

Monday Morning, October 29, 2012

Spectroscopic Ellipsometry Focus Topic

Room: 19 - Session EL+TF+AS+EM+SS+PS+EN+NM-MoM

Spectroscopic Ellipsometry for Photovoltaics and Semiconductor Manufacturing

Moderator: M. Creatore, Eindhoven University of Technology, the Netherlands, H. Wormeester, MESA+ Institute for Nanotechnology, University of Twente, Enschede, The Netherlands

8:20am **EL+TF+AS+EM+SS+PS+EN+NM-MoM1 Multichannel Spectroscopic Ellipsometry: Applications in I-III-V₂ Thin Film Photovoltaics**, *R.W. Collins, D. Attygalle, P. Aryal, P. Pradhan, N.J. Podraza*, University of Toledo, *V. Ranjan, S. Marsillac*, Old Dominion University **INVITED**

Multichannel spectroscopic ellipsometry (SE) has been applied successfully as an in situ, real time tool for optimizing, monitoring, and controlling multi-stage deposition processes in various thin film photovoltaics (PV) technologies. A particularly challenging process optimization problem involves the thermal co-evaporation of individual elements of Cu, In, Ga, and Se in a three-stage process, which has proven to produce high quality Cu(In_{1-x}Ga_x)Se₂ (CIGS) materials and high performance PV devices. This three-stage process provides a high level of flexibility in determining the phase, composition, and microstructure of the film, but also generates greater challenges in run-to-run reproducibility of the optimized process. Information extracted from real time SE measurements includes the evolution of the bulk layer and one or more surface layer thicknesses, as well as layer dielectric functions. The layer dielectric functions can be analyzed further to extract the phase and alloy compositions and the defect density or grain size, which can assist in understanding the fabrication process, in optimizing solar cells, and ultimately in monitoring and controlling the optimized process for improved reproducibility. In this study, the focus is on analysis of ellipsometric (ψ , Δ) spectra acquired by real time SE in order to characterize (i) the structural and compositional evolution in (In,Ga)₂Se₃ film growth from In, Ga, and Se fluxes in the first stage, (ii) the transition from Cu-poor to Cu-rich CIGS at the end of the second stage, which occurs under Cu and Se fluxes, and (iii) the transition from Cu-rich to the desired Cu-poor CIGS, which defines the end of the third and final stage, and occurs under a second application of In, Ga, and Se fluxes. After the transition from Cu-poor to Cu-rich material in the second stage, a Cu_{2-x}Se phase near the surface of the bulk layer is tracked. In the Cu-rich to Cu-poor transition, this Cu_{2-x}Se phase has fully reacted with In, Ga, and Se to form CIGS. Studies using a standard Mo substrate and 2 μ m thick CIGS for solar cells have also revealed features in the (ψ , Δ) spectra characteristic of the anticipated changes in the near surface phase composition as established by detailed modeling on thinner and smoother films. Although careful analysis of real time SE is expected to provide quantitative information on the surface properties and their evolution in this case of solar cells, control of the deposition has been successful simply by monitoring real time changes in the ellipsometric (ψ , Δ) spectra.

9:00am **EL+TF+AS+EM+SS+PS+EN+NM-MoM3 Contribution of Plasma Generated Nanoparticles to the Growth of Microcrystalline Silicon Deposited from SiF₄/H₂/Argon Gas Mixtures**, *J.-C. Dornstetter, S. Kasouit, J.-F. Besnier*, Total S.a, France, *P. Roca i Cabarrocas*, LPICM-CNRS, Ecole Polytechnique, France

Despite the low fabrication cost of thin film silicon solar modules, this type of technology remains non competitive in main stream markets because of the high BOS costs, due to the low energy conversion efficiency of this type of modules (~10%). We have recently shown that microcrystalline silicon films deposited using SiF₄/H₂/Argon RF capacitive plasmas have excellent structural and transport properties, compared to films deposited using conventional SiH₄/H₂ mixtures, allowing for a very good carrier collection, even for thick cells, and Voc values of 0.55 V, without device optimization, thus opening up the path for the realization of high performance solar cells. However, little is known so far about the growth mechanism of this type of materials and the reason for such interesting properties. Studies of silicon thin films deposition from SiF₄/H₂ mixes, under conditions different from ours, suggested that the growth is due to the deposition of SiF₂ radicals, followed by the abstraction of fluorine by hydrogen. Previous work within our group has also shown that deposition occurs only when particles are present in the plasma, and that growth starts from crystallites without any amorphous phase. We present here a systematic study of the growth of

microcrystalline films, together with the composition of nanoparticles attracted by thermophoresis to cold traps located both on the walls of the plasma chamber and in the fore line as a function of deposition conditions. The composition of the deposit on the traps is found to be amorphous at low power/ low hydrogen conditions and becomes crystalline when either of them increases. This correlates well with an increase in atomic hydrogen concentration in the plasma, as estimated by actinometry. The crystalline fraction of the deposited film was measured using in-situ ellipsometry and was found to correlate with the composition of the deposit on the cold traps. Deposition rate is drastically reduced when a water cooled trap is installed on the walls of the plasma chamber, and switches off at high H₂ flow rates. Under these conditions, TEM and AFM images, show that at the initial stages of the growth the film is constituted of sparse, hexagonal crystalline particles, having sizes on the order of few tens of nanometers. We interpret the data above as a result of plasma-generated nanocrystals being a significant contribution to the deposited film. This may explain the excellent electronic properties of the films, as the particles are formed in the bulk of the plasma region, free from energetic ions bombardment. We will correlate the structural properties and the film growth mechanisms to the properties of solar cells.

9:20am **EL+TF+AS+EM+SS+PS+EN+NM-MoM4 Multichannel Spectroscopic Ellipsometry for CdTe Photovoltaics: from Materials and Interfaces to Full-Scale Modules**, *P. Koirala, J. Chen, X. Tan, N.J. Podraza*, The University of Toledo, *S. Marsillac*, Old Dominion University, *R.W. Collins*, The University of Toledo

Real time spectroscopic ellipsometry (RTSE) has been implemented in studies of the evolution of the semiconductor structural and optical properties during sputter deposition of thin film polycrystalline CdS/CdTe solar cells on transparent conducting oxide (TCO) coated glass substrates. Analysis of the real time optical spectra collected during CdS/CdTe deposition requires an optical property database as a function of measurement temperature for all substrate components. These include not only soda lime glass, but also an SiO₂ layer and three different SnO₂ layers. We report optical functions parameterized versus temperature for the glass substrate and its overlayers starting from room temperature and ending at elevated temperature above which the semiconductor layers are deposited. In fact, such a database has additional applications for on-line, through-the-glass monitoring applications of coated glass at elevated temperature. In the RTSE studies, knowledge of the temperature dependent optical functions of the substrate components enables an accurate substrate temperature determination before the onset of deposition and is critical for accurate extraction of the semiconductor layer optical properties. We implement RTSE to study the filling process of the surface roughness modulations on the top-most SnO₂ substrate layer and modification of the optical properties of this layer. This modification is further studied post-deposition by infrared spectroscopic ellipsometry. In addition to providing information on interface formation to the substrate during film growth, RTSE also provides information on the bulk layer CdS growth, its surface roughness evolution, as well as overlying CdTe interface formation and bulk layer growth. Information from RTSE at a single point during solar cell stack deposition assists in the development of a model that can be used for mapping the completed cell stack properties, which can then be correlated with device performance. Independent non-uniformities in the layers over the full area of the cell stack enable optimization of cell performance combinatorially.

9:40am **EL+TF+AS+EM+SS+PS+EN+NM-MoM5 Determination of Electronic Band Gaps from Optical Spectra**, *R.A. Synowicki*, J.A. Woollam Co., Inc.

The band gap of a material E_g is defined theoretically as the lowest energy for electronic transition from the valence to conduction bands in a solid. For an ideal material free of defects this is the photon energy or wavelength where the optical properties change from transparent to absorbing. However, real materials contain defects which cause absorption to begin below the band gap (i.e. the Urbach Tail) making determination of the true band gap position difficult. For example, in a solar cell the measured absorption edge represents the onset of transitions first due to defects, then from band to band. Empirical methods used to determine the band gap in real materials with defects include the Tauc plot and the Mott-Davis plot. More theoretical mathematical dispersion models such as the Tauc-Lorentz, Cody-Lorentz, and Herzinger-Johs models have been developed which include an adjustable band gap parameter. The various plots and dispersion model methods will be discussed and applied to different materials measured optically via spectroscopic ellipsometry, intensity transmission, reflection, absorption, or a combination of these methods.

10:00am **EL+TF+AS+EM+SS+PS+EN+NM-MoM6 Optical Modeling of Plasma-Deposited ZnO: Extended Drude and its Physical Interpretation**, *H.C.M. Knoop, M.V. Ponomarev, J.W. Weber, N. Leick, B.W.H. van de Loo, Y.G. Melese, W.M.M. Kessels, M. Creatore*, Eindhoven University of Technology, the Netherlands

High-quality transparent conductive oxides such as ZnO are important due to their electrical and optical properties. To improve these properties the responsible physical processes have to be understood. Traditionally, charge-carrier-scattering processes are investigated by combining morphology data and Hall measurements. This contribution discusses the extensive optical modeling of plasma-deposited ZnO and how its interpretation directly provides insight into the relevant charge-carrier-scattering processes at different length scales. The interpretation is generalized to the concept of frequency-dependent resistivity, which is used to explain the applicability of different Drude models.

Thin films (50-1000 nm) of Al-doped and undoped ZnO were deposited using an expanding thermal plasma MOCVD process.¹ Conditions of high pressure and high diethyl zinc flow allowed for dense films with low electrical resistivities (e.g., $4 \times 10^{-4} \Omega \text{ cm}$ at 300 nm). The films were analyzed with variable-angle spectroscopic ellipsometry (SE) (0.75 – 5.0 eV), FTIR reflection spectroscopy (0.04 – 0.86 eV), Four-point-probe (FPP), and Hall measurements.

The SE and FTIR data were combined and fitted with classical and extended Drude² models. The high intensity of the Drude in the FTIR range resulted in a high sensitivity with which the carrier concentration and mobility could even be determined for thin (~40 nm) undoped ZnO films. An extended Drude model was needed to correctly model the SE energy range, which was explained by the dominance of ionized impurity scattering and a reduction of this scattering for higher photon energies. The grain-boundary-scattering mobility could be determined by the difference between optical and Hall mobilities.³ When combined with FPP results, the effective mobility can be determined from these optical techniques without the use of Hall measurements. The optical response above the band gap was modeled by a PSEMI or Tauc-Lorentz oscillator model, where a broadening and shift of the transition was seen for increasing carrier concentration.⁴

These insights and a generalized view of electron scattering in ZnO at different length scales will be presented.

1. Ponomarev et al., *J. Appl. Phys.* **Submitted** (2012)
2. Ehrmann and Reineke-Koch, *Thin Solid Films* **519**, 1475 (2010)
3. Steinhäuser et al., *Appl. Phys. Lett.* **90**, 142107 (2007)
4. Fujiwara and Kondo, *Phys. Rev. B* **71**, 075109 (2005)

10:40am **EL+TF+AS+EM+SS+PS+EN+NM-MoM8 The Ellipsometric Response of Single-Crystal Silicon to Doping**, *H.G. Tompkins*, Consultant

The current wisdom is that for ellipsometry in the UV-vis-NIR spectral range, doping of single-crystal silicon can be ignored. We study the ellipsometric response of silicon doped with arsenic at various levels. We also studied the response after implant (before activation) and after the activation (anneal). We find that for samples implanted with 1×10^{18} atoms/cm³, the single-crystal silicon was not amorphized. Implants of 2×10^{19} atoms/cm³ and higher left an amorphous layer on the surface of the wafer the thickness of which was about the depth of the implant. Activation of the sample implanted with 2×10^{19} atoms/cm³ returned the sample to single-crystal silicon and the ellipsometric response in the UV-vis-near-IR is essentially that of undoped silicon. However, the response in the mid-IR is that the extinction coefficient is no longer zero. For samples implanted with 2.5×10^{20} atoms/cm³ and greater, annealing did not return the UV-vis-near-IR ellipsometric response to that of single-crystal silicon. Although this amount of other material (arsenic) is still less than about one tenth of one percent, our conjecture is that the microstructure simply could not be returned to that of a single crystal. As with the lower doped sample, the mid-IR spectral region showed significant increase in the extinction coefficient.

11:00am **EL+TF+AS+EM+SS+PS+EN+NM-MoM9 The Effect of Stress on the Optical Properties Semiconductor Films**, *A.C. Diebold, G.R. Muthinti, M. Medikonda, T.N. Adam*, College of Nanoscale Science and Engineering, University at Albany, *A. Reznicek, B. Doris*, IBM Research at Albany Nanotech

Here we review the impact of stress on the complex dielectric function of semiconductor films measured using spectroscopic ellipsometry. Two relevant examples of stressed semiconductor layers are pseudomorphic epitaxial layers fabricated during semiconductor manufacturing and strained silicon on insulator (sSOI) wafers. Stress is known to shift the energies of direct gap critical point transitions in semiconductors. The biaxial stress in pseudomorphic films grown on silicon wafers can be as high as that used during opto-elastic studies of bulk semiconductors. The amount of stress in

un-relaxed, pseudomorphic films of $\text{Si}_{1-x}\text{Ge}_x$ on Si (100) reaches 1 GPa for alloys with 20% Ge and is more than 3 GPa for films with > 50% Ge. The bi-axial stress in sSOI is typically ~1 GPa. An elastic theory approach for the effect of strain on the k^*p determined band structure and optical transition energy is well known. Both low shear stress and high shear stress approximations can apply to the shift in transition energy depending on the magnitude of the spin orbit splitting energy vs the magnitude of the shear stress. Until recently it was difficult to obtain sets of samples that test both approximations. Here we discuss results from our recent study of pseudomorphic films of $\text{Si}_{1-x}\text{Ge}_x$ on Si (100) from $x=0.05$ to 0.75 which covers both low and high shear regimes. We also present our recent study of the dielectric function of thinned sSOI which illustrates the impact of stress on the optical transitions for the Si layer on sSOI. All of these samples are examples of new materials being used in semiconductor research. The results of this study are directly transferred into cleanroom spectroscopic ellipsometry systems used for process control during manufacturing.

11:20am **EL+TF+AS+EM+SS+PS+EN+NM-MoM10 Numerical Ellipsometry: Spectroscopic n-k Plane Analysis of Thin Films Growing on Unknown Layered Substrates**, *F.K. Urban, D. Barton*, Florida International University

Spectroscopic ellipsometry measurements on thin films commonly make use of prior knowledge of the structure and optical properties of the underlying substrate. However, imprecision in substrate statistics propagates into the solution for the film of interest. Thus it is more accurate to have a method for solving for film properties which simultaneously obtains whatever is needed about the substrate. And it makes solutions possible whether or not book data or previous substrate solutions are available. In this work we apply Complex Analysis in the n-k plane to achieve solutions employing the well-know reflection equations. The method is carried out at each measured wavelength and does not necessitate an *a-priori* assumption of optical property dependencies on wavelength. The mean square error has been improved by many orders of magnitude, a selected limit of 10^{-14} as opposed to 1 to 30 or so for least squares. Thus the full accuracy of the ellipsometer is now available for more accurate measurements of film thickness and optical properties. The method requires six measurements during growth. The first is used to determine the relationship between R_p and R_s at the film-substrate interface. The following four are used to uniquely determine the values of R_p , R_s , and film n , k , and d . The final measurement confirms the unique solution. Suitability of the model is tested by comparing measurements at two of more wavelengths for self consistency. Results for n and k of the growing film are examined across the measurement spectrum in comparison with parameterizations in common use.

Energy Frontiers Focus Topic

Room: 15 - Session EN+NS-MoM

Nanostructured Solar Cells

Moderator: M.S. Arnold, University of Wisconsin Madison

8:20am **EN+NS-MoM1 Doping Control for the Development of Silicon Quantum Dot Solar Cell**, *K.J. Kim, J.H. Park*, Korea Research Institute of Standards and Science (KRISS), Republic of Korea, *H.-J. Baek, H.H. Hwang*, University of Science and Technology (UST), Republic of Korea, *J.S. Jang*, Chungbuk National University (CBNU), Republic of Korea

Si quantum dots (QDs) imbedded in a SiO_2 matrix is a promising material for the next generation optoelectronic devices, such as solar cells and light emission diodes (LEDs). However, low conductivity of the Si quantum dot layer is a great hindrance for the performance of the Si QD-based optoelectronic devices. The effective doping of the Si QDs by semiconducting elements is one of the most important factors for the improvement of conductivity. High dielectric constant of the matrix material SiO_2 is an additional source of the low conductivity.

Active doping of B in Si nano structures and the effect of internal polycrystalline bridge layer were investigated by secondary ion mass spectroscopy (SIMS) depth profiling analyses. Phosphorous and boron doped-Si / SiO_2 multilayers on Si wafers were fabricated by ion beam sputtering deposition as a model structure for the study of the diffusion behavior of the dopants. The distributions of the dopants after annealing at high temperatures were analyzed by SIMS depth profiling analyses.

In this study, the diffusion behaviors of various dopants in silicon nanostructures will be discussed and the effects of the various parameters for the improvement of conversion efficiency in Si quantum dot solar cell will be introduced.

8:40am **EN+NS-MoM2 Photocarrier Generation in Si Quantum-dot Sensitized Solar Cells**, *G. Uchida, H. Seo, Y. Wang, K. Kamataki, N. Itagaki, K. Koga, M. Shiratani*, Kyushu University, Japan

The pressing need for massively scalable carbon-free energy sources has focused attention on both increasing the efficiency and decreasing the cost of solar cells. Quantum-dot (QD) solar cells employing multiple exciton generation (MEG) have attracted much attention as a candidate for the third generation solar cells, because MEG represents a promising route to increased solar conversion efficiencies up to about 44 % in single junction. Our interest has been concerned with QD sensitized solar cells using Si nanoparticles [1]. The main purpose of this study is to discuss the characteristic of the quantum yield in view of the MEG effect.

QD thin films composed of size-controlled Si nanoparticles were deposited using double multi-hollow discharge plasma chemical vapour deposition (CVD) of a SiH₄/H₂ and CH₄ or N₂ gas mixture [2]. Short-circuit current density of Si QD sensitized solar cells increases by a factor of 2.5 by irradiation of CH₄ or N₂ plasma to Si nanoparticle surface. We also have measured incident photon-to-current conversion efficiency (IPCE) in the near-ultraviolet range using quartz-glass plates as front panels of QD sensitized solar cells. IPCE gradually increases by light irradiation in a wavelength range less than 600 nm around optical band-gap (E_g) of Si nanoparticle films, and then steeply increases below 280 nm around 2E_g. This rapid increase of IPCE under the ultraviolet light incidence may be explained by the theoretically predicted MEG, the creation of two electron-hole pairs from one high-energy photon incidence, in Si nanoparticle QDs.

[1] G. Uchida, et al., *Phys. Status Solidi C* 8 (2011) 3021.

[2] G. Uchida, et al., *Jpn. J. Appl. Phys.* 51 (2011) 01AD01-1.

9:00am **EN+NS-MoM3 Quantum Dot Solar Cells with External Quantum Efficiency Exceeding 100% by Multiple Exciton Generation**, *J.M. Luther, M.C. Beard, A.J. Nozik, O.E. Semonin*, National Renewable Energy Laboratory **INVITED**

Traditional semiconductors used in photovoltaic devices produce one electron from each absorbed photon. On the other hand, new materials such as quantum dots, nanorods, carbon nanotubes and graphene can more efficiently convert high-energy photons into multiple electron-hole pairs through a process titled multiple exciton generation (MEG) provided that the energy of the photon is at least twice the bandgap of the absorber. This process has been shown to be more efficient in highly confined quantum dots than other forms of carrier multiplication (such as impact ionization) in bulk materials. Photovoltaic devices can benefit greatly from MEG by producing increased photocurrent from the multiple electrons and thus allowing a single junction solar cell to yield a theoretical maximum efficiency as high as 44% compared to 33% for bulk semiconductors. In this talk, we will present recent findings from incorporating PbSe quantum dots (QDs) into semiconducting arrays that make up the absorber layer in prototype solar cells. In these devices, MEG is confirmed by demonstrating the first solar cell with external quantum efficiency (EQE) exceeding 100% for solar relevant photon energies. The EQE in our device reaches a maximum value of 114% at 380 nm and we have employed an optical model to determine that the PbSe QD layer produces as many as 1.3 electrons per photon (on average) for these photons. These findings are compared to ultrafast time resolved measurements of carrier quantum yields where we find reasonable agreement. We will also discuss future directions for materials designs that increase the quantum yield through more efficient MEG.

9:40am **EN+NS-MoM5 Quantum-Confined Nanocrystals as Building Blocks for Low-Cost Solution-Processed Multi-Junction Solar Cells**, *T. Hanrath, J.W. Choi, W.N. Wenger, R.S. Hoffman*, Cornell University

In light of recent advances in synthesis, characterization, and the emerging understanding of their size-dependent properties, there are many exciting opportunities for semiconductor nanomaterials to contribute to the development of next-generation energy conversion technologies. Semiconductor nanocrystal quantum dots are particularly attractive material candidates for the efficient capture of solar emission in inexpensive, thin film photovoltaic devices due to their large absorption cross sections, low-cost solution-phase processing and size-tunable energy gaps. The prospect of exploiting colloidal nanostructures for the creation of low-cost multi-junction solar cells has garnered immense scientific and technological interest. We recently demonstrated solution-processed tandem solar cells created from nanocrystal quantum dots with size-tuned energy levels. Bringing this prospect to fruition requires the connection of absorber layers with cascaded energy gaps subject to stringent electrical and optical constraints. We show that interlayers composed of ZnO/Au/PEDOT provide appropriate carrier density and energy-level alignment to resolve this challenge. With such interlayers we have been able to create nanocrystal quantum dot tandem cells that exhibit IR sensitivity and an open circuit voltage approaching 1V. These advances provide guidelines for the design

of an effective interlayer in tandem cell devices and suggest a promising future for solution-processed nanocrystal quantum dot solar cells.

10:00am **EN+NS-MoM6 Improvement of Carrier Transport in PbSe Quantum Dot-Embedded Polymeric Solar Cells Fabricated by a Laser Assisted Spray Process**, *C. Hettiarachchi, D.M. Feliciano, D. Mukherjee, P. Mukherjee, S. Witanachchi*, University of South Florida

PbSe quantum dots (QD) in the size range of 4-8 nm are promising candidates for solar energy harvesting as they exhibit multi-exciton generation with ultraviolet (UV) photon absorption. While generation of multi-excitons has been demonstrated, dissociation of excitons to enhance current densities has not been realized. One of the main bottlenecks has been the difficulty in removing the surfactants on QDs to form a clear interface between the QD and the polymer matrix. We have developed a Laser Assisted Spray (LAS) deposition technique to deposit uniform coatings of surfactant-free QDs on substrates. This technique involves the transient heating of aerosols containing PbSe QDs by a CO₂ laser-gas interaction to burn the organic surfactants. Transmission electron micrographs and absorption spectroscopy show, under optimum conditions, the particles remain as single crystals and maintain quantum confinement. Growth parameters are optimized by monitoring the degree of surfactant removal by studying the Fourier Transform Infrared (FTIR) spectra of coatings grown by LAS technique. Two-layer solar cell structures of PbSe/polymer that is sandwiched between ITO and Al electrodes have been fabricated. Comparison of the IV characteristics of these cells and cells fabricated by PbSe QDs with ligand-exchange will be presented.

10:40am **EN+NS-MoM8 Single and Multiple Exciton Dissociation in Colloidal Nanoheterostructures**, *T. Lian*, Emory University **INVITED**

The ability to control charge transfer dynamics to and from quantum dots (QDs) is essential to many QD-based devices, such as solar cells and light emitting diodes. Recent reports of multiple exciton generation (MEG) by one absorbed photon in some QDs offer an exciting new approach to improve the efficiency of QD-based solar cells and to design novel multi-electron/hole photocatalysts. Two major challenges remain. First, the efficiency of MEG process needs to be significantly improved for practical applications. Second, the utilization of multi-excitons requires ultrafast exciton dissociation to compete with the exciton-exciton annihilation process, which occurs on the 10s to 100s ps time scale. In this presentation we report a series of studies of exciton dissociation dynamics in QDs and nanorods by electron transfer to adsorbed electron acceptors. We show that excitons in CdX (X=S, Se, Te) and PbS QDs can be dissociated on the picosecond and faster timescales and multiple excitons (generated by multiple photons) per QD can be dissociated by electron transfer to adsorbed acceptors. We discuss approaches for optimizing the single and multiple exciton dissociation efficiencies by controlling the spatial distributions of the electron and hole (i.e. wave-function engineering) in type II core/shell QDs and nanorods.

11:40am **EN+NS-MoM11 Intermediate Band Upconversion for Low-Cost, Solution Processed Photovoltaics**, *J. Lewis, E.J.D. Klem, C.W. Gregory, G.B. Cunningham, S. Hall, D.S. Temple*, RTI International

PV devices based on disordered semiconductors such as polymers, organic small molecules, and colloidal quantum dots have seen gradually improving performance in recent years, but are likely to be limited to efficiencies in the range of 10–15%. To increase efficiency further would require the use of tandem cells, which adds complexity and cost. Alternatively one can pursue devices such as intermediate band solar photovoltaics (IBPV) that can exceed the Shockley-Queisser efficiency limit. In an IBPV device mid-gap states are incorporated into a wider band-gap host, allowing infrared photons to contribute to the photocurrent of the device via sequential absorption of two photons. Ideally this occurs without compromising the open circuit voltage. We will present the first example of an IBPV solar cell using solution processed, low-cost disordered materials. We show that the nature of the defect states in Pb-salt quantum dots is uniquely suited to efficient upconversion at optical power densities that are relevant for unconcentrated solar illumination. This demonstration provides a path for a step-change in the efficiency of low-cost PV.

Monday Afternoon, October 29, 2012

Energy Frontiers Focus Topic

Room: 15 - Session EN+TF-MoA

Chalcogenide Solar Cells I

Moderator: J. Luther, NREL

2:00pm EN+TF-MoA1 **Research Strategies and Results Toward Improving Thin Film CdTe Photovoltaic Devices Beyond 20% Conversion Efficiency**, T.A. Gessert, National Renewable Energy Laboratory **INVITED**

Recent studies of thin-film CdS/CdTe photovoltaic (PV) devices have suggested that significantly higher device performance will not be achieved unless recombination in the CdTe is reduced. Specifically, unless high recombination in the CdTe quasi-neutral region is reduced, benefits of increasing CdTe net-acceptor doping cannot be realized—because resulting higher open-circuit voltage will be accompanied by lower fill factor. Although some control of CdTe recombination has been achieved historically through the careful incorporation of oxygen, chlorine, and copper, many technologists believe a more promising avenue to higher device performance is by understanding and controlling the defects in the as-deposited CdTe. This is supported by theoretical studies that suggest much of the improvement associated with oxygen, chlorine, and copper is due to the interaction of these species with intrinsic defects related cadmium and tellurium (i.e., vacancies, interstitial, and anti-site defects). Although CdTe is a relatively simple semiconducting material that exists only near its 50%/50% composition, even at thermodynamic equilibrium, the material can sustain a small stoichiometric deficiency (~0.01%). Even this small extent of stoichiometry variation can produce intrinsic defects at a sufficient concentration to significantly alter device performance. Further, the typical techniques used in PV film deposition are not equilibrium processes, and so the extent of non-stoichiometry could be greater. Several research projects at NREL are currently focused on altering CdTe deposition and post-deposition processes to allow for an enhanced control of the as-deposited intrinsic defects. Related defect changes are being assessed using a combination of device analysis, time-resolved photoluminescence, low-temperature photoluminescence, and microscopic techniques. The presentation will discuss initial results where process changes expected to alter the as-deposited defects also affect junction evolution and device functionality. *This abstract is subject to government rights.*

2:40pm EN+TF-MoA3 **Nanocrystal-Ink and Soluble-Precursor Routes to Earth Abundant Element Kesterite Solar Cells**, H.W. Hillhouse, University of Washington **INVITED**

Given the terawatt scale of future energy needs, the most promising future photovoltaic materials should be Earth abundant with their primary mineral resources distributed across several geographic regions and their supply chains robust to reduce concerns of price volatility. In addition, the process of forming the solar cell should be scalable, low-cost, and not utilize dangerous or toxic materials. The strongest initial candidate appears to be kesterite structures of $\text{Cu}_2\text{ZnSnS}_4$ (CZTS) and similar materials. The presentation will review the progress in developing photovoltaics devices based on these materials and our group's recent experimental and modeling results.

CZTS thin film solar cells have historically been synthesized by evaporating or sputtering metals (Cu, Zn, & Sn) followed by sulfurization or selenization. More recently, two potentially low-cost high-throughput approaches have been demonstrated that form the quaternary or pentenary chalcogenide directly from solution-phase processes. One is based on first synthesizing multinary sulfide nanocrystals and then sintering them to form a dense layer. The other approach utilizes molecular precursors dissolved in hydrazine. Both new approaches reach their highest device efficiencies by incorporating Se to form $\text{Cu}_2\text{ZnSn}(\text{S}_x\text{Se}_{1-x})_4$ devices, and each has yielded substantially higher efficiency devices than the best vacuum deposited absorbers. The hydrazine route has yielded the most efficient CZTS-based devices thus far. The presentation will highlight our recent progress in CZTS-based nanocrystal-ink devices. In particular, we have shown that germanium may be alloyed with CTZS (at least up to Ge/(Sn+Ge) ratios of 0.7) to form $\text{Cu}_2\text{Zn}(\text{Sn,Ge})\text{S}_4$ nanocrystals that have an increased bandgap. The defect chemistry is serendipitous, and yields devices at with greater than 8% power conversion efficiency. This exciting prospect may be used to create a back surface field and direct carriers in a similar manner to how gallium is used in high efficiency CIGS devices. In addition, we will report recent results from high throughput experiments focused on identifying doping and passivation agents.

3:40pm EN+TF-MoA6 **Developing Earth Abundant and Quantum Dot Materials for Thin-Film Photovoltaics**, M. Law, University of California Irvine **INVITED**

This talk describes projects in our group to develop thin-film photovoltaics based on earth-abundant iron pyrite (FeS_2) active layers and PbSe quantum dot (QD) solids. I will first introduce the promise and challenge of pyrite, describe solution- and gas-phase syntheses of pyrite films, and present preliminary electrical characterization of pyrite layers and device stacks. Then I will switch gears to highlight several projects focused on the chemistry/physics of QD solids, including our use of atomic layer deposition to produce environmentally-robust PbSe QD films with long carrier diffusion lengths for next-generation solar cells.

4:20pm EN+TF-MoA8 **Synthesis of Photovoltaic $\text{Cu}_2\text{ZnSnS}_4$ via *Ex Situ* Sulfidation of Co-Sputtered Cu-Zn-Sn Thin Films**, M. Johnson, M. Manno, X. Zhang, C. Leighton, E.S. Aydil, University of Minnesota

$\text{Cu}_2\text{ZnSnS}_4$ (CZTS) is an emerging low-cost solar absorber for thin film photovoltaics based on non-toxic, high earth-abundance elements. While *ex situ* sulfidation of Cu-Zn-Sn precursor films in S vapor is a popular synthesis route for CZTS, much remains to be understood with regard to the sulfidation mechanisms, microstructural control, and structure-property relationships. In this work, DC magnetron co-sputtered Cu-Zn-Sn films, of varying composition, were sealed with 1.0 mg of S in evacuated (10^{-6} Torr) quartz ampoules, and then isothermally heat treated at sulfidation temperatures in the range $100^\circ\text{C} \leq T_S \leq 700^\circ\text{C}$. The films were then characterized structurally by scanning electron microscopy, Raman spectroscopy, and X-ray diffraction, and electrically via resistivity measurements between 4.2 K and 300 K. We find that the phase purity of the resultant films depends strongly on T_S , with complete conversion of the precursor film to CZTS occurring only at $T_S \geq 550^\circ\text{C}$. The final phase purity of *ex situ* sulfidized CZTS films is however remarkably insensitive to modest amounts of excess Zn and Sn in the Cu-Zn-Sn precursor film. Excess Zn or Sn in the precursor is readily ejected during sulfidation, via elemental or binary sulfide evaporation, respectively, while Sn-deficiency can also be corrected by introducing elemental Sn to the sealed quartz ampoule. However, due to the low melting point of Sn, and the absence of appropriate Sn-Zn alloys, the precursor composition *does* play a significant role in defining the final CZTS film microstructure, and the lateral homogeneity. In addition to detailed discussion of the physics and chemistry underlying the above observations we will also provide data on the transport properties of such films, including observations of hopping conduction.

Work supported by NSF (CBET-0931145) and IREE (RL-0004-11)

4:40pm EN+TF-MoA9 **Crossover from Intergranular Hopping to Conventional Charge Transport in Pyrite FeS_2 Thin Films**, X. Zhang, M. Manno, A. Baruth, M. Johnson, E.S. Aydil, C. Leighton, University of Minnesota

Pyrite FeS_2 is undergoing a tremendous resurgence of interest as a candidate thin-film solar absorber based on abundant, low-cost, non-toxic elements. Historically, FeS_2 -based Schottky solar cells have suffered from low open circuit voltages (~100 mV), and thus low efficiency, although the origins of this behavior are not entirely clear. In fact, even the electronic properties of FeS_2 are not well understood, including the conduction mechanisms and doping behavior. Understanding these issues could contribute significantly to improvements in FeS_2 -based solar cells, particularly if doping can be understood and controlled. In this work, we present a comprehensive study of the conduction mechanism in FeS_2 thin films synthesized via the *ex situ* sulfidation of Fe films in a S vapor at sulfidation temperatures in the range $100^\circ\text{C} \leq T_S \leq 700^\circ\text{C}$. The resultant films were characterized structurally, using X-ray diffraction, scanning electron microscopy, energy dispersive spectroscopy, and confocal Raman microscopy; electrically, via transport and magnetoresistance measurements between 4.5 and 300 K; and magnetically with high-sensitivity dc magnetometry. At T_S around 500°C we observe a crossover in the conduction mechanism from some form of hopping conduction to a more conventional band transport-type mechanism. Through detailed analysis of the hopping parameters, measurement of the Fe spin-state, and simple calculations based on S diffusion in Fe, we demonstrate that intergranular hopping occurs via highly conductive, S-deficient, nanoscopic grain cores separated by nominally stoichiometric FeS_2 shells. We find that the approach towards more conventional band transport as T_S is increased above 500°C is due to an increase of S diffusion into the FeS_2 grains. Moreover, this conduction mechanism crossover is found to be accompanied by a sign reversal of the Hall coefficient, from hole-like (in the hopping regime) to electron-like. In addition to placing hard constraints on the conditions under which useful properties can be

obtained from FeS₂ synthesized under diffusion-limited conditions, these results also highlight potential problems with prior conclusions on the dominance of *p*-type behavior.

The work was supported by the Initiative for Renewable Energy & the Environment, IREE (RL-0004-11). Part of this work was carried out in the University of Minnesota Characterization Facility, a member of the NSF-supported Material Research Facilities Network.

5:00pm EN+TF-MoA10 Plasma Assisted Synthesis of Pyrite Absorbers, R. Morrish, R. Silverstein, C.A. Wolden, Colorado School of Mines

Pyrite (FeS₂) is a non-toxic, earth abundant chalcogenide with desirable characteristics for application as a photovoltaic absorber including a modest band gap of 0.95 eV and a large optical absorption coefficient (>10⁵ cm⁻¹). Although theoretically capable of >20% efficiency, to date pyrite devices have displayed poor performance. One key challenge has been the production of stoichiometric material that is free of impurity phases. Conventional approaches employ thermal sulfurization of iron-based films or precursors. These routes inherently produce contaminate phases (troilite, pyrrhotite, marcasite), that once formed, are difficult to completely remove. Thermodynamics suggests that hematite (α -Fe₂O₃) may be directly converted to pyrite in the presence of sufficiently high sulfur activity. In this work, we demonstrate pyrite synthesis using a H₂S plasma to sulfurize hematite nanorods produced using chemical bath deposition. Conversion to pyrite was achieved by exposure to a 90% Ar-10% H₂S plasma at moderate temperature (350 - 450 °C). The application of plasma dramatically enhances both the rate of conversion and the quality of the resulting material. Composition analysis using both Raman and X-ray photoelectron spectroscopy confirm that the resulting pyrite is free of common impurity phases. The degrees of sulfur incorporation could be precisely controlled by plasma exposure, and the apparent optical band gap could be systematically reduced from 2.2 to 1.0 eV. Electron microscopy images showed the surface maintained a nanostructured architecture following sulfurization, and a 150 nm thick film was sufficient to absorb 99% of incident visible light. In this presentation we discuss the kinetics of this solid state transformation, as well as report on the optoelectronic properties of these materials.

Thin Film

Room: 11 - Session TF+EN-MoA

ALD for Energy

Moderator: R.K. Grubbs, Sandia National Laboratories

2:00pm TF+EN-MoA1 Atomic Layer Deposition for the Synthesis of Nanostructured Catalysts, J.W. Elam, C. Marshall, Argonne National Lab, E. Stach, F. Ribeiro, Purdue Univ., J. Greeley, Argonne National Lab, J. Notestein, K. Poepelmeier, Northwestern Univ., L. Curtiss, Argonne National Lab, M. Kung, P.C. Stair, Northwestern Univ., L. Winans, Argonne National Lab, S. Nguyen, Northwestern Univ. **INVITED**

The successful transition to an energy economy based on biomass will require radical advances in catalyst science. This challenge demands a new paradigm in catalyst synthesis whereby inorganic components can be assembled at the atomic scale to yield complex, multifunctional catalysts rivaling Nature's enzymes in their specificity. To this end, we have developed a novel approach combining templated synthesis for shape-selectivity with the atomically-precise positioning of discrete functionalities. In this approach we begin with a supporting scaffold for catalyst growth upon which we chemically attach molecular templates. Next, atomic layer deposition is used to build a structure around each template in an atomically precise, layer-by-layer fashion where the thickness and composition can be tuned at each layer. Finally, the template is removed yielding a "nanobowl" defining a structured catalytic environment. The molecular template can be synthesized to contain bulky organic ligands surrounding a catalytic atom or cluster which remains anchored to the bottom of the bowl after ligand removal. Furthermore, one or more layers in the bowl wall can be selected to serve as a co-catalyst (e.g. Lewis acid group) positioned at a well-defined distance from the catalyst at the bottom of the bowl. This presentation will review our recent progress synthesizing, characterizing, modeling, and testing these unique catalytic materials.

2:40pm TF+EN-MoA3 Using Metalcone Films Grown by Molecular Layer Deposition to Form Conducting Metal Oxide-Carbon Composite Films, A. Abdulagatov, K. Terauds, J. Travis, A. Cavanagh, R. Raj, CU Boulder, S.M. George, University of Colorado, Boulder

Metalcone films grown using molecular layer deposition (MLD) techniques with metal and organic precursors are metal alkoxide polymers. These hybrid organic-inorganic films can serve as precursors to conducting metal oxide-carbon composite films. In this study, titanocene MLD films were deposited by sequential, self-limiting exposures of TiCl₄ and glycerol at 150°C. These films were then annealed in argon at temperatures ranging from 500 to 1200 °C. Under argon, the hydrogen is removed from the hybrid organic-inorganic titanocene films and the carbon remains. Raman spectroscopy measurements showed the progressive growth and sharpening of the D and G signature peaks for graphitic carbon after annealing from 600 to 900 °C. The sheet resistance of the annealed films was also found to progressively decrease with increasing annealing temperature. X-ray photoelectron spectroscopy depth profiling confirmed the presence of carbon throughout the annealed film. X-ray diffraction measurements also observed the formation of rutile TiO₂ diffraction peaks. The annealing of metalcone MLD films in argon is a general method to deposit metal oxide-carbon composite films. Conducting metal oxide-carbon composite films are desirable because many electrochemically important metal oxides have low electrical conductivities. The metal oxide-carbon composite films with graphitic carbon have much higher electrical conductivities that will enable their electrochemical application for Li ion batteries and pseudocapacitance supercapacitors.

3:00pm TF+EN-MoA4 In Situ Growth Study and Material Characterization of Plasma-Assisted Atomic Layer Deposition of Palladium, M.J. Weber, A.J.M. Mackus, M.A. Verheijen, N. Leick-Marius, A. Bol, W.M.M. Kessels, Eindhoven University of Technology, Netherlands

Palladium thin films are object of great interest in catalysis, as well as in hydrogen sensing, storage and generation. Noble metals such as Palladium are the most effective if deposited as ultrathin films on a large surface area. Atomic layer deposition (ALD) is considered to be the method of choice to grow ultrathin films on various substrates with demanding surface topologies. This contribution will present *in situ* and *ex situ* studies of Palladium films grown by plasma-assisted ALD. The Pd films were deposited on alumina at 100°C using Pd(hfac)₂ (hfac= hexafluoroacetylacetonate) as the precursor, and H₂ gas and H₂ plasma as reducing agents. *In situ* spectroscopic ellipsometry (SE) has been used to monitor the film growth and obtain detailed information about the optical properties of Palladium. The nucleation and subsequent island growth have been characterized by Transmission Electron Microscopy (TEM). X-Ray diffraction, X-ray photoelectron spectroscopy and Rutherford backscattering spectrometry have been carried out in order to characterize the grown films. The thermal ALD process only allowed for growth of Pd on a Pd or Pt seed layer, while the plasma-assisted ALD process also led to growth on an alumina surface. In both cases the steady-state growth rate was ~ 0.17 Å/cycle as determined by *in situ* SE. The observed selective growth on catalytic Pd or Pt seed layer of the thermal process holds promises for nanopatterning applications, whereas the plasma-assisted process can be used to deposit Pd nanoparticles and films at low-temperature on oxide substrates, which has considerable potential for catalysis and hydrogen sensor applications.

3:40pm TF+EN-MoA6 ALD-enabled Nanostructures for High Rate Li-ion Storage, X. Chen, H. Zhu, L. Hu, G.W. Rubloff, University of Maryland

A major challenge for Li-ion batteries is to achieve high rates (power) by overcoming the long charge/discharge time caused by low Li diffusivity in active storage materials. Nanostructured electrodes provide a potential solution by reducing the thickness of active storage layers, since the diffusion time is proportional to the square of diffusion length. Our strategy to improve the rate performance of Li-ion battery is to use atomic layer deposition (ALD) to grow thin active battery materials on highly conductive current collecting scaffolds with high surface area. The unprecedented conformality of ALD allows maximum utilization of high surface area, while the highly conductive scaffold facilitates easy electron transport and Li⁺ migration in electrolyte as also needed for high power. We report two embodiments of this heterogeneous nanostructure configuration, both with ALD V₂O₅ storage layers.

First, we used highly porous multiwall carbon nanotube (MWCNT) sponge as the scaffold. The V₂O₅-MWCNT-coaxial sponge achieves a stable high areal capacity as 816 μAh/cm² over voltage range 4.0-2.1 V at current density of 1.1 mA/cm² (i.e., 1C rate). This capacity is 450X that of a corresponding planar V₂O₅ thin film cathode. For the same voltage range but 50X higher current, the areal capacity of the V₂O₅-MWCNT sponge is 155 μAh/cm², giving a high power density of 21.7 mW/cm². The areal capacity increases further to 1284 μAh/cm², when cycled over a larger

voltage window (4.0-1.5 V), but this incurs deteriorated cycling performance as expected from the intrinsic properties of V_2O_5 .

Second, we employed well-ordered anodic aluminum oxide (AAO) templates to with ALD current collecting layers as a scaffold for the storage material. ALD TiN was first deposited into the AAO nanopores to form current collecting nanostructures, after which ALD V_2O_5 was deposited on TiN as the active Li storage medium, with both layer thicknesses precisely controlled and highly conformal. The resulting structures, with electrolyte filling the remaining pore volume, provide test structures to understand regimes where either Li^+ transport or electron transport can be rate-limiting.

4:00pm TF+EN-MoA7 Enhancement of the Heat Recovery Mechanism in Infrared Photovoltaic Devices Promoted by Thin Planar ALD Oxide Films, *A.J. Vincent-Johnson, H.S. Mann, Y. Schwab*, James Madison University, *A.E. Masters*, Custom Thermoelectrics Inc., *X. Hu, G. Scarel*, James Madison University

Infrared photovoltaic devices absorb infrared radiation and transform it into electricity through the heat recovery mechanism [1,2]. In thin planar oxide films, the mechanism is mediated by the excitation of radiative polaritons, as shown by investigations carried out immediately after beginning the exposition to infrared radiation [1,2]. Here we present the results of our investigation on the evolution of the heat recovery mechanism; and the electricity production over time through illumination by infrared radiation. We compare the results on systems including atomic layer deposited (ALD) Al_2O_3 , Al foil, and the bare thermoelectric power generator used for the detection of the heat recovery mechanism. We show that ALD oxide films promote the largest amount of electricity production under long term exposition to both polarized and non-polarized infrared radiation.

[1] A.J. Vincent-Johnson, K.A. Vasquez, J.E. Bridstrup, A.E. Masters, X. Hu, and G. Scarel, *Appl. Phys. Lett.* **99**, 131901 (2011).

[2] A.J. Vincent-Johnson, A.E. Masters, X. Hu, and G. Scarel. Submitted.

4:20pm TF+EN-MoA8 Ultra-thin TiO_2 Blocking Layer by Atomic Layer Deposition for Dye-Sensitized Solar Cells, *D.H. Kim, M. Woodroof, K.M. Lee, B. Kalanyan, G.N. Parsons*, North Carolina State University

In dye-sensitized solar cells (DSSCs), one of major recombination routes occurs at the interface of fluorine-doped tin oxide (FTO) glass and electrolyte solution. Typically, a thin and compact blocking layer (B/L) on the FTO-glass has been introduced to reduce electron loss before mesoporous TiO_2 layer integration. A variety of deposition methods have been tried and studied to make efficient B/L on the FTO-glass. Optimal thickness that suppresses the recombination on the interface of FTO glass and electrolyte, is typically 25 to 450 nm, depending on deposition methods and conditions. Compared to other methods, atomic layer deposition (ALD) with TiO_2 is not well established and investigated for blocking layers even though it is a valuable process in making pin-hole, crack-free, and dense TiO_2 films.

In this study, ALD TiO_2 was performed on FTO-glass with titanium isopropoxide and H_2O as precursors, producing B/L thickness from 5 to 100 nm. Cells without mesoporous titania but with ALD TiO_2 B/L were also made. We find the optimal thickness of the ALD TiO_2 blocking layer is 10 nm. This blocking layer thickness significantly reduces recombination, resulting in an average overall efficiency of 8.5%, compared to 7.1% for similar cells without the blocking layer present. We also find that a blocking layer of 4.3 nm effectively prevents electrons of FTO surface from recombining with I_3^- in the electrolyte. On the other hand, a thick ALD TiO_2 blocking layer in excess of 10 nm tended to reduce the overall efficiency because the thick ALD TiO_2 film increases the charge transfer resistance and hinders the electron transport to FTO-glass. This work contributes to understand effective blocking layer from TiO_2 ALD process for DSSCs and other high-performance electrical devices

Tuesday Morning, October 30, 2012

Actinides and Rare Earths Focus Topic

Room: 6 - Session AC+EN-TuM

Energetic Materials Issues for Nuclear Power: Fuels, Corrosion and Waste Disposal

Moderator: J.G. Tobin, Lawrence Livermore National Laboratory

8:00am AC+EN-TuM1 Novel Concepts for Enhanced Metallic Nuclear Fuel Performance, *J.R. Kennedy, R.D. Mariani, D.L. Porter, S.L. Hayes, H.J.M. Chichester*, Idaho National Laboratory, *A.E. Wright, Y.S. Kim, A.M. Yacout, G.L. Hofman*, Argonne National Laboratory, *R.P. Ombreg, D.J. Senior*, Pacific Northwest National Laboratory

INVITED

The Advanced Fuels Campaign of the Fuel Cycle Research and Development (FCRD) program of the Office of Nuclear Energy (DOE/NE) is charged with the mission to develop and qualify fuel forms that can be used 1) to close the nuclear fuel cycle, 2) to increase fuel performance in reactor, and 3) to be accident tolerant. In the first case, metallic fuels composed of (U,Pu,Np,Am)Zr alloys are being developed with the intention to transmute the transuranic isotopes in fast spectrum reactors. In the second case, increasing fuel performance, fuel forms are being developed that may, for example, allow higher levels of burnup in either fast spectrum or thermal spectrum reactors (lightwater reactors - LWR). In the final case, fuel forms that have an inherently higher level of tolerance to off-normal conditions are being developed in response to the Fukushima Daiichi accident. A number of innovative concepts will be presented with respect to the above including decreased fuel smear densities, annular fuel forms, cladding coatings or liners to prevent fuel-cladding chemical interactions, gas vented fuel pin designs, advanced fabrication methods such as fuel-clad co-extrusion, U-Mo based fuel alloys, and, of particular interest to this session's topical area, targeted fuel alloy additions into the actinide fuel composition that will sequester rare earth fission product migration to the fuel-cladding interface. Rare earth fission products have been implicated in enhancing detrimental fuel-cladding chemical interactions. These fuel development activities are a collaboration of Idaho National Laboratory with Argonne National Laboratory and with Pacific Northwest National Laboratory.

8:40am AC+EN-TuM3 Low Temperature Oxidation of Plutonium: A Mott-Cabrera Mechanism, *P. Roussel*, AWE, UK, *A.J. Nelson*, Lawrence Livermore National Laboratory

INVITED

X-ray photoelectron spectroscopy was used to study the oxidation of d-stabilized plutonium between 190K and 300K. The gas-solid reaction on this highly reactive surface depends on the surface energy, electronic structure and temperature along with radiological dissociation of the O₂ molecule. The initial oxidation of sputter cleaned Pu metal by O₂ forms Pu₂O₃ followed by formation of PuO₂ on the Pu₂O₃ surface. Angle-resolved measurements indicate that the PuO₂ layer thickness is limited to 1.2 nm after continued O₂ dosing at the lower temperatures. These results suggest the Mott-Cabrera mechanism of oxidation at low temperature where the rate limiting step is the diffusion of O⁻ anions through the oxide film to the oxide/Pu interface increasing only the thickness of the Pu₂O₃ layer.

This work was performed under the auspices of the U.S. Dept. of Energy by Lawrence Livermore National Laboratory under Contract DE-AC52-07NA27344.

9:40am AC+EN-TuM6 The Sputtering Yields of Depleted Uranium and Uranium Carbide Bombarded and Alloyed by Either 30 keV Gallium or 16 keV Cesium Ions, *W.J. Siekhaus, N.E. Teslich, P.K. Weber*, Lawrence Livermore National Laboratory

A sample of depleted uranium was abraded with 1200 grid SiC paper and subsequently polished with 3µm and 1µm diamond to a mirror finish. Areas 20µm x 20µm wide that included uranium carbide inclusions were ion-etched with 30 keV Gallium ions with a current of 2.8 nA, for up to 5 minutes. The depths of the "craters" thus generated were measured by electron microscopy and by profilometry and the ratio of the number of uranium atoms removed and the ion fluence was used to determine the sputtering yield for both uranium and uranium carbide.

We show the results in SEM images of sputtered areas and depth measurements on "craters" that include uranium carbide inclusions.

The same procedure was used to determine the sputtering yield of 16keV Cesium ions bombarding uranium. At their respective energies the depth of penetration of Gallium and Cesium (109Å and 50Å, respectively, as calculated by the TRIM[1] code) is much smaller than the crater depths.

The measured depth increases represent therefore the sputtering yields of the Uranium-Gallium and Uranium-Cesium alloys created by ion implantation, since sputtered atoms originate almost exclusively from the first atomic layers of the substrate[2]. Comparison of the measured sputtering yields with those of pure U using Matsunami's equation[3] demonstrates the effect of alloying on sputtering yield.

This work performed under the auspices of the U.S. Department of Energy by Lawrence Livermore National Laboratory under Contract DE-AC52-07NA27344.

[1] Sputtering by Particle Bombardment. Behrisch, R. Ed. Springer Verlag GmbH., 2007.

[2] Burnett, J.W. et al., Journal of Vac. Science & Technology A., **6**, 3, 2064-2068, 1988.

[3] Matsunami, N. et al., Atomic Data and Nuclear Data Tables, **31**, 1-80, 1984.

10:40am AC+EN-TuM9 Actinide Subsurface Chemistry in Waste Isolated Pilot Plant, Recent Development, *M. Borkowski, J.-F. Lucchini, M.K. Richmann, D.T. Reed*, Los Alamos National Laboratory

Waste Isolation Pilot Plant (WIPP) is designed to permanently dispose radioactive waste generated by the US defense program. Waste is placed in a salt bed 2150 feet below the ground level. During the regulatory time repository may be filled with brine and interaction of brine components with actinide is objective of the Actinide Chemistry Repository Science Program. One of the brine components is borate (up to ~160 mM), present in the brine by the dissolution of Borax mineral. Borate chemistry especially in basic media is still unknown and in this study the interesting borate speciation in the basic media is presented. Recently it was reported that neodymium, analog for trivalent actinides, is complexed by tetraborate ion with log K ~4 and that plutonium forms a stronger complex than that of neodymium. Also neptunium (V) forms complexes with borate and spectrophotometric evidence will be presented. Further investigations of borate chemistry and borate complexing properties are also discussed. Complexation power of different polyborate forms may be different. Some are able to form a covalent bond but other forms can only attract cation by a weak electrostatic interaction. Borate provides a wide range of pH buffering capacity from 6 to 12.

11:00am AC+EN-TuM10 XPS Study of Uranium Oxides with Various Precipitating Agents, *K.S. Holliday*, Lawrence Livermore National Laboratory, *J. Plaue*, University of Nevada, Las Vegas, *W.J. Siekhaus, A.J. Nelson*, Lawrence Livermore National Laboratory

X-ray photoemission spectroscopy (XPS) and Auger electron spectroscopy (AES) are powerful tools for materials characterization by determining chemical shifts in core level spectra. By combining XPS data with the X-ray excited Auger transitions one is able to have a two dimensional analysis based on both initial state effects and final state relaxation energies. Specifically, combining the chemical shift of the U NOV Auger lines with the chemical shift of the U 4f photoelectron lines defines the Auger parameter (difference in the binding energy of the photoelectron and Auger lines) and results in a reliable method for determining oxidation states independent of calibration. Here, XPS analysis of core-level excitation and X-ray excited Auger transitions were combined to determine the Auger parameter and produce chemical state (or Wagner) plots for various uranium and thorium compounds. In addition this method is combined with valence band spectra to characterize uranium oxides precipitated with different reagents. The calcination of these precipitates is followed at various temperatures in an effort to identify unique characteristics associated with the precipitating reagent.

Energy Frontiers Focus Topic

Room: 15 - Session EN+TF-TuM

Chalcogenide Solar Cells II

Moderator: H.W. Hillhouse, University of Washington

8:00am EN+TF-TuM1 Thin Film Solar Cells: Present Status and Future Prospects, *C.S. Ferekides*, University of South Florida

INVITED Thin film photovoltaics (TF PV) have long been viewed as a low cost option for solar electricity. Two very promising TF technologies are based on Cu(In,Ga)(S,Se)₂ (CIGS) and CdTe. The former has achieved the highest thin film laboratory efficiency (over 20%) and the latter is the lowest cost PV product on the market today (@ \$0.74/Watt). Recently, another thin

film technology based on the kesterites $\text{Cu}_2\text{ZnSn}(\text{S,Se})_4$ (CZTS) has received significant attention due to the abundance of the constituent elements, and small area cells have reached the 10% efficiency level. Despite all the successes achieved at the laboratory and manufacturing environments, TF technologies continue to face challenges some of which are unique to the specific material system. The presentation will provide an overview of thin film photovoltaics by comparing and contrasting the devices and technologies described above. Material, device and fabrication issues will be discussed with emphasis placed on some of the unique aspects of each technology: the need for sodium for CIGS and the importance of the co-evaporation process, the use of a chloride based treatment for CdTe and the challenge in forming back contacts to this device, and the loss of tin for CZTS.

8:40am EN+TF-TuM3 Materials and Process Options for Cu(InGa)Se₂ Thin Film Solar Cells, W.N. Shafarman, University of Delaware

INVITED

Two approaches to depositing thin films of $\text{Cu}(\text{InGa})\text{Se}_2$ and related alloys have been developed in the laboratory and are being implemented in large scale photovoltaics manufacturing. Precursor reaction processes use precursor films containing Cu, Ga, and In deposited by methods such as sputtering, printing, or electrodeposition chosen to provide potential manufacturing benefits. These are reacted in hydrogen selenide gas or elemental Se vapor to form the semiconductor absorber layer. Elemental co-evaporation is a single step process in which fluxes of all species are delivered to a hot substrate. Advantages and critical issues for these processing approaches will be compared. One of the materials options for $\text{Cu}(\text{InGa})\text{Se}_2$ -based absorber layers is the opportunity to alloy the film to increase its bandgap. This is desirable because the increased solar cell voltage can be advantageous for large scale module performance. Wider bandgap can be achieved by increasing the relative Ga content or by alloying with S, Al or Ag, but in all cases the cell efficiency decreases as the absorber layer bandgap increases beyond 1.2-1.3 eV. Alloying and composition control is generally straightforward using co-evaporation since these alloys form continuous solutions. With precursor reaction, however, chemical pathways to film formation are partly controlled by preferential reaction of Se with In instead of Ga, leading to aggregation of the Ga at the back of the film and, effectively, low bandgap. Multi-step reaction profiles can be used to control through-film composition in this case. For wide bandgap cells, recent results with the combination of Ag alloying and higher Ga content show promise. This includes improved optical properties, evidence of reduced structural disorder and improved performance with high open circuit voltage solar cells. The incorporation of Ag in both the precursor reaction and co-evaporation processes will be described.

9:20am EN+TF-TuM5 Why Are We Making CIGS Solar Cells from Cu-poor Material?, S. Siebentritt, University of Luxembourg

INVITED

CIGS can be prepared single phase in a large range of Cu-poor compositions. When prepared under Cu-excess a secondary phase of Cu selenide is formed which can be etched. Record solar cells as well as commercial modules are prepared from Cu-poor absorbers. However, the transport and recombination properties of material prepared under Cu-excess are superior. It has been known that the interface in cells with absorbers prepared under Cu-excess leads to increased recombination and thus limits the efficiency. The properties of the surface of CIGS absorbers prepared under Cu-excess is not well understood so far. We are preparing solar cells with absorbers grown under Cu-excess, where we make the surface Cu-poor to get the best from both worlds.

10:40am EN+TF-TuM9 Zn_xCd_{1-x}S Thin Films for Chalcopyrite Solar Cells Deposited through Batch and Continuous-Flow Chemical Bath Deposition, B.S. Tosun, C. Pettit, S.A. Campbell, E.S. Aydil, University of Minnesota

Copper indium gallium diselenide (CIGS) thin film solar cells already exceed 20% overall power conversion efficiencies. These high efficiencies are achieved using an n-type cadmium sulfide (CdS) buffer layer deposited on the p-type CIGS absorber using chemical bath deposition. CdS buffer layers are also used in the emerging copper zinc tin sulfide/selenide (CZTSSe) based solar cells. In some cases, it is desired to grade and widen the band gap of the buffer layer away from the CdS-absorber interface by alloying CdS with Zn to form $\text{Zn}_x\text{Cd}_{1-x}\text{S}$ films. In this work, we demonstrate the ability to manipulate Zn fraction, x , as a function of distance from the absorber-buffer layer interface and investigate the fundamental factors that govern the evolution of the film composition as a function of depth. Specifically, $\text{Zn}_x\text{Cd}_{1-x}\text{S}$ films were grown from solutions containing cadmium sulfate ammonium hydroxide, ethylenediaminetetraacetic acid disodium, zinc sulfate and thiourea in two different types of chemical baths, a traditional batch-type chemical bath and a continuous-flow chemical bath. By changing the initial concentrations of Zn and Cd sulfate in the batch-type chemical bath deposition, the entire range of overall compositions

ranging from primarily cubic ZnS to primarily hexagonal CdS could be deposited. Using Auger depth profiling, we show that a CdS rich layer forms at the film/substrate interface due to the faster reaction of Cd than Zn. The formation of Cd-rich $\text{Zn}_x\text{Cd}_{1-x}\text{S}$ layer at film/substrate interface followed by Zn-rich $\text{Zn}_x\text{Cd}_{1-x}\text{S}$ is favorable for solar cells. Thicker films with increasing band gap towards the surface can be deposited to increase the shunt resistance without sacrificing light transmission. In addition, we have developed a continuous chemical bath deposition system that allows deposition of $\text{Zn}_x\text{Cd}_{1-x}\text{S}$ films on 4-inch diameter substrates at temperatures as high as 80 °C without significant liquid temperature rise and without homogeneous nucleation and growth. Structure and composition of the films from the batch and continuous flow systems will be discussed and compared.

11:00am EN+TF-TuM10 Selenization of Cu-Ga-In Precursors for Synthesis of CIGS Absorbers: Equilibrium and Kinetic Studies, C. Muzzillo, R. Krishnan, University of Florida, W.K. Kim, Yeungnam University, Republic of Korea, E.A. Payzant, Oak Ridge National Laboratory, Y.H. Sohn, B. Yao, University of Central Florida, J. Shen, General Research Institute for Non-ferrous Metals of Beijing, China, C. Campbell, National Institute of Standards and Technology, T.J. Anderson, University of Florida

The emerging $\text{CuIn}_x\text{Ga}_{1-x}\text{Se}_2$ (CIGS) PV industry is primarily differentiated on the basis of the process used to synthesize the CIGS absorber. The most common approach is a 2-step metal deposition/selenization with differentiation occurring on the method of metal deposition and Se source for selenization. Typical champion cell efficiencies, however, are slightly lower for 2-step processes as compared to co-evaporation. This has been attributed to difficulty in creating a 'U-shaped' Ga profile, void formation near the back contact, and differences in diffusion/reaction rates of Ga and In during synthesis. Furthermore, cost pressures are driving reduction of the selenization time (up to 8 hr) and thinning of the absorber layer. A better understanding of the thermodynamic and kinetic elements of the precursor Cu-Ga-In metal system offers the potential to exploit faster pathways, assist in scale-up, and ensure robust processing of CIGS. This study includes a critical assessment of thermochemical and phase equilibria data of the Cu-Ga-In ternary metal system. The calculated phase diagram includes 11 binary intermetallic phases and no ternary compounds. Of particular interest are the 4 phases which exhibit ternary solubility: $\alpha\text{-Cu}$ (fcc), $\gamma\text{-Cu}_9(\text{Ga}_x\text{In}_{1-x})_4$ (sc), and $\eta\text{-Cu}_{16}(\text{In}_x\text{Ga}_{1-x})_9$ (hcp) are all modeled with a sublattice formalism, and an ionic two-sublattice liquid model is employed. Time-resolved *in situ* high temperature X-ray diffraction data for selenization of metallic precursors have also been collected. Reaction pathways and kinetics of temperature ramp and isothermal anneal experiments have both been examined, and kinetic rate parameters for the Avrami and parabolic growth models have been estimated from the data. As examples, MBE deposited bilayer metal precursor structures (e.g. CuIn/CuGa) and elemental stacked layers (e.g. $(\text{Cu}/\text{Ga}/\text{In})_n$) were selenized and the Ga distribution measured. The formation of $\text{Cu}_{11}\text{In}_9$, textured indium, and the solid solution $\gamma\text{-Cu}_9(\text{Ga}_x\text{In}_{1-x})_4$ were also evident as well as formation of CuGaSe_2 and CIGS simultaneously for selected structures. Rietveld refinement of temperature ramped selenized samples was performed to estimate the Ga distribution. TEM-EDS results confirm that the Ga distribution after selenization depended on the order of deposition of the precursor structure. The samples were further characterized by SEM (microstructure) and ICP (final composition). The activation energy for formation of CIGS was estimated from isothermal studies, and gave values of $76(\pm 14)$ for the $\text{glass}/\text{Mo}/\text{CuIn}/\text{CuGa}$ and $93(\pm 4)$ and $101(\pm 9)$ kJ/mole for the $\text{glass}/\text{Mo}/\text{CuGa}/\text{CuIn}$ precursor.

11:20am EN+TF-TuM11 Fabrication of $\text{CuIn}_{1-x}\text{Ga}_x\text{S}_2$ Thin-Film Solar Cells on Single Layer Molybdenum, A. Kaul, E. Schneller, N. Shiradkar, S. Pethe, N. Dhere, Florida Solar Energy Center, University of Central Florida

Considering the various advantages of a single pass operation, efforts have been made to develop a recipe for device quality single layer molybdenum back contact film that has good adhesion to the soda-lime glass substrate and at the same time lower resistivity values. $\text{CuIn}_{1-x}\text{Ga}_x\text{S}_2$ (CIGS2) thin film solar cells with reasonable efficiencies were successfully fabricated on the single layer molybdenum film without any signs of peeling or back contact degradation during processing. The molybdenum films were also subjected to various processing conditions of temperature and gas ambient and the subsequent results from these tests are also being presented.

11:40am EN+TF-TuM12 Investigation of Elemental Composition for $\text{Cu}(\text{InGa})\text{Se}_2$ Thin Films by Various Analytical Techniques, J.H. Lee, S.H. Kim, J.-H. Yoon, S.-O. Won, Y.H. Lee, Korea Institute of Science and Technology, Republic of Korea

$\text{Cu}(\text{InGa})\text{Se}_2$ (CIGS) solar cells are very promising films for use in photovoltaic devices, as they feature a high absorption coefficient and a

high conversion efficiency at a relatively low manufacturing cost. In order to develop an efficient CIGS solar cell, the relative ratio of the major elements should be determined quantitatively. In this study, a quantitative analysis of Cu(InGa)Se₂ (CIGS) was performed using an electron probe micro analysis (EPMA), x-ray fluorescence (XRF), inductively coupled plasma-optical emission spectrometry (ICP-OES), Auger electron spectroscopy (AES), time-of-flight secondary ion mass spectrometry (TOF-SIMS), and dynamic secondary ion mass spectrometry (dynamic SIMS). Surface roughness was observed by using atomic force microscopy (AFM) to identify the effect of the surface roughness on the reproducibility of the measurements. The relative sensitivity factors (RSF) of AES and SIMS were obtained by using ungraded CIGS thin film of known composition as the standard sample. Quantitative analysis of several CIGS samples were performed using the relative sensitivity factor (RSF) value calculated from the depth profile results of the standard film. The Cu/(In+Ga) ratio and the Ga/(In+Ga) ratio of SIMS results are relatively reproducible and close to those of the AES results. Overall, results from Composition of CIGS thin films by a variety of analytical methods were compared and their discrepancies were interpreted.

In Situ Microscopy and Spectroscopy Focus Topic

Room: 7 - Session IS+AS+SS+EN-TuM

In Situ Spectroscopic Studies of Catalysis and Gas-Solid Reactions

Moderator: B. Roldan Cuenya, University of Central Florida

8:00am **IS+AS+SS+EN-TuM1 Ambient Pressure XPS for Alternative Energy Research and Environmental Science, H. Bluhm**, Lawrence Berkeley National Laboratory **INVITED**

Solid/vapor and liquid/vapor interfaces play a major role in many processes in the environment and technology. Examples include heterogeneous catalysis, fuel cell technology, aerosol chemistry, and weathering of minerals and rocks. The measurement of these interfaces under realistic conditions of gas pressure and temperature has gained increasing importance over the last decades. Ambient pressure photoelectron spectroscopy (APXPS) is a promising technique for the investigation of liquid and solid surfaces in the presence of gases at pressures in the Torr range. The heart of an APXPS instrument is a differentially pumped electrostatic lens system that separates the sample, which is in a gas atmosphere at pressures of up to 5 Torr, from the electron spectrometer, which is kept in vacuum. This talk will discuss the history and basics of APXPS and show examples of the application of APXPS to the study of aqueous solution, metal oxides, soot, and fuel cell electrodes under reaction conditions.

8:40am **IS+AS+SS+EN-TuM3 In Situ Soft X-ray Photon-in/Photon-out Spectroscopy of Photo-electrochemical Reactions of Hematite in Water Splitting, J.H. Guo**, Lawrence Berkeley National Laboratory, *A. Braun*, Empa, Swiss Federal Laboratories for Materials Science and Technology, *K. Sivula*, Ecole Polytechnique Fédérale de Lausanne (EPFL), Switzerland, *D. Bora*, Lawrence Berkeley National Laboratory, *J.F. Zhu, L. Zhang*, University of Science and Technology of China, *M. Grätzel*, Ecole Polytechnique Fédérale de Lausanne (EPFL), Switzerland, *E.C. Constable*, University of Basel, Switzerland

Hydrogen fuel generation by solar water splitting in photoelectrochemical cells (PEC) is one of the first steps in artificial photosynthesis and an essential part of the holy grail of solar energy conversion. Iron oxide, literally "rust", is an interesting PEC photoanode material because of its affordability, good stability, good spectral match of the solar spectrum, and yet controversial because of its poor electronic structure. At present, iron oxide is taking center stage as prospective PEC anode material.

PEC electrodes are typically semiconducting metal oxides to form electron-hole pairs when struck by light. In the photoanodes such as hematite, the generated holes must diffuse to the iron oxide surface where they can oxidize water to oxygen. However, the electronic structure of iron oxide is such that the photogenerated holes tend to recombine and annihilate with the electrons before reaching the surface and performing the required chemical work on water splitting. Currently, researchers worldwide try to understand the peculiarities of iron oxide so as to invent strategies to improve this material.

The Advanced Light Source produces soft X-rays which are optimally suited to study the electronic structure of electrode materials and which can detect electron holes. But the holes needed for solar water splitting by iron oxide require an anodic electric bias plus the illumination. Moreover, the

holes are transitional and quite elusive. Also, soft X-rays cannot easily peek into a PEC cell. The unique design of the in-situ cell at the ALS has overcome the burden [1-3]. Recently the experiment has been performed for studying, under in-situ and operando conditions, the hole generation in a specifically designed photoelectrochemical cell. The oxygen valence band signature was recorded while tuning the PEC relevant parameters, two different types of holes in the valence band near the Fermi energy are discovered [4].

References:

[1] "X-ray Emission Spectroscopy of Hydrogen Bonding and Electronic Structure of Liquid Water", J.-H. Guo et al., *Phys. Rev. Lett.* **89**, 137402 (2002).

[2] "Electronic Structure of Cobalt Nanocrystals Suspended in Liquid", H. Liu et al., *Nano Lett.* **7**, 1919 (2007).

[3] "In situ soft X-ray absorption spectroscopy investigation of electrochemical corrosion of copper in aqueous NaHCO₃ solution", P. Jiang et al., *Electrochem. Comm.* **12**, 820 (2010).

[4] "Direct Observation of Two Electron Holes in a Hematite Photoanode during Photoelectrochemical Water Splitting", A. Braun et al., *J. Phys. Chem. C* **116**, 16870 (2012).

9:00am **IS+AS+SS+EN-TuM4 XANES and Ambient Pressure XPS (APXPS) Study: Investigations of the Local Structure and Final-State Effect in Partially Reduced SnOx Nanoislands on Pt(111), S. Axnanda, Z. Liu, B. Mao**, Lawrence Berkeley National Laboratory

Heterogeneous catalysts consisting of small particles having a high concentration of structural defects and under-coordinated sites make up the majority of the catalytic processes in industrial chemistry. One important recent example of interest shows that the interface-confined coordinatively unsaturated ferrous (CUF) sites together with the metal supports (FeO_x/Pt(111)) are active for dioxygen activation which causes the ensemble to be highly efficient for CO oxidation at low temperature under typical operating conditions of a proton-exchange membrane fuel cell.[1-2] In this work, we report another spectroscopic evidence to further confirm an enhanced reactivity at the edges of small catalyst particles. The system of interest is partially oxidized SnO_x (Sn²⁺) nanoislands supported on Pt(111) for ethanol oxidation reaction (EOR), an electrode material in a direct alcohol fuel cell (DAFC). Our findings suggested that SnO_x/Pt(111) inverse catalysts have improved activity for EOR in acidic media as compared to a bare Pt(111) surface.[3] We also found that the most active surface had a small coverage of SnO_x (0.3- 0.4 ML). Water activation at low potentials is currently attributed to be the promoting effect of SnO_x nanoparticles, since this enhances the oxidation of chemisorbed CO formed on Pt sites during the EOR.[4] To better understand this increased activity, we performed study with the goal to indicate the actual state of Sn in SnO_x nanoislands before and after the SnO_x /Pt(111) is used in EOR showing the increased activity: purely oxide Sn or mixed Sn alloy and Sn oxide, using a combination of APXPS and XANES techniques. BE shift in the XPS core-line spectra of Sn and O, soft X-ray XANES spectra (Sn M4,5-edge, O K-edge) will be collected and compared to the corresponding XPS spectra (Sn 3d, O 1s) to explain the actual state of Sn before and after the SnO_x/Pt(111) is used in the EOR.

1. Fu, Q., et al., Interface-Confined Ferrous Centers for Catalytic Oxidation. *Science*, 2010. 328: p. 1141.

2. Deng, X., et al., Reactivity Differences of Nanocrystals and Continuous Films of α-Fe₂O₃ on Au(111) Studied with In Situ X-ray Photoelectron Spectroscopy. *J. Phys. Chem. C*, 2010. 114: p. 22619.

3. Zhou, W.P., et al., Enhancement in Ethanol Electro-Oxidation by SnOx Nanoislands Grown on Pt(111): Effect of Metal Oxide-Metal Interface Sites. *Journal of Physical Chemistry C*, 2011. 115: p. 16247.

4. Axnanda, S., W.P. Zhou, and M.G. White, CO Oxidation on Nanostructured SnOx/Pt(111) surfaces: Unique Properties of Reduced SnOx. *Phys. Chem. Chem. Phys.*, 2012. Submitted.

9:20am **IS+AS+SS+EN-TuM5 Epitaxial Strontium Substituted Lanthanum Cobalt Oxides Investigated using In Situ Ambient Pressure X-ray Photoelectron Spectroscopy Near Operating Conditions Under Applied Potentials, E. Crumlin, E. Mutoro**, Massachusetts Institute of Tech., *Z. Liu*, Lawrence Berkeley National Lab, *M.D. Biegalski*, Oak Ridge National Lab, *W.T. Hong*, Massachusetts Institute of Tech., *H.M. Christen*, Oak Ridge National Lab, *H. Bluhm*, Lawrence Berkeley National Lab, *Y. Shao-Horn*, Massachusetts Institute of Tech.

Operating conditions for solid oxide fuel cell (SOFC) are typically at high temperatures (~500 – 1000 °C) and ambient pressures (~1 atm). We have to understand how the physical and chemical properties of SOFC materials, particularly the cathode which is responsible for a majority of the fuel cells area specific resistance, change under operating conditions. Such data can

provide insights into the mechanism of the oxygen reduction reaction (ORR) which may lead to material development strategies to improve the cathode performance. However, these operating conditions are far away from conventional characterization techniques that are often applied at room temperature or even in ultrahigh vacuum (UHV). Our recent work using *in situ* ambient pressure X-ray photoelectron spectroscopy (APXPS) has shown that (001) oriented epitaxial films of $\text{La}_{0.8}\text{Sr}_{0.2}\text{CoO}_{3-\delta}$ (LSC_{113}) can exhibit Sr enrichment in the near-surface perovskite lattice structure ("lattice") as temperatures were raised from 220 °C to 520 °C in a $p(\text{O}_2)$ of 1×10^{-3} atm. In contrast under the same conditions, a bulk pellet of LSC demonstrated no changes in Sr content within the "lattice" region. The Sr enrichment is believed to play a key role in the observed one order of magnitude enhancement in ORR activity (as measured by the surface exchange coefficient, k^0) of the (001) epitaxial films relative to bulk LSC_{113} . In this work, we continue the previous investigations of the chemical properties of (001) epitaxial LSC_{113} as a function of temperature cycling between 220 °C and 520 °C at a $p(\text{O}_2)$ of 1×10^{-3} atm. Additionally, the comparison of LSC_{113} , $(\text{La}_{0.5}\text{Sr}_{0.5})_2\text{CoO}_{4-\delta}$ (LSC_{214}), and LSC_{214} -decorated LSC_{113} ($\text{LSC}_{113/214}$) at $p(\text{O}_2)$ of 1×10^{-3} atm as a function of temperature and under applied cathodic potentials will be presented in order to provide insights into the physical origin responsible for the observed ~3 orders of magnitude ORR activity enhancement of $\text{LSC}_{113/214}$ relative to (001) epitaxial LSC_{113} .

9:40am IS+AS+SS+EN-TuM6 Probing Nitrogen and Metal Speciation in Non-Platinum Electrocatalysts by Ambient Pressure X-ray Photoelectron Spectroscopies and DFT Calculations. *K. Artyushkova, B. Halevi, A. Serov, The University of New Mexico, B. Kiefer, New Mexico State University, P. Atanassov, The University of New Mexico*

X-ray Photoelectron Spectroscopy (XPS) has been the main surface analysis method for determining the chemical environment and coordination of nitrogen and transition metal (TM) in the non-precious group metal oxygen reduction reaction (ORR) electrocatalysts. Even though there is an agreement that Me-N_x serve as one of the possible active sites in ORR, the distribution of Me-N₂ vs Me-N₄ centers and their specific role still remains unresolved. XPS which heavily relies on use of reference spectra in accurate identification of species cannot address this issue directly as no reference compounds with Me-N₂ moieties are available. The assignment of peaks and nitrogen coordination is not straightforward due to overlapping peaks that appear within a narrow energy window of 2.5-eV and the full width half maximum (fwhm) for individual species is on the order of 1.2-1.5-eV. Being able to calculate binding energy shifts based on molecular structure can be very important tool for assisting in this task. We will report on BE shifts that have been calculated at the DFT level and their comparison to experimentally obtained values for metal-less and metal-containing porphyrins. Information obtained from the DFT calculations will be used as input into curve-fitting XPS spectra for various model N-Me containing compounds as well as from electrocatalyst. We will compare chemical information derived from conventional XPS as well as *in-situ* ambient-pressure XPS using variable energy synchrotron source.

10:40am IS+AS+SS+EN-TuM9 Resolving Growth of Palladium Nanocatalysts Using *In Situ* FT-IR, XAS and PDF under Practical Atomic Layer Deposition Conditions. *Y. Lei, J. Lu, B. Liu, H. Zhao, J. Greeley, P. Chupas, J. Miller, J.W. Elam, Argonne National Laboratory*

Nanostructured Pd catalysts prepared by ALD have been demonstrated highly active for alkene hydrogenation, methanol decomposition reaction, and alcohol oxidation for fuel cells. Development of supported Pd nanoparticles with controlled size/structure relies on the fundamental understanding of the two half reactions with high precision during Pd ALD. However, evolution of Pd surface species, as well as the subsequent nucleation and growth of palladium nanoparticles during Pd ALD is still not clear.

Mechanism of assembly of highly dispersed Pd nanoparticles on TiO₂ surfaces from palladium hexafluoroacetylacetonate ($\text{Pd}(\text{hfac})_2$) were investigated by means of *in situ* Infrared (IR) spectroscopy, X-ray absorption spectroscopy (XAS) and pair distribution function (PDF) under practical atomic layer deposition condition simultaneously. Density function theory simulation was applied to understanding the reaction mechanism. On chlorine-containing TiO₂ surface, $\text{Pd}(\text{hfac})_2$ primarily adsorbed on TiO₂ surface as $\text{Pd}(\text{hfac})\text{Cl}_2^*$ species, confirmed by both XAS and DFT calculations. *In-situ* FT-IR results reveal that deligation of $\text{Pd}(\text{hfac})\text{Cl}_2^*$ species began at as low as 100 °C with the present of formalin. Further on, *in-situ* XAS results indicated that cleavage of Pd-O bond occurred first, followed by cleavage of Pd-Cl bond. Sequentially, Pd atoms started to gain mobility and agglomerate to small nanoparticles. The hfac ligands spilled to TiO₂ surface as site blockers for ALD. The surface poisons were eventually removed at 225 °C. Nano-size palladium-carbon phase was also found after long exposure of formalin. Atomic resolution aberration-corrected STEM image showed one nanometer size crystalline

Pd particles were synthesized using ALD. The catalytic performance of these Pd nanocatalysts was further demonstrated in several applications.

In summary, dynamic growth of Pd nanocatalysts was obtained utilizing a combination of *in-situ* techniques.

11:00am IS+AS+SS+EN-TuM10 Catalyst Characterization using *In Situ* XAS and XPS: From Nanoparticles Synthesis to Evolution of Structural/Electronic Properties under Reaction Conditions. *A.M. Karim, Pacific Northwest National Laboratory* **INVITED**

Catalysts are used to facilitate the important industrial chemical processes, leading to products valued in the trillions of dollars annually just in the U.S and most catalysts used in large-scale processes are solids. To maximize the number of sites available for reaction, catalysts are typically comprised of metallic/metal oxide nanoparticles dispersed on high surface area supports. The activity and selectivity of metallic nanoparticles strongly depend on their size, shape and composition [1-8]. In order to design more active and selective catalysts, it is essential to identify the catalytically active sites and understanding their geometric and electronic properties which requires: (1) synthesis of well-defined catalyst structures and (2) the ability to correlate individual reaction pathway(s) with the type of active site(s) available on the catalyst surface under reaction conditions.

This talk is going to cover our work on *in situ* characterization of nanoparticles from the synthesis stage to the evolution of their structural/electronic properties under reaction conditions using X-ray photoelectron and X-ray absorption spectroscopies. The catalyst systems that will be covered include:

Pd nanoparticles synthesis in solution: Understanding the nucleation and growth mechanisms.

Supported Pt, PtRe and PtNi nanoparticles under aqueous phase reaction condition: Correlating the structural and electronic properties with the catalytic activity and selectivity.

References:

- [1] Boudart, M. *Adv. Catal.* 1969, 20, 153.
- [2] Boudart, M. *Journal of Molecular Catalysis* 1985, 30, 27.
- [3] Ichikawa, S.; Poppa, H.; Boudart, M. *Journal of Catalysis* 1985, 91, 1.
- [4] Somorjai, G. A.; Carrazza, J. *Industrial & Engineering Chemistry Fundamentals* 1986, 25, 63 [5] Liu, Z.; Hu, J. E.; Wang, Q.; Gaskell, K.; Frenkel, A. I.; Jackson, G. S.; Eichhorn, B. *Journal of the American Chemical Society* 2009, 131, 6924.
- [6] Alayoglu, S.; Nilekar, A. U.; Mavrikakis, M.; Eichhorn, B. *Nature Materials* 2008, 7, 333.
- [7] Sinfelt, J. H. *Journal of Catalysis* 1973, 29, 308.
- [8] Sinfelt, J. H. *Accounts of Chemical Research* 1977, 10, 15.

11:40am IS+AS+SS+EN-TuM12 *In Situ* Study of the Oxidation of CO over Ir(111). *J. Knudsen, Lund University, Sweden, Y. Monya, Keio University, Japan, J. Schnadt, M.A. Arman, E. Grånäs, Lund University, Sweden, H. Kondoh, Keio University, Japan, J.N. Andersen, Lund University, Sweden*

The platinum group metals are known to be excellent catalysts for the oxidation of carbon monoxide, and the reaction mechanisms over the surfaces of these metals have been studied for a long time. Nevertheless, only during recent years a new picture has emerged which suggests that the catalytically active phase often is formed first under reaction conditions – which implies realistic pressures rather than ultrahigh vacuum (UHV) – and that it is different from the adsorption structures known from UHV experiments. In the case of the Pt(111) surface a very oxygen-rich chemisorbed phase has been suggested as the catalytically active phase [1], whereas a surface oxide has been suggested for the Ru(0001) surface [2]. Thus, for each different surface different phases and mechanisms might be at play, and, moreover, the phase might depend quite strongly on the conditions (pressure and temperature) used.

With this in mind we have studied the CO oxidation reaction over the Ir(111) surface and the related adsorption systems of CO and oxygen on Ir(111) using a combination of *in situ* Ambient pressure x-ray photoelectron spectroscopy (APXPS) – carried out at the new APXPS instrument at the Swedish synchrotron radiation facility MAX IV Laboratory – and *ex situ* Scanning tunnelling microscopy (STM) and x-ray photoelectron spectroscopy (XPS) measurements performed in UHV.

A recent surface x-ray diffraction study reports different oxygen phases for the Ir(111) surface at oxygen pressures from 10^{-6} to 100 mbar – chemisorbed oxygen, a trilayer, a multilayer oxide, and a bulklike oxide [3]. Concentrating on pressures at around 1 mbar, we find a variety of oxygen-rich structures. The corresponding CO adsorption phase formed at 1 mbar

CO pressure is an assembly of separated CO₁₆ clusters with the CO molecules sitting in on-top sites [4].

The reactivity at 1 mbar total pressure (O₂:CO ratio 9:1) and at different temperatures was studied by APXPS and simultaneous monitoring of the gas composition. We find that the phase with the highest activity for the oxidation of CO is a surface phase which contains both CO and oxygen. By comparing with the measured adsorption structures of oxygen we find that the oxygen structure is quite similar to the p(2x1)-O structure formed on Ir(111) under UHV conditions. This contrasts with what is found for other platinum group metals such as the Pt(111) surface [2], for which CO oxidation is favoured over oxygen rich phases.

[1] A. L. Gerrard, J. F. Weaver, *J. Chem. Phys.* **123** (2005) 224703.

[2] H. Over et al., *Science* **287** (2000) 1474.

[3] Y. B. He et al., *J. Phys. Chem.* **112** (2008) 11946.

[4] L.-M. Yang, S.-L. Yau, *J. Phys. Chem. B.* **104** (2000) 1769.

Nanometer-scale Science and Technology

Room: 12 - Session NS+EN-TuM

One-Dimensional Nanowires and Nanotubes

Moderator: M.C. Hersam, Northwestern University

8:00am **NS+EN-TuM1 Direct Observation of Selective Band Engineering of an Isolated Subnanometer Wire.** *I. Song, D.-H. Oh, C.-Y. Park, J.R. Ahn*, Sungkyunkwan University, Republic of Korea

Band engineering has been achieved mainly by substituting an atom of a pristine nanomaterial with an extra atom. At the ultimate nanometer scale, subnanometer scale, a nanowire becomes closer to an ideal 1D system and the band engineering by the atomic substitution enters a different regime. The strong disorder by the atomic substitution tends to break a pristine 1D system. In the band engineering of the subnanometer wire (hereafter subnanowire), we need to find a way of circumventing the dilemma of doping and disorder. There is another challenging problem to find out a conclusive experimental proof that its electronic band structure is changed within a single isolated subnanowire. A unique experimental way is to measure its electronic band structure by angle-resolved photoemission spectroscopy (ARPES). Because a photon beam in ARPES measurement cannot be focused down to subnanometer scale, a single subnanowire cannot be used and rather subnanowires have to be aligned along a specific direction on a surface. A fundamental requirement to resolve the puzzling problem is that subnanowires have to be aligned by a self-assembly method. In comparison to the atomic structure, its electronic structure is required to be decoupled to observe a 1D electronic structure change of a single isolated subnanowire by a dopant. In this study, self-assembled subnanowires on a stepped surface, Au-induced subnanowires on a Si(553) surface, were chosen. A Si(553) surface, which is one of stepped Si(111) surfaces, has an appropriate terrace width to assemble subnanowires along its step edge direction and its step edge structure can decouple subnanowires electronically. Three different metallic subnanowires exist on its single terrace and each metallic wire has only a single metallic band. After extra Au atoms were adsorbed on the self-assembled subnanowires at room temperature, only one of metallic bands moved rigidly to a higher binding energy without a change in other metallic bands, which was directly observed by ARPES measurement. Here we note that if the three metallic subnanowires are coupled electronically to each other, all of the three metallic bands have to shift rigidly. This experimentally proves that only one of self-assembled multiple metallic wires can be controlled electronically by a dopant and the electronic structure of an isolated wire can be controlled down to a subnanometer scale.

8:20am **NS+EN-TuM2 Growth of ZnO Nanowires on Retroreflector Microspheres and the Resulting Plasmonic Light Channeling Properties.** *S.M. Prokes, O.J. Gembocki, E. Cleveland*, Naval Research Laboratory

We investigated the growth of ZnO nanowires on retroreflectors in order to potentially enhance the optical response of these composite structures. Results show that the growth of ZnO aligned NW arrays can be achieved on the retroreflectors, but it occurs far away from the Zn vapor source compared to the standard ZnO nanowire growth on a flat Si substrate. In the case of the ZnO nanowires on flat Si, the nanowires that formed in nearly aligned arrays were short and significantly thicker, suggesting that the growth occurred both longitudinally and laterally in this process. For the NW growth on the curved retroreflectors, as the distance from the vapor source increased, the NW density increased and for the substrates farthest from the source, growth of nearly aligned NW arrays was noted. Initially, the ZnO growth on the retroreflectors resulted in a high rate of deposition of

a polycrystalline ZnO film and as the amount of Zn vapor decreased, the vapor-solid (VS) nucleation of random NWs began, and aligned nanowire arrays only formed where the vapor supply was the lowest. The fact that it is more difficult to nucleate and grow ZnO NW arrays on the retroreflectors is likely due to the surface roughness, as well as the crystal structure of the retroreflector bead.

Once nearly aligned arrays of ZnO nanowires on the retroreflectors were formed, we investigated their optical properties by forming ZnO/Ag composite NW structures and using a self-assembled monolayer of benzenethiol to measure a surface enhanced Raman (SERS) response. The ZnO/Ag NW composites were formed by atomic layer deposition (ALD) of Ag, and the surface enhanced Raman (SERS) response was measured and compared to nanowire composites deposited on a flat Si substrate. Results indicated that the SERS response was 29 times greater in the case of the ZnO/Ag NW aligned arrays grown on the retroreflectors. Since one would only expect a factor of 4 enhancement due to the light reflecting properties of the retroreflector, it is suggested that the enhancement in the SERS signal is due to light channeling by the nearly aligned nanowire arrays as a result of plasmonic effects. These results have been modeled using COMSOL electric field simulations, which support the light channeling concept.

8:40am **NS+EN-TuM3 Optical and Electrical Characteristics of Al-doped ZnO Nanowires Grown by Chemical Vapor Deposition.** *G. Shen, N. Dawahre, J. Waters, J. Krafcik, S.M. Kim, P. Kung*, University of Alabama, Tuscaloosa

Zinc oxide (ZnO) is a well-known major semiconductor material for optoelectronic devices due to its wide bandgap (~3.3 eV) and large exciton binding energy (~60 meV). One dimensional ZnO nanowires have been successfully synthesized by various techniques ranging from as simple as thermal chemical vapor deposition and solution growth, to more complex such as metal organic chemical vapor deposition, with good structural, optical and electrical properties. These are promising as an alternative to indium tin oxide as a more abundant, lower cost transparent window for a number of optoelectronic devices, including photovoltaics, while at the same time offering potentially more efficient electron charge transport. ZnO is also capable of harvesting the short wavelength spectral bands more efficiently.

In this work, we present the growth, doping and characterization of vertical well-aligned ZnO nanowire arrays. The wires are synthesized without metal catalyst by thermal chemical vapor deposition on basal plane sapphire substrates following the carbo-thermal reduction of zinc oxide powder. Control of the aluminum doping is accomplished by adjusting the ratio of Al and ZnO in the source material. The effects of doping and synthesis conditions on the nanowire optical and electrical properties are investigated through a number of techniques. The concentration of Al in the crystal is determined by energy dispersive spectroscopy, while atom probe tomography enables us to investigate the distribution of aluminum within the ZnO matrix. Micro-Raman spectroscopy and micro-photoluminescence, including their temperature dependence, are used to probe the vibrational and optical properties of the nanowires as a function of doping. It is observed that a defect related radiative green emission in ZnO is significantly reduced after Al doping. The electrical characteristics of undoped and doped nanowires are compared by leading electrical nano-connections to individual nanowires, which show a more than 1 order of magnitude decrease in the resistivity after doping down to 1 ohm.cm.

9:00am **NS+EN-TuM4 Rational Defect Engineering in Silicon Nanowires.** *N. Shin, M. Filler*, Georgia Institute of Technology

Group IV nanowires synthesized via the vapor-liquid-solid (VLS) technique do not frequently exhibit planar defects and/or polytypic domains. Even in group III-V nanowires, where these structural motifs are common, rational control of their position remains challenging. Since defect energetics are similar in both systems, the observed structural differences are especially striking and indicate that the underlying physical phenomena are not sufficiently well understood. Here, we demonstrate how user-defined changes in surface chemistry near the triple-phase line can introduce twin planes and stacking faults during the growth of <111> oriented Si nanowires. More specifically, the addition of atomic hydrogen during Si nanowire growth enables {111} defects that begin at the <112> sidewall and continue to propagate across the nanowire even after the flux of atomic hydrogen ceases. Real-time *in-situ* infrared spectroscopy measurements reveal that covalent Si-H bonds are responsible for the defect initiation process and a simple mechanistic model will be presented to explain these results. Our findings are an important step toward a fundamental understanding of the chemistry that governs semiconductor nanowire synthesis and suggest a new route to engineer the properties of Si.

9:20am **NS+EN-TuM5 Ultrafast Carrier Dynamics of Si Nanowires Grown by LPCVD**, A. Seyhan, Tokyo Institute of Technology and Nigde University, Turkey Japan, T. Ishikawa, S. Koshihara, M. Simanullang, K. Usami, S. Oda, Tokyo Institute of Technology, Japan

This paper report the ultrafast carrier dynamics in silicon nanowires (NWs) grown by vapour-liquid-solid (VLS) mechanism in the low pressure chemical vapour deposition (CVD) reactor at 425°C. The femtosecond transient absorption measurements were studied by tuning probe wavelength in visible range to investigate the effect of pump and probe beam polarization, NW diameter, and pump fluence on the carrier dynamics. The fast carrier relaxation with lifetime of several picosecond in Si NWs can be attributed to surface trap states. This study has important implications in the understanding of ultrafast carrier dynamics of Si NWs.

9:40am **NS+EN-TuM6 Selective Deposition of Germanium Nanowire Segments via a Hybrid Oxide-Stabilized/Vapor-Liquid-Solid Growth Method**, C.J. Hawley, T. McGuckin, J.E. Spanier, Drexel University

The introduction low levels of oxygen during the vapor-liquid-solid growth (VLS) of germanium nanowires causes an oxide sheath to form at the catalyst/nanowire/vapor interface for the extent that the growth persists. This results in extremely high aspect ratio nanowires due to the removal of homoepitaxial deposition and the finite energy required for heterogeneous nucleation of germanium on its oxide. Furthermore, with the removal of oxygen, the catalyzed oxide sheath terminates and conventional growth with finite sidewall deposition dominates subsequent growth. The successful transition between the aforementioned oxide-stabilized and conventional VLS regimes can be deliberately manipulated to grow finite conical nanowires segments with discontinuous changes in diameter.

Work was supported by the U.S. Army Research Office (W911NF-08-1-0067).

10:40am **NS+EN-TuM9 Electronics and Opto-Electronics with Semiconducting Carbon Nanotube Arrays**, M.B. Steiner, IBM TJ Watson Research Center **INVITED**

While field-effect transistors made of single semiconducting carbon nanotubes have excellent electrical DC characteristics, the measurement of their AC characteristics is complicated and their output current is not sufficient for technological applications. Utilizing an array of semiconducting carbon nanotubes could resolve these problems. However, there are issues associated with the separation of carbon nanotubes with respect to the electronic type, their aligned assembly in high densities, as well as the scaling of device dimensions.

In this talk, I will present recent advancements with respect to the solution-assisted, electric-field driven assembly of highly separated (>99%) semiconducting carbon nanotubes into regular arrays on a device platform with embedded electrodes. The planar device platform is based on manufacturing processes known to the semiconductor industry and provides a basis for future enhancements of the carbon nanotube assembly and the scaling of critical device dimensions. Electrical transport measurements (AC and DC) of assembled carbon nanotube array transistors reveal intrinsic current gain cut-off frequencies of 150GHz and electrical current saturation behavior at a gate length of 100nm. The requirements for future applications of carbon nanotube array transistors in high-frequency electronics will be discussed.

In the second part of my talk, I will discuss high-resolution optical mapping of the internal electrostatic potential landscape of carbon nanotube array devices. Laser-excited photocurrent measurements provide insights into the physical principles of device operation and reveal performance-limiting local heterogeneities that cannot be detected with the electron microscope. The experiments deliver photocurrent images from the underside of nanotube-metal contacts and enable the direct measurement of the charge carrier transfer length at a nanotube-metal interface. Moreover, the external control of the electrostatic potential profile in carbon nanotube array devices by means of local metal electrodes is demonstrated. The results are important for the design and optimization of optoelectronic devices based on carbon nanotube arrays, such as polarized light detectors and emitters.

11:20am **NS+EN-TuM11 Observation of the Impact of Pseudospin Conservation in Carbon Nanotubes**, R. Tsuchikawa, University of Central Florida, Z. Zhang, X. Guo, J.C. Hone, Columbia University, M. Ishigami, University of Central Florida

It has long been accepted that pseudospin conservation in metallic carbon nanotubes prevents backscattering by long-range potentials such as Coulomb potential. This unique property is expected to be valid only for metallic nanotubes [1]. Here, we have directly tested this yet untested theoretical result by measuring the impact of charged impurities on transport property of chiral-angle known carbon nanotubes. Single-walled carbon nanotubes (SWNTs) were grown to as long as a few hundred microns with minimal number of defects, followed by Rayleigh scattering

spectroscopy to identify the chirality. In order to minimize the extrinsic impurities, electron transport measurements were performed in an ultra high vacuum environment after cleaning nanotubes down to atomic scale. Furthermore, we employed length-dependent resistance measurements to eliminate the impact of the metal-nanotube contact. Finally, transport property was measured at increasing coverage of cesium to determine the impact of charged impurities. Our results show chiral angle dependence of the impact of cesium and enable us to directly test the properties of pseudospin in carbon nanotubes.

1. P.L. McEuen, M. Bockrath, D.H. Cobden, Y.-G. Yoon, and S.G. Louie, Disorder, Pseudospin, and Backscattering in Carbon Nanotubes, Physical Review Letters, 83, 5098 (1999)

11:40am **NS+EN-TuM12 Properties and Application of Electronically Monodisperse Carbon Nanomaterials Functionalized with Nonionic Block Copolymers**, J.-W.T. Seo, Northwestern University

Carbon nanomaterials, including carbon nanotubes and graphene, have garnered significant attention from the research community in recent years. In an effort to refine their properties and better integrate them into device structures, chemical functionalization methods have been employed including aqueous dispersion with ionic surfactants, proteins, and DNA. While these strategies have proven effective for tuning the optical properties of carbon nanomaterials, the residual charge from the ionic dispersants complicate efforts to utilize them in electronic and/or electrochemical technologies. In contrast, we demonstrate here that nonionic, amphiphilic block copolymers (e.g., Pluronics and Tetronics) are effective surfactants for grapheneⁱ and carbon nanotubes,ⁱⁱ thus yielding chemically and electronically monodisperse samples without spurious charged impurities.

Pluronics and Tetronics are biocompatible block copolymers that are composed of hydrophilic polyethylene and hydrophobic polypropylene oxide domains. By tuning the relative length of these domains, their dispersion efficiency for carbon nanomaterials can be tailored. For example, Pluronics possess the ability to sort semiconducting single-walled carbon nanotubes (SWCNTs) via density gradient ultracentrifugation with shorter hydrophobic domains resulting in higher purity levels. Furthermore, Pluronic F68 has shown pH-sensitive, switchable sorting affinity towards both metallic and semiconducting SWCNTs, thus providing a novel route for the production of electronically monodisperse SWCNTs that are encapsulated with biocompatible, nonionic speciesⁱⁱⁱ. In addition to biomedical applications, the nonionic character of these block copolymers yields more reliable and enhanced performance of SWCNT-based electronic and electrochemical devices such as thin film transistors and lithium ion batteries.

Tuesday Afternoon, October 30, 2012

Energy Frontiers Focus Topic

Room: 15 - Session EN+TF-TuA

Thin Film, Heterostructured, and Organic Solar Cells

Moderator: M. Filler, Georgia Institute of Technology

2:00pm EN+TF-TuA1 **Photonic Materials for Solar Energy Conversion at the Thermodynamic Limit**, H.A. Atwater, California Institute of Technology **INVITED**

Ever since serious scientific thinking went into improving the efficiency of photovoltaic energy conversion more than 50 years ago, thermodynamics has been used to assess the limits to performance, guiding advances in materials science and photovoltaic technology. Photovoltaics have advanced considerably, resulting in single-junction solar cells with a record efficiency of 28.8% and multi-junction cells with an efficiency of 43.5%. As impressive as these advances are, these record efficiencies and also today's manufactured cell efficiencies in the 10–18% range fall far short of the thermodynamic limits. Why such a large gap? There is no fundamental reason, and in this talk, I will discuss methods for systematically addressing the thermodynamic efficiency losses in current photovoltaics that can enable a next phase of photovoltaic science and engineering – ultrahigh efficiency photovoltaics. This development takes advantage of recent advances in the control of light at the nanometer and micron length scales, coupled with emerging materials fabrication approaches, and will allow the development of solar cells with efficiencies in the 50–70% range.

Web resources:

<http://www.lmi.caltech.edu/>

<http://daedalus.caltech.edu/>

2:40pm EN+TF-TuA3 **Semiconducting Carbon Nanotubes as Polymer-Like Near-Infrared Bandgap Photoabsorbers**, M.S. Arnold, D.J. Bindl, M.-Y. Wu, M.J. Shea, University of Wisconsin Madison **INVITED**

We are pioneering the exploration of semiconducting carbon nanotubes as the light-absorbing components of polymer-inspired solar cells and photodetectors.[1-2] Carbon nanotubes are conjugated polymer-like materials with built-in long-range crystallinity that gives rise to exceptional charge and energy transport characteristics, strong light absorption tunable throughout the visible and near-infrared spectra, and outstanding stability in air. We have discovered how to efficiently harvest photogenerated charges and excitons from optically excited nanotubes by pairing them in donor / acceptor heterojunctions with more electronegative electron accepting semiconductors. In particular, semiconducting nanotubes form a type-II heterojunction with C60 fullerenes and C60 derivatives with energy offsets sufficient to drive electron transfer from the optically excited nanotubes to C60, with an internal quantum efficiency (QE) for exciton dissociation and charge transfer > 75%, for nanotubes of diameter < 1 nm and gaps > 1 eV. Thus, we have identified the nanotube / C60 materials pair as a promising basis for future nanotube-based light harvesting devices.

In order to further guide the implementation of nanotubes in devices, we have also characterized exciton transport in nanotube films and shown that excitons can migrate in films by two mechanisms: (i) over short distances of ~ 5 nm via slow inter-nanotube diffusion and (ii) potentially over much longer distances via rapid intra-nanotube diffusion. As a proof-of-principal, we have fabricated both bilayer and blended nanotube / C60 heterojunction devices, which are analogous to polymer solar cells with nanotubes taking on the role of the semiconducting “polymer”. Thus far, we have realized a peak external QE > 20% across 1000 – 1365 nm and a monochromatic power conversion efficiency of 7% at 1050 nm. Our results show that AM1.5G photovoltaic power conversion efficiency > 10% should be possible with future optimization of: (a) the nanotube bandgap (and diameter) distribution and (b) improved control over morphology.

[1] D. J. Bindl, M.-Y. Wu, M. S. Arnold, *Nano Letters* (2011).

[2] D. J. Bindl, A. S. Brewer, M. S. Arnold, *Nano Research* (2011).

4:00pm EN+TF-TuA7 **Understanding Vertical Stratification in Polymer:Fullerene Bulk Heterojunction Solar Cells**, M.D. Clark, Air Force Research Laboratory, M.L. Jespersen, University of Dayton Research Institute, B.J. Leever, Air Force Research Laboratory

In the bulk heterojunction architecture of polymer-based solar cells (PSCs), the separate acceptor-donor phases form a bi-continuous inter-penetrating network by simultaneous casting from solution with morphological control stemming from external parameters such as thermal annealing, co-solvent inclusion, and drying conditions. While such treatments enhance device performance, a fundamental understanding of vertical concentration gradients within the fabricated active layer has been limited. In an effort to understand such morphological changes, several reports have explored 3D bulk heterojunction nanostructure using electron tomography,¹ ellipsometry,² neutron scattering,³ and spectroscopic techniques.⁴ This work, however, has yielded somewhat contradictory conclusions about fundamental network development and the origin of emerging concentration gradients. For example, some studies reported nearly equal blends at the PEDOT:PSS surface of annealed samples,^{2,4c} while others found P3HT^{1,4a,4c} or PCBM^{3,4b,4d,4f} preferentially decorating the buried interface. Several groups^{2b,3,4c,4f} further reported annealing causes PCBM diffusion towards the exposed surface, suppressing as cast vertical composition gradients. However, Xu et al.^{4b} detected PCBM migration towards the PEDOT:PSS interface upon annealing, while Xue et al.^{4a} suggested PCBM diffusion away from both interfaces. Here we report a combined experimental and theoretical analysis of phase segregation. The vertical stratification within a P3HT:PCBM bulk heterojunction solar cell is examined by depth profiling using both x-ray photoelectron spectroscopy (XPS) and time of flight secondary ion mass spectrometry (ToF-SIMS), with the effects of thermal annealing and P3HT:PCBM ratio being explored. In addition, the vertical phase stratification is predicted on thermodynamic grounds based on measured interfacial energies of the PSC constituents. Using these results, a fundamental understanding of the thermodynamic driving force for bulk heterojunction phase segregation and vertical stratification is then presented.

References

1 van Bavel, S.S. et al. *Nano Lett.* **9**, 507 (2009).

2 (a) Germack, D.S. et al. *Macromolecules* **43**, 3828 (2010); (b) Campoy-Quiles, M. et al. *Nat. Mater.* **7**, 158 (2008).

3 Parnell, A.J. et al. *Adv. Mater.* **22**, 2444 (2010).

4 (a) Xue, B. et al. *J. Phys. Chem. C* **114**, 15797 (2010); (b) Xu, Z. et al. *Adv. Funct. Mater.* **19**, 1227 (2009); (c) Yu, B.-Y. et al. *ACS Nano* **4**, 833 (2010); (d) Vaynzof, Y. et al. *ACS Nano* **5**, 329 (2011); (e) Wang, H. et al. *Chem. Mater.* **23**, 2020 (2011); (f) Germack, D.S. et al. *Appl. Phys. Lett.* **94**, 233303 (2009).

4:20pm EN+TF-TuA8 **Novel, Single-Crystalline-like Silicon on Low-Cost, Flexible Substrates for High Efficiency Thin Film Photovoltaics**, V. Selvamani, P. Dutta, R. Wang, Y. Gao, M. Yang, G. Majkic, E. Galtysyan, University of Houston

Thin film photovoltaics (PV) is being pursued by several institutions as a lower cost alternative to crystalline wafer technologies. The use of much less materials and roll-to-roll continuous processing in thin film technologies have been touted as the pathway to low-cost PV. However, the efficiencies of production thin film Si solar cells are about one half that achieved with crystalline silicon. Hence, achievement of single-crystalline-like silicon photovoltaics on flexible, low-cost substrates can be game changing by combining high efficiency with low cost. We are developing such a technology by creation of an architecture that yields single-crystalline-like thin films even on polycrystalline or amorphous substrates. This technology has been very successfully demonstrated and being commercialized in the superconductor field and inserted in the U.S. electric power grid [1].

The enabler that we have employed in this work is a single-crystalline-like thin film template of MgO made by Ion Beam-Assisted Deposition (IBAD). Such IBAD films have been successfully employed as templates for epitaxial growth of cube-textured superconducting films on polycrystalline substrates with critical current densities as high as those achieved on single crystal substrates [1].

MgO templates made by IBAD on flexible metal substrate have been used for epitaxial growth of germanium films using intermediate oxide layers. All layers were deposited by reel-to-reel magnetron sputtering and strongly (400) textured Ge films with an in-plane texture spread of just 1° FWHM

were achieved [2]. Optical properties of the germanium films are found to be comparable to that single crystal Ge and Hall mobility values over 700 cm²/Vs have been achieved. Epitaxial (400) textured silicon films have been grown by reel-to-reel magnetron sputtering on the Ge films. A continuous grading of germanium to silicon has been done to accommodate for the lattice mismatch. While excellent epitaxial growth has been achieved in Si and Ge on flexible metal substrates, the defect density of the films showed a high value of 10⁸ per cm². Cross sectional TEM of the multilayer architecture showed concentration of threading dislocations near the semiconductor-oxide interface. Defect reduction strategies are being employed and recent progress in use of single-crystalline-like templates on low-cost, flexible substrates for high-efficiency silicon photovoltaics will be discussed in this presentation.

1. V. Selvamanickam et al. *IEEE Trans. Appl. Supercond.* **19** (2009) 3225.
2. V. Selvamanickam et al. *J. Crystal Growth* **311**, (2009) 4553.

4:40pm **EN+TF-TuA9 High-Efficiency Multijunction Solar Cells Employing Dilute Nitrides**, V.A. Sabnis, H.B. Yuen, M. Wiemer, Solar Junction **INVITED**

Concentrating photovoltaic (CPV) systems have the opportunity to provide the lowest cost of electricity in hot, sunny climates. The advantages of CPV are based, in part, from the high performance offered by multijunction solar cells made from group III-V compound semiconductors. Unlike traditional PV, high concentration systems utilize mm-scale solar cells that comprise only 10-15% of the overall system cost. This low cost share means that increasing cell efficiency has significant leverage in driving down upfront capital costs and the leveled cost of electricity of a CPV project.

Production cell efficiencies for triple junction solar cells have reached 40% under concentration (25°C, AM 1.5D spectrum). We will review a number of exciting approaches for increasing cell efficiency that are being investigated world wide. Solar Junction has developed a set of dilute-nitride compound semiconductors that offer broad bandgap tunability over the infrared while retaining lattice matching to GaAs and Ge substrates. While significant efforts have been undertaken to develop dilute nitrides for multijunction solar cells over the last 15 years, these approaches have resulted in films that exhibited poor minority carrier properties resulting in low current drives and output voltages. Solar Junction has developed a molecular beam epitaxy process utilizing antimony as a surfactant that significantly enhances the minority carrier properties. Triple junction cells utilizing GaInNAsSb bottom junctions have achieved a world record efficiency of 43.5% under concentration. When used in conjunction with well known InAlGaP and AlGaAs compounds, GaInNAsSb films complete a lattice-matched epitaxial platform for enabling 4-, 5-, and 6-junction cells for achieving > 50% efficiencies in the coming years.

5:20pm **EN+TF-TuA11 Non-Radiative Carrier Recombination in InGaAs/GaAsP Strain-Balanced Superlattice Solar Cell**, T. Aihara, University of Miyazaki, Japan

An inserting of the quantum wells (QWs) to GaAs p-i-n solar cells could be a promising candidate to solve the current matching issue in the multi-junction solar cells[1]. We have successfully obtained the non-radiative recombination process for excitonic and subband absorptions in the GaAs/AlAs multiple QWs (MQWs) by using PPT methods [2]. In this study, we investigate escape, radiative and non-radiative recombination mechanisms of photo-generated carriers in the strain-balanced InGaAs/GaAsP MQWs or superlattice (SL) inserted into GaAs p-i-n solar cell structure to improve the photovoltaic performance. We then evaluated above three processes by using the surface photovoltage (SPV), photoluminescence (PL), and piezoelectric photothermal (PPT) spectroscopies, respectively. A InGaAs/GaAsP MQWs absorbing layer that inserted into GaAs p-i-n junction was composed of 10 stacks of 7.4-nm-thick InGaAs well and 10.8-nm-thick GaAsP barrier. For SL absorbing layer, ultra-thin GaAsP barriers of 3.7 nm thickness with 0.56-nm-thick GaAs buffer were prepared. All the layers were grown by metal-organic vapor phase epitaxy on the GaAs substrate. The PPT detects a heat generated by the non-radiative recombination by the PZT directly attached to rear surface of the sample. Figures 1 and 2 show the temperature change of PPT spectra of MQWs and SL with GaAs thin buffer samples, respectively. For MQWs sample, three peaks were observed and A-peak was concluded to be due to the excitonic transition associated with the electron transition between first electron (e1) and heavy-hole subbands (hh1) in QW. On the other hand, B-peak was concluded to be the electron transition between 1st minibands in conduction and valence bands in SL. As the temperature decreased, peak intensities of A and B increased, whereas corresponding SPV peaks decreased. The temperature dependence of PL, PPT, and SPV signal intensities can be fitted with the Arrhenius equation. Figure 3 shows the fitting results of PPT A (MQWs) and B (SL) and SPV A peaks. As shown in Fig. 3, activation energy of SL was smaller than that of

MQWs. This result implied that carrier escape from the QWs was enhanced for the case of SL. References [1] K. W. J. Barnham and G. Duggan, *J. Appl. Phys.* **67** (1990) 3409. [2] P. Wang et al.: *Jpn. J. Appl. Phys.* **46** (2007) 6857.

5:40pm **EN+TF-TuA12 Piezoelectric Photothermal Spectra and Carrier Nonradiative Recombination in InGaAs/GaAsP Super Lattice Structured Solar Cells**, T. Ikari, T. Aihara, Y. Nakano, University of Miyazaki, Japan, Y. Wang, M. Sugiyama, Y. Nakano, University of Tokyo, Japan, A. Fukuyama, University of Miyazaki, Japan

Fabrication of multi quantum well (MQW) or superlattice (SL) structures embedded in an absorption layer of solar cell is a promising idea for developing higher efficient devices. This is because the quantum well can extend the absorption to longer wavelength region and enhance the short-circuit current. However, recombination centers for carriers are simultaneously generated at the boundaries, leading to the degradation of conversion efficiency. Although optical absorption and spectral response spectroscopy are usually used for investigating absorption and recombination mechanism in the solar cell, no direct technique for characterizing nonradiative recombination is presented. We have developed the piezoelectric photothermal (PPT) spectroscopy for detecting such nonradiative recombination in the QW [1]. Heat generated by a nonradiative recombination of photoexcited carriers were detected as PPT signal by using a piezoelectric transducer. In this paper, we report on the PPT spectra of InGaAs/GaAsP SL layer and show that this technique is sensitive and powerful to investigate the absorption spectra of SL. It is, then, becomes possible to discuss a recombination mechanism of the photo-excited carriers in the solar cell structure from the non-radiative transition point of view.

A strain-balanced InGaAs/GaAsP SL layer embedded into the intrinsic region of the GaAs p-i-n solar cell were prepared. The SL absorbing layer was prepared in the structure of InGaAs(3.7nm)/GaAsP(5.4nm) with 0.56-nm-thick GaAs buffer layer by MOVPE technique on the GaAs substrate [2]. PPT spectrum at 100K shows two dominant peaks. The conventional absorbance of SL and the PPT spectrum of the MQW (InGaAs(7.4nm)/GaAsP (10.8nm)) samples were also discussed for comparison. A signal from SL is more clearly observed in the PPT than the absorbance spectra. Although the step like signals accompanied with the exciton transition are well resolved for MQW samples, no step but broad peaks around 1.395 and 1.45 eV were observed for SL sample. The energies of these peaks were as expected from the calculation of the single QW without any interaction of the neighboring QW, i.e. tunneling. Since the wave function of quantized level spread into the next well for the SL structure, broad peaks were, then, observed. Although the step like density of states should appear even in the SL, drastic decrease of the PPT signal beyond the peak was observed. One possible reason is that the number of carriers that recombine nonradiatively inside the quantum well decreases by tunneling.

- [1] T. Ikari, et al., *Phys. Rev. B* **77** (2008) 125311.
- [2] M. Sugiyama et al.: *J. Cryst. Growth* **315** (2011) 1.

Magnetic Interfaces and Nanostructures
Room: 6 - Session MI+EN+BI-TuA

Fundamental Problems in Magnetism

Moderator: G.J. Szulczewski, The University of Alabama

2:00pm **MI+EN+BI-TuA1 Spintronics – Implications for Energy, Information and Medical Technologies**, S.D. Bader, Argonne National Laboratory and Northwestern University **INVITED**

Spintronics encompasses the ever-evolving field of magnetic electronics.[1,2] Fields such as spintronics are hold the potential to extend the information technology revolution as the semiconductor road map reaches its end. A major issue with present day electronics is in its demand for increased power. Spintronics offers the possibility to communicate via pure spin currents as opposed to electric charge currents. The talk provides a brief perspective of recent developments to switch magnetic moments by spin-polarized currents, electric fields and photonic fields. Developments in the field of spintronics continue to be strongly dependent on the exploration and discovery of novel nanostructured materials and configurations. An array of exotic transport effects dependent on the interplay between spin and charge currents have been explored theoretically and experimentally in recent years. The talk highlights select promising areas for future investigation, and, features recent work at Argonne, [3,4] including, most strikingly, in the realm of medical applications. [5]

* Work supported by the U.S. Department of Energy, Office of Science, Basic Energy Sciences, under contract No. DE-AC02-06CH11357.

1. S. D. Bader and S. S. P. Parkin, "Spintronics," in *Ann. Rev. of Cond. Matt. Phys.*, 1, 71-88 (2010).
2. S. D. Bader, *Rev. Mod. Phys.* 78, 1-15 (2006).
3. O. Mosendz, J. E. Pearson, F. Y. Fradin, G. E. W. Bauer, S. D. Bader, A. Hoffmann, *Phys. Rev. Lett.* 104, 046601 (2010).
4. J. S. Jiang, J. E. Pearson, S. D. Bader, *Phys. Rev. Lett.* 106, 156807 (2011).
5. D.-H. Kim, E. A. Rozhkova, I. V. Ulasov, S. D. Bader, T. Rajh, M. S. Lesniak, V. Novosad, *Nature Mat.* 9, 165-171 (2010).

Samuel D. Bader, Materials Science Division and Center for Nanoscale Materials, Argonne National Laboratory, Argonne, Illinois 60439, and Department of Physics and Astronomy, Northwestern University, Evanston, Illinois 60208 USA

2:40pm **MI+EN+BI-TuA3 Multiscale Modeling for Spintronics**, *K.A. Mewes, T. Mewes, W.H. Butler*, University of Alabama **INVITED**

The next generation of spintronic devices relies strongly on the development of new materials with high spin polarization, optimized intrinsic damping and tunable magnetic anisotropy. Therefore technological progress in this area depends heavily on the successful search for new materials as well as on a deeper understanding of the fundamental mechanisms of the spin polarization, the damping and the magnetic anisotropy. My talk will focus on different aspects of materials with high spin polarization, low intrinsic relaxation rate and perpendicular anisotropy. Our results are based on first principles calculations in combination with a non-orthogonal tight-binding model to predict those material properties for complex materials which can be used for example in new spin based memory devices or logic devices. Future progress in spintronics not only requires a better understanding of the underlying physical principles but also hinges strongly on the development of theoretical models capable of describing the expected performance of realistic device structures. As an example I will discuss the challenges in the Spin Transfer Torque Random Access Memory. This memory is dense, fast and nonvolatile and has the capability of a universal memory possibly even replacing today's Dynamic Random Access Memory (DRAM).

4:00pm **MI+EN+BI-TuA7 Anomalous Magneto Transport in Amorphous TbFeCo Film with Perpendicular Magnetic Anisotropy**, *N. Anunivat, M. Ding, J. Poon, S.A. Wolf, J.W. Lu*, University of Virginia

TbFeCo has attracted some interests because of its high perpendicular anisotropy and tunable magnetic properties for nanomagnetic and spintronics application. Due to the fact that electronic device is getting smaller, fundamental understanding of size and geometry dependent is crucial. In this study, we report a strong size dependence of the coercive field in 15 - 100nm thick Tb₃₀Fe_{63.5}Co_{6.5} films with MgO capping. Magneto Optical Kerr effect (MOKE) and Vibrating Sample Magnetometer are performed on unpatterned films. The films exhibited strong PMA characteristics. The films were then fabricated into Hall bars with 10 μ m, 50 μ m, 100 μ m and 500 μ m in width. From anomalous Hall effect (AHE), HC was determined for these patterned films. We observed coercivity enhancement as the width of the hall bar decreases (up to 200% at room temperature). The temperature dependent of the coercivity is also studied. There exhibits the local minimum as the temperature change from 50 - 300K. The correlation between HC_{min} and dimensions of the hall bar are discussed. The magnetic domain structures and surface morphology analysis were performed using magnetic force microscopy and atomic force microscopy respectively. The variation in domain sizes, structures for different hall bars as well as possible origins of the coercivity enhancement are also discussed.

4:20pm **MI+EN+BI-TuA8 Magnetic Properties of Fe Clusters: A DFT+U vs Nano DFT+DMFT Analysis**, *A.K. Kabir, V. Turkowski, T.S. Rahman*, University of Central Florida

We use our recently proposed combined density-functional-theory/dynamical-mean-field-theory (DFT + DMFT) approach for molecules and nanosystems [1] to study the magnetic properties of Fe clusters consisting of 15, 17 and 19 atoms. This method has several advantages compared with the widely-used DFT + U approach for systems with localized electron states, the most important of which is that it takes into account dynamical correlation effects. These effects are especially important in the case when the kinetic (hopping) and the local Coulomb repulsion energies have the same order of magnitude. In particular, we study the size-dependence of the magnetic properties of the clusters by using the nanoDMFT code developed in our group using the iterated-perturbation theory approximation in the impurity solver. We find that the DFT+DMFT approach yields much better agreement for the magnetization with experimental data as compared to DFT and DFT+U methods, both of which generally overestimate the magnetization.

Work supported in part by DOE Grant No. DOE-DE-FG02-07ER46354

1. V. Turkowski, A. Kabir, N. Nayyar and T.S. Rahman *J. Phys.: Condens. Matter* 22, 462202 (2010) and *J. Chem. Phys.* 136, 114108 (2012)

4:40pm **MI+EN+BI-TuA9 Rationally-designed Iron Oxide Nanostructures for Bioimaging**, *Y. Bao*, The University of Alabama **INVITED**

Iron oxide nanoparticles have been extensively studied in targeted delivery, localized therapy, and as contrast agents for magnetic resonance imaging (MRI). In fact, sugar coated iron oxide NPs have been clinically used as the liver/spleen-specific contrast agents in MRI, indicating the biocompatibility and potential of iron oxide nanoparticles in nanomedicine. This presentation will discuss how rationally designed iron oxide nanoparticles can achieve highly effective MRI contrast agents. The talk will primarily focus on the shape control of iron oxide nanoparticles and the surface functionalization. The formation and magnetic properties of various shaped-iron oxides (e.g., cubes, nanoworms, nanoplates, and nanowires) will be elaborated. In particular, ultrathin iron oxide nanowires will be discussed in details, such as synthesis, property, and their potential as MRI contrast agents.

5:40pm **MI+EN+BI-TuA12 3D Vector Magnetometry of Thin-Films using Generalized Magneto-Optical Ellipsometry (GME)**, *J.A. Arregi, J.B. González-Díaz, O. Idigoras, A. Berger*, CIC nanoGUNE Consolider, Spain

Generalized Magneto-Optical Ellipsometry (GME) has emerged in the last decade as a methodology to characterize magnetic materials with a high degree of precision, by means of utilizing the magneto-optical Kerr effect [1]. Compared to other magneto-optical characterization methods based on the same effect, GME has two key advantages: it can measure both the optical and magneto-optical constants, and it allows full vector magnetometry, all with one simple experimental set-up. The technique has been successfully employed in the study of diverse magnetization reversal processes, for the purpose of identifying spin-polarized electronic states in multiferroic materials [2], as well as for the measurement of the magnetization orientation using 2D vector magnetometry [3].

Even if some works have suggested the possibility to perform quantitative 3D vector magnetometry using the GME technique [4], actual measurements have not been demonstrated so far. Here, we extract the field dependent evolution of the three magnetization components during the reversal process. In order to do so, we exploit the different symmetries of the longitudinal, transverse and polar Kerr effect around different polarizer/analyzer crossing points, which allows us to separate the information of each of the magnetically induced contributions to the non-diagonal reflection matrix elements. By combining the presence of in-plane uniaxial anisotropy as well as out-of-plane applied magnetic fields in our Co and Co-alloy based thin films, we manage to monitor the evolution of the full magnetization vector as a function of the field.

In addition to this full vector magnetometry capability, we have recently improved this technique to enhance measurement reliability [5] and we also extended its capabilities to characterize materials that are magneto-optically active and optically anisotropic at the same time [6].

References:

- [1] A. Berger and M. R. Pufall, *Appl. Phys. Lett.* **71**, 965 (1997)
- [2] M. Bastjan, S. G. Singer, G. Neuber *et al.*, *Phys. Rev. B* **77**, 193105 (2008)
- [3] A. Berger and M. R. Pufall, *J. Appl. Phys.* **85**, 4583 (1999)
- [4] K. Mok, N. Du, and H. Schmidt, *Rev. Sci. Instrum.* **82**, 033112 (2011)
- [5] J. A. Arregi, J. B. Gonzalez-Diaz, E. Bergaretxe, O. Idigoras, T. Unsal, and A. Berger, accepted for publication in *J. Appl. Phys.*
- [6] J. B. González-Díaz, J. A. Arregi, E. Bergaretxe, M. J. Fertin, O. Idigoras, and A. Berger, submitted to *Appl. Phys. Lett.*

Nanometer-scale Science and Technology

Room: 12 - Session NS+EN+GR-TuA

Nanomaterials in Two and Three Dimensions

Moderator: V.P. LaBella, University at Albany-SUNY

2:20pm **NS+EN+GR-TuA2 Nanopatterning of SPRi Sensor Surfaces for Sub-Nanomolar Biomarker Detection**, *M.A. Parracino, M.J. Perez Roldan, J. Hanus, V. Spampinato, G. Ceccone, P. Colpo, F. Rossi*, Nanobiosciences Unit, JRC, Italy

In this work we report the detection of low-molecular weight biomarkers on two kinds of nanostructured surfaces by using a SPRi sensor. Nanopatterned

surfaces are fabricated by combining functionalization and patterning techniques. Two different methods were used for the surface nanopatterning: electro-beam lithography (EBL) and colloidal lithography (CL). Maltose binding protein (MBP) and transthyretin (TTR) are respectively immobilized on the two types of nanopatterns and used as biological recognition elements. Chemical contrast adhesive/non adhesive at nanoscale has been created in order to control protein binding at nanoscale. Plasma deposited (PEO)-like film was used as passivation layer to prevent non-specific binding of protein in between the protein adhesives nano-areas. All the fabrication steps of both surfaces have been carefully controlled and analyzed using several techniques such as AFM, XPS, and SEM. The gold nanostructures were 185 nm width lines, for the patterned created with EBL, and holes of 250 nm in diameters for the pattern fabricated using CL. The gold grating surface made using EBL was functionalized with sugar via a thiol-linker. Maltose Binding Protein (MBP) was bound on sugar modified surface in order to develop a competitive assay for maltose detection. In this competitive assay, the protein binding on the sugar functionalized surface depends on the concentration of his free competitor in solution: by measuring the protein binding, it is possible to evaluate the concentration of the small molecule in solution. In the second methods, NTA functionalized nanoholes in PEO like background were fabricated and subsequently activated with nickel (Ni II) for a selective immobilization of histidines tagged TTR, which underlies to a direct detection of Thyroxine 4 (T4). In both case, the biological intermediates, MBP and TTR, are selectively immobilized onto nanopatterned surfaces. The ligand protein binding on the nanostructure is higher than on the flat surface. The better ligand orientation and immobilization on the nanostructures results in analyte detection at sub-nanomolar concentration. The combination of nanopatterning features with the two different methods of detection presented in this work provides a description for a more generalized approach for the development of stable and reliable biosensor platforms for the detection of different small molecules having an high impact in environmental, and biomedical field.

4:00pm NS+EN+GR-TuA7 Single Layer of MoS₂ on Close-Packed Metal Surfaces, D. Le, T.S. Rahman, University of Central Florida

We present results of first principles electronic structure calculations, using van der Waals density functional theory, of the adsorption of a single layer of Molybdenum disulfide (MoS₂) on several close-packed metal surfaces. On Cu(111) we find three energetically equivalent stacking types and a Moiré pattern whose periodicity is in agreement with experimental findings [1]. The layer is found not to be purely physisorbed on the surface, rather there exists a chemical interaction between it and the Cu surface atoms. We also find that the MoS₂ film is not appreciably buckled, while the top Cu layer gets reorganized and vertically disordered. The sizes of Moiré patterns for a single layer of MoS₂ adsorbed on other close-packed metal surfaces are also estimated by minimizing the lattice mismatch between the film and the substrate. The Moiré patterns on Ir(111), Pt(111), and Ru(0001) are particularly interesting as the MoS₂ layer is found to bind more strongly on them than on Cu(111). We compare the nature of the bond in these three substrates with that on Cu(111).

[1] D. Kim, D. Sun, W. Lu, Z. Cheng, Y. Zhu, D. Le, T. S. Rahman, and L. Bartels, *Langmuir* **27**, 11650 (2011).

* This work was supported in part by the U.S. Department of Energy under Grant No. DE-FG02-07ER15842.

4:20pm NS+EN+GR-TuA8 Chemically Exfoliated Two Dimensional Materials for Energy Applications, M. Chowalla, Rutgers University
INVITED

Chemical exfoliation of layered two-dimensional materials such as graphite and transition metal chalcogenides allow access to large quantities of atomically thin nanosheets that have properties that are distinctly different from their bulk counterparts. Although 2D materials have recently become popular, their fabrication via exfoliation of bulk crystals has been known for decades. For example, Brodie first exfoliated graphite into atomically thin oxidized form of graphene in 1859. In the case of layered transition metal dichalcogenides (LTMDs) such as MoS₂, WS₂, MoSe₂, WSe₂, etc., Frindt et al. performed seminal work in the '70s and '80s. We have revived these techniques to obtain a wide variety of chemically exfoliated two-dimensional nanosheets and utilized these materials in wide variety of electronic and energy applications. In this presentation, I will highlight some of our key contributions with graphene oxide (GO) and LTMD nanosheets. Specifically, I will present their implementation into large area electronics, strategic implementation into solar cells, and as catalyst for hydrogen evolution.

5:00pm NS+EN+GR-TuA10 Isolation and Surface Structure of Ultrathin Nanosheets formed by Atomic Layer Deposition, K.M. Lee, D.H. Kim, G.N. Parsons, North Carolina State University

Ultrathin nanosheets are two-dimensional structures that are often exfoliated from layered compounds. The nanosheets are flat with large surface area (100's of nm²) but with very small thickness in several nm scale. A common example of a nanosheet is graphene which is exfoliated from graphite. Other nanosheet materials that are chemically exfoliated from layered crystals include MoS₂, VS₂, and many oxide materials such as MnO₂, TiNbO₅, or LaNb₂O₇. These materials show unique capabilities for nanoelectronic devices, photocatalysts, and electrochemical sensor applications. For our work, we explore atomic layer deposition (ALD) as an effective technique to fabricate metal oxide nanosheets with precisely controlling thickness and chemical composition. To form nanosheets, we spin-coated a substrate with polymer such as polymethylmethacrylate (PMMA), polyvinyl alcohol (PVA), or polyacrylic acid (PAA) as a sacrificial layer, then deposited TiO₂, Al₂O₃ or ZnO on polymer layer by ALD. Dissolving the polymer in solvent releases nanosheets from the substrate. We successfully attained two dimensional TiO₂ nanosheets with several hundred μm in lateral size and less than 10 nm in thickness. Attaining nanosheets with thickness near 1nm proved to be rather challenging. For Al₂O₃ and TiO₂, nanosheets with thickness of ~ 1 nm can be isolated by two-immiscible liquid separation process. For ZnO, the thinnest nanosheet obtained to date is closer to 15 nm. We characterized nanosheets using AFM to confirm their thickness and found that the surface structure and roughness depends on the materials and thickness. We also examined the functionality of TiO₂ nanosheets as an agent for photocatalytic degradation of organic dyes. This work demonstrates and defines the capabilities and limits for functional nanosheets fabrication by atomic layer deposition.

5:20pm NS+EN+GR-TuA11 All Solution Processed InGaO₃(ZnO)_m Thin Films with Layered Structure and their Thermoelectric Properties, J.H. Kim, H.K. Cho, Sungkyunkwan University, Republic of Korea

As the materials currently in use have been reached terminal and showed low productivity in a few field, the development of advanced materials are demanded. In the middle of atmosphere, low-dimensional nanostructures have been introduced in recent studies such as 1-D nanowire and 2-D superlattice. Among them, a multi-layered structure shows unique properties originating from the confinement of carriers in the two-dimensional layer. For example, LaFeO₃-LaCrO₃ superlattice structures fabricated by pulsed layer deposition (PLD) have shown enhanced ferromagnetism [1] and InGaO₃(ZnO)_m superlattice structure grown by sputtering method has improved thermoelectric properties [2].

These homologous series of RAO₃(MO)_m (R=In or rare earth elements; A=Ga, In, Al, or Fe ; M=Mg, Co, Cu, or Zn ; m=integer) comprise alternating stacks of RO₂⁺ and AO⁺(MO)_m layers and are candidate to exhibit the quantum effect due to its natural superlattice [3]. Despite these materials being widely investigated, the fabrication of RAO₃(MO)_m thin film with layered structure is limit due to their fabrication which requires expensive high-vacuum equipment and shows low productivity.

In this study, all solution process (an epitaxial ZnO buffer layer growth on sapphire substrate, amorphous IGZO layer on ZnO buffer layer by composition controlled solution process, and post-annealing at 900°C for 9hours) enables us to fabricate InGaO₃(ZnO)_m thin film with periodic superlattice structure. Crystallinity of thin film was analyzed by X-ray diffraction and TEM results. And also, TE properties such as Seebeck coefficient, electrical conductivity, thermal conductivity were evaluated to identify the degree of crystallization of superlattice with layered structure.

Reference

- [1] K. Ueda, H. Tabata and T. Kawai, *Science*, 1998, **280**, 1064
- [2] D. K. Seo, B. H. Kong and H. K. Cho, *Cryst. Growth Des.*, 2010, **10**, 4638
- [3] J. L. F. Da Silva, Y. F. Yan and S. H. Wei, *Physical Review Letters*, 2008, **100**, 255501.

Energy Frontiers Focus Topic

Room: 15 - Session EN+PS-WeM

Plasmas for Photovoltaics and Energy Applications

Moderator: J.-P. Booth, LPP-CNRS, Ecole Polytechnique, France

8:00am EN+PS-WeM1 **Electron Driven C₁-chemistry: Direct Conversion of Methane to Synthetic Fuels**, T. Nozaki, Tokyo Institute of Technology, Japan **INVITED**

Currently, industrial material and energy conversion technology platform consists of thermochemical processes including various catalytic reactions. Existing industry scale technology and related science has already been well established; nevertheless, further improvement in energy efficiency and material saving are demanded. Drastic reduction of CO₂ emission is also drawing keen attention with growing concern of energy and environmental issues. Green chemistry is a rapidly growing field of science and technology, and often highlights renewable bioenergy, bioprocesses, solar photocatalysis of water splitting, and CO₂ regeneration as synthetic fuels. Plasma catalysis of hydrocarbon feedstock is also highlighted as an important part of the innovative next generation green technologies that meet the need for energy saving, environment protection, and material preservation [1-4]. Non-thermal plasma uniquely generates reactive species independently of reaction temperature, and these species are used to initiate chemical reactions at unexpectedly lower temperatures than normal thermochemical reactions. Non-thermal plasma thus broadens the operation window of existing chemical conversion processes, and ultimately allows modification of the process parameters to minimize energy and material consumption. We specifically focus on dielectric barrier discharge (DBD) as one of the viable non-thermal plasma sources for practical fuel reforming. In the presentation, room-temperature one-step conversion of methane to synthetic fuels such as methanol, hydrogen, and syngas (H₂+CO) using a microplasma reactor is highlighted. Not only practical background of the project, but also unique characteristics of plasma fuel reforming such as non-equilibrium product distribution is presented [5-7].

1. T. Nozaki et al: *Journal of the Japan Petroleum Institute*, **54**(3) (2011) 146.
2. The special issues on " Non-thermal Plasma Assisted Fuel Conversion for Green Chemistry ", *J Phys D: Appl Phys.*, **44**(23), 2011
3. A Gutsol: *Handbook of Combustion*, Vol.5 New Technology, Wiley-VCH, 323 (2010)
4. H L Chen et al: *Appl. Catal. B: Environmental*, **85** (2008) 1.
5. T. Nozaki et al: *Chemical Engineering Journal*, **166** (2011) 288–293.
6. T. Nozaki et al: *Energy & Fuels*, **22** (2008) 3600–3604.
7. T. Nozaki et al: *Pure and Applied Chemistry*, **78**(6) (2006) 1147–1162.

8:40am EN+PS-WeM3 **Plasma-assisted CO₂ Conversion as Candidate Element in Future Solar Fuel Economy**, S. Welzel, S. Ponduri, F. Brehmer, M. Ma, M.C.M. van de Sanden, R. Engeln, Eindhoven University of Technology, the Netherlands

Recently research in 'solar fuels' has been stimulated by the forthcoming depletion of fossil fuels along with a slowly increasing share of intermittently available renewable sources. New efficient methods of harvesting renewable (e.g. solar) energy and its storage in high energy density chemical fuels are therefore highly desirable. CO₂ and its recycling into 'solar fuels' will be an essential element in the future transport and energy infrastructure. Plasma-processing of CO₂ in the gas phase under low-temperature non-equilibrium conditions is thereby a promising alternative to specifically tackle the rate-limiting dissociation into CO. Two aspects of such a plasma-assisted CO₂ treatment have been studied and are detailed in this contribution.

Firstly, the direct hydrogenation of CO_x in a plasma-expansion created from mixtures of Ar and H₂ was investigated. Different (metallic) surface materials were employed to assess the influence of surface reactions on the molecule formation. Mass-spectrometry and infrared absorption spectroscopy were applied to quantify the gas phase composition of such argon-ion and hydrogen-radical enhanced plasmas. Although CO was a main product with up to 50 % conversion yield, the separation of CO₂ dissociation and subsequent hydrogenation was strongly suggested to optimise both processes individually. Furthermore it transpired that plasma-catalysis require new surface materials that are different from conventional catalysts: a copper surface typically reduced the CO and CH₄ yields by 50 %.

Secondly, to particularly account for the individual optimisation of the CO₂ dissociation and scrutinise the (energy) efficiency of the conversion process dielectric barrier discharges in CO₂ were studied. The focus was on establishing a consistent energy-balance of the proposed plasma-assisted route and involved the analysis of energy injected to the power supply, the transfer to the discharge and the correlation with the CO₂ conversion. Through reduction of loss channels in the resonance circuit operated in the kHz-range clearly more than 50 % of the input power were directly injected to the plasma. Plasma parameters such as electron and vibrational temperatures and the population distribution of excited species were determined to further characterise the excitation and dissociation channels in the CO₂ plasma.

9:00am EN+PS-WeM4 **Novel Processing Routes of Silicon Nanocrystals in a Remote Expanding Thermal Plasma for Photovoltaic Applications**, I. Dogan*, Eindhoven University of Technology, Netherlands, S.L. Weeks, Colorado School of Mines, K. Dohnalova, T. Gregorkiewicz, University of Amsterdam, Netherlands, S. Agarwal, Colorado School of Mines, M.C.M. van de Sanden, Dutch Institute for Fundamental Energy Research, Netherlands

The interest in silicon nanocrystals (Si-NCs) has considerably increased since the observation of carrier multiplication and separation between adjacent Si-NCs. This mechanism might potentially enable a more efficient solar spectrum conversion. For successful integration of Si-NCs into solar cells, the key issues are size control, crystalline quality, surface preparation and cost efficient production of Si-NCs. Previous works have failed to address the latter point because they require multiple production steps yet with an insufficient amount of produced Si-NCs. Here, a novel synthesis method of Si-NCs by using a remote expanding thermal plasma (ETP) is presented, that allows a direct utilization for large scale production. One-step route synthesis of Si-NCs is realized in an argon/silane plasma with remarkable throughputs above 100mg/min of Si-NCs. Formation of Si-NCs is favoured by means of silane polymerization reactions. In contrast to the common belief of particle coagulation, all Si-NCs are found to be formed by nucleation as revealed from TEM analysis of the Si-NCs produced. TEM, Raman spectroscopy (RS) and photoluminescence spectroscopy (PL) consistently demonstrate that the Si-NCs have a size distribution in the range 2-140nm which is related to differences in residence times in the different zones of the reactor. To move towards a better control of the size distribution, a series of size separation experiments is discussed. Two approaches are proposed: spatial confinement of the plasma zones where the smaller Si-NCs are formed or a time modulation of the silane flow injected into the reactor. It will be shown that using these methods an average Si-NC size distribution of 5nm can be reached. Moreover, based on the results of time modulation, the role of different plasma species on the formation of small and large Si-NCs will be discussed. The observation of step-like enhancement of luminescence quantum yield with increased photon energy, which is a sign of carrier multiplication between Si-NCs will be discussed. It is expected that the ETP approach is capable to dramatically increase the production efficiency of Si-NCs to scalable throughputs without any loss of quality.

9:20am EN+PS-WeM5 **Growth of Microcrystalline Silicon using Tailored Voltage Waveform Driven Plasma Processes: From Materials to PV Devices**, E.V. Johnson, LPICM-CNRS, Ecole Polytechnique, France, S. Pouliquen, P.A. Delattre, J.-P. Booth, LPP-CNRS, Ecole Polytechnique, France **INVITED**

The use of non-sinusoidal, radio-frequency (RF) « tailored » voltage waveforms (TVW's) to drive plasma processes in a capacitively coupled plasma reactor allows one to decouple the injected power from the mean ion bombardment energy (IBE) at the substrate. Also known as the Electrical Asymmetry Effect (EAE), this decoupling stems from a controllable division of the sheath voltage between the two electrodes when an asymmetric voltage waveform is applied to one of the electrodes. In a symmetric reactor, this effect manifests itself through the presence of a self-bias voltage (V_{DC}), and as dramatic changes in this parameter in an asymmetric one. For example, the application of a "peaks" waveform to the RF electrode - consisting sharp pulses separated by plateaus - results in a large, negative V_{DC}, and thus a reduction in the IBE at a substrate on the grounded electrode. A "valleys" waveform results in the opposite, while both waveforms inject the same power into the plasma.

Such independent control over the sheath voltages is very useful when applied to the deposition by PECVD of thin-films of materials needing a high radical flux but low IBE, such as hydrogenated microcrystalline silicon

* Coburn & Winters Student Award Finalist

($\mu\text{-Si:H}$). By controlling the growth conditions of the $\mu\text{-Si:H}$ thin films through the shape of the waveform, one can control many aspects of the film properties (Raman crystallinity, density, hydrogen bonding, surface morphology, and electronic properties) without changing any other process conditions. In particular, the optical response of the films (and film surfaces) can be observed in-situ during growth using spectroscopic ellipsometry, thus linking the redistribution of the sheath voltages to the growth dynamics. Furthermore, we show that when TVW's are used to decrease the IBE during the growth of the absorber layer of thin-film solar cells, good device properties at acceptable deposition rates are obtained.

A promising aspect of this technique is the prospect of achieving process control without modifying the core of an existing reactor chamber. However, the counteracting challenge is that of efficiently coupling multiple harmonics to the reactor simultaneously, and these two facets will also be discussed.

10:40am EN+PS-WeM9 Measurement and Control of Ion Energies in Dual Frequency Capacitive Hydrogen Discharges, E. Schuengel, S. Mohr, J. Schulze, U. Czarnetzki, Ruhr-University Bochum, Germany

In plasma processing applications, capacitively coupled radio frequency (CCRF) discharges are widely used. A typical example is the manufacturing of silicon thin film solar cells using PECVD in a geometrically almost symmetric capacitively parallel plate discharge. For these applications, one of the major aims is the control of the fluxes and properties of radicals and ions at the substrate surface, thus controlling the surface chemistry and optimizing the (electrical) properties of the deposited film and/or the deposition rate. In particular, the shape of the ion velocity distribution function (IVDF) plays a crucial role [1]. The IVDF can be controlled to some extent in CCRF discharges driven by two substantially different frequencies, where the low frequency component is used to modify the ion energy while the total ion flux should be adjusted via the high frequency component. However, recent investigations have shown that this method is limited to a rather narrow window of discharge operating conditions [2]. As opposed to this concept, the Electrical Asymmetry Effect (EAE) uses the excitation via two consecutive harmonics to generate an asymmetric discharge even in geometrically symmetric discharge configurations [3]. Here, the symmetry of the discharge, the DC self bias, and the ion energy at the electrode surfaces are controlled via the phase angle between the two frequencies. In this study, the EAE is investigated in a discharge setup, which is similar to the ones described in the above example. A combination of 13.56 MHz and 27.12 MHz is applied to one electrode. The discharge is ignited in pure hydrogen at pressures of several hundred Pascals. Under these conditions, H_3^+ ions are the dominant ion species. A plasma process monitor is implemented into the center of the grounded electrode, allowing to measure the H_3^+ IVDF. The results show that the mean ion energy changes as a function of the phase angle, while the ion flux is kept almost constant. However, the control range of the ion energy via the EAE is limited and the shape of the IVDF shows a dependence on the phase angle. These experimental findings are understood in the frame of a simple model.

Funding by the German Federal Ministry for the Environment, Nature Conservation and Nuclear Safety (0325210B) is gratefully acknowledged.

- [1] S. Nunomura and M. Kondo 2008 Appl. Phys. Lett. **93** 231502
- [2] J. Schulze et al. 2009 Plasma Sources Sci. Technol. **18** 034011
- [3] U. Czarnetzki et al. 2011 Plasma Sources Sci. Technol. **20** 024010

11:00am EN+PS-WeM10 Raman Study of the Properties of Free Standing Silicon Nanocrystals Using Laser Induced Thermal Heating, L. Han, A.H.M. Smets, M. Zeman, Delft University of Technology, Netherlands

Nanocrystals (NCs) exhibit unique physical properties which might open routes to new photovoltaic concepts conquering the Shockley-Queisser limit of single junction solar cell devices, such as multiple-exciton-generation (MEG) and down conversion using space-separated-quantum-cutting (SSQC). In addition, the strong dependence of the band gap of NCs on their sizes, allows the design of novel multi-junction solar cells. For these reasons, NCs made of variety of direct and indirect semiconductor materials, have been extensively studied in recent years. In this contribution we focus on silicon, the most dominant material in PV technology. Challenges in the processing of Si NCs are controlling their size distribution and passivation of surfaces to prevent unwanted Shockley-Read-Hall recombination of generated charge carriers.

The Si NCs studied in this paper are synthesized using the expanding thermal plasma chemical vapor deposition (ETP-CVD) technique with the advantage of incredible high yield, deposition rate, room temperature fabrication, low cost, high purity and post-surface passivation treatment based on plasma processing. Using the ETP-CVD technique free standing Si NCs with a wide variety of properties have been processed. The

dependence of the processing conditions are studied using high resolution transmission electron microscopy. Furthermore, the surface oxidation kinetics of free standing Si NCs without any post-deposition surface-passivation-treatment is studied using IR absorption spectroscopy.

The main focus in this contribution is an unconventional Raman spectroscopy analysis on the free standing Si NCs. In this approach, Si NCs are additionally heated using a laser probe to study the quantum confinement effects of the Si NCs in more detail. An interesting huge red Raman peak shift for the transverse optic mode (520 cm^{-1}) of around 30 cm^{-1} and a width enhancement of 19.1 cm^{-1} are observed with the increasing power of the probe laser. We argue that the shift is due to the laser induced thermal heating of the Si NCs in line with analysis based on the ratio of the Anti-Stokes-to-Stokes peak of the free standing Si NCs [1]. As a reference, the Raman spectra of amorphous silicon and microcrystalline silicon thin films are studied using the same approach. This experiment shows that thermal conduction between the free standing Si NCs is inefficient in contrast to the Si films, which allows the Si NCs to be heated up by laser light more efficiently.

- [1] Khriachtchev et al., JAP 100, 053502 (2006)

11:20am EN+PS-WeM11 Fabrication of 3D Array Si Quantum Dots Superlattice using Biotemplate and Neutral Beam Etching, M.E. Fauzi, M. Igarashi, W. Hu, S. Samukawa, Tohoku University, Japan

Quantum dots have been used in many novel optoelectronic devices due to its quantum effect characteristics. To further improve quantum dots light absorption efficiency, it is vital to increase number of quantum dots while keeping straight alignment in vertical direction. However, in the conventional method using bottom-up approach, fabricated quantum dots structure is not uniform and well-aligned in vertical direction, while the conventional top-down etching has limitations in fabrication of nanometer size and leaves high-density defects. In previous study, we have fabricated well-ordered arrangement of high-density 2 dimensional (2D) array ($7 \times 10^{11}\text{ cm}^{-2}$) silicon nanodisk (Si-NDs) with a new process using bio-template and damage-free neutral beam etching (NBE). In this paper, we developed technology for fabricating 3D array of Si NDs with single step NBE technique and biotemplate technology, focusing on well-aligned structure in vertical direction.

Firstly, we deposited 4 layers of 4 nm-thick Si layer with 2 nm-thick silicon carbide (SiC) as its matrix using thin film deposition technique. Then, biotemplate was quasi-hexagonally arranged and used as mask during our etching process. These bio-templates provide 6 nm space between etching masks. After NBE process, high aspect ratio of 12 is achieved. The key technology in our approach is to utilize low-selectivity etching process to etch high aspect ratio structure in single step. Single step etching is made possible for three reasons. First, oxide layer on top of our Si/SiC structure was first removed by NF_3 gas/hydrogen radical treatment. Secondly, SiC that was used as matrix material has a comparable etching rate compare to Si. In our research, we make use of Si/SiC's low selectivity (1.3) to conduct a well-aligned vertical etching process. Thirdly, a high selectivity for Si/SiC structure to iron-core etching mask. After chlorine NBE process, iron-core mask pattern was precisely transferred, and anisotropic etching profile was achieved. Our SEM images of the top-view and cross-section view exhibits well-aligned, uniformity, high aspect ratio nano-columns. Lastly, we deposit SiC layer to complete Si/SiC matrix. As a result, we successfully fabricated 4 layers-stacked Si-NDs with sub-10 nm in diameter and 2 nm space between nanodisks.

We hope quantum dots superlattice fabricated by our technology could be used in quantum dot solar cell application for higher conversion efficiency.

11:40am EN+PS-WeM12 Two-dimensional Simulations of Hydrogen and Hydrogen/Silane Capacitively Coupled Dual Frequency Discharges, S. Mohr, E. Schuengel, J. Schulze, U. Czarnetzki, Ruhr University Bochum, Germany

Capacitively coupled radio-frequency (CCRF) discharges are commonly used in surface processing applications, for example the deposition of thin films. One of the most important challenges in optimizing CCRF discharges for this usage is achieving the ample and independent control of flux and energy of ions and reactive species at the surfaces, as these properties determine the quality and deposition rate of the films. This independent control can be attained by using electrically asymmetric discharges which use two consecutive harmonics to excite the plasma; the ion energy can be controlled by the phase between the two frequencies while the flux stays constant. The feasibility of this method has been demonstrated by both experiments and simulations in various gas mixtures [1-3], although limitations have been observed, for example in highly electronegative discharges.

Hydrogen is part of many gas mixtures used in industrial applications such as hydrogen/silane mixtures in the production of solar cells. Two traits, which distinguish hydrogen discharges from the already investigated gas mixtures, are the high ion mobility and the regular occurrence of field reversals during the sheath collapse. Additionally, deposition processes are usually carried out at quite high pressures of several 100 Pa. We conduct two-dimensional simulations of such discharges covering a wide range of discharge conditions (pressure: 20 Pa – 500 Pa, pure hydrogen discharges and hydrogen/silane mixtures) using the simulation tool Hybrid Plasma Equipment Model (HPEM) by Mark Kushner [4]. The focus of our investigations lies on the influence of high pressures, field reversals, and high ion mobilities on the separate control of ion energy and ion flux. For example, we observe a significant reduction of the ion energy control range, if field reversals are the main ionization source of the discharge. The physical mechanisms behind this effect and others occurring in hydrogen and hydrogen/silane - discharges will be discussed.

Funded by the German Federal Ministry for the Environment, Nature Conservation and Nuclear Safety (0325210B).

[1] U. Czarnetzki et al. 2011 *PSST***20** 024010

[2] E. Schüngel et al. 2011 *J. Phys. D.***44** 285205

[3] J. Schulze et al. 2011 *PSST***20** 045008

[4] M. Kushner 2009 *J. Phys. D***42** 194013

Wednesday Afternoon, October 31, 2012

Energy Frontiers Focus Topic

Room: 15 - Session EN+TF-WeA

Thin Films for Energy Applications

Moderator: M. Filler, Georgia Institute of Technology

2:00pm EN+TF-WeA1 Batteries and Battery Materials by Vapor Deposition, N. Dudney, Oak Ridge National Laboratory INVITED

Although most commercial rechargeable batteries are prepared by bulk and powder processing methods, vapor deposition of materials has led to important advances for fundamental research, for modification of battery materials and interfaces, and also for commercialization of thin film batteries. Each of these areas will be illustrated with our studies of thin film materials for the electrolyte, anode, and cathode components of rechargeable lithium and lithium-ion batteries with both planar and 3-dimensional architectures.

4:00pm EN+TF-WeA7 Efficient Radiative and Non-Radiative Energy Transfer from Quantum Dots to Silicon Nanomembrane. Evidence of Waveguiding Phenomena, O. Seitz, H.M. Nguyen, W. Peng, Yu.N. Gartstein, Y.J. Chabal, A.V. Malko, University of Texas at Dallas

Nanostructured materials attract a considerable attention as potential candidates for practical photovoltaic (PV) devices. The majority of current hybrid PV architectures are based on charge transfer schemes, which frequently suffer from bad interface quality and poor carrier transport, consequently lowering the light conversion efficiency. An alternative is offered by non-contact energy transfer-based hybrid nanostructures, which combine strongly absorbing components, such as inorganic nanocrystal quantum dots (NQDs), and high-mobility semiconductor (SC) layers. It is envisioned that in such hybrid systems, the excitonic energy would be transferred via non-radiative energy transfer (NRET) and radiative (RET) waveguide coupling across the interface with the subsequent separation and transport of charge carriers entirely within the SC-based component. In this talk, we demonstrate the efficient excitonic sensitization of crystalline Si nanomembranes via combined effects of radiative (RET) and non-radiative (NRET) energy transfer from a proximal monolayer of colloidal semiconductor nanocrystals. Ultrathin, 25–300 nm Si films are prepared on top of insulating SiO₂ substrates and grafted with a monolayer of CdSe/ZnS nanocrystals via carboxy-alkyl chain linkers. The wet chemical preparation ensures that Si surfaces are fully passivated with a negligible number of non-radiative surface state defects and that the separation between nanocrystals and Si is tightly controlled. Combining atomic force microscopy (AFM), ellipsometry, time-resolved photoluminescence measurements and theoretical modeling, we could identify and quantify the individual contributions from RET and NRET, which all combined exceed 85% efficiency of energy transferred into the Si substrate when the nanocrystals are at about 4 nm from the interface. This demonstration supports the feasibility of an advanced thin-film hybrid solar cell concept that relies on energy transfer between strong light absorbers and adjacent high-mobility Si layers.

4:40pm EN+TF-WeA9 Synthesis of a Thin-Film Yttria-Stabilized-Zirconia (Y₂O₃-ZrO₂) Thin Films by Radical Enhanced Atomic Layer Deposition for μ -Solid Oxide Fuel Cell Applications, J. Cho, D. Membreno, B. Dunn, J.P. Chang, University of California, Los Angeles

Solid Oxide Fuel Cells (SOFCs) is one outstanding alternative energy devices, owing to its significantly higher fuel conversion efficiency than that of fossil fuel based ones while being more environmentally benign. Despite its tremendous advantages and potentials, however, the commercial applications of this technology have been restrained due to its intrinsic problems such as the use of expensive interconnectors and long start-up time, which are inevitably tied to its high operation temperatures (650–1000°C) to maintain high ionic conductivity of electrolytes. To fully utilize the revolutionary potentials of SOFCs in commercial applications, it is imperative to lower its operation temperatures to intermediate temperatures, below 700°C without sacrificing the efficiency of the cell.

Yttria-Stabilized-Zirconia (YSZ, (Y₂O₃)_x-(ZrO₂)_(1-x)) has been implemented as the electrolyte material of choice in SOFCs because of their high structural, chemical stability with along with high ionic conductivity at the operation temperatures of the cell. While the temperature of the cell could not be lowered as it compromises its conductivity, recent pioneering studies of YSZ in nanoscales have reported significantly enhanced ionic conductivities which could not only lower the working temperature of the cell much below 700°C, but will also allow an expansion in their potential applications even to power portable electronics, resulting in strong scientific

and technological interests in investigating the feasibility of developing YSZ in nanoscale for electrolyte applications in next-generation SOFCs, including μ -SOFCs for portable electronics. A thin-film YSZ has been synthesized by Radical Enhanced Atomic Layer Deposition (REALD), with thickness and composition controllability. The metal precursors, Tris(2,2,6,6-tetramethyl-3,5-heptanedionato)yttrium(III) [Y(tmhd)₃] and Bis(cyclopentadienyl)dimethylzirconium [Cp₂Zr(CH₃)₂] with Oxygen radicals as oxidant, were used to deposit Y₂O₃ and ZrO₂ with the deposition rates of 0.47 Å/cycle and 0.62 Å/cycle, respectively at ~250°C. The composition of each metal cations in YSZ thin films synthesized as a solid solution of Y₂O₃-ZrO₂ was found to correlate closely to the number of ALD cycles of each constituent oxide. The crystalline structures as well as the local environment of the deposited YSZ thin films were studied by X-ray diffraction (XRD) and Extended X-ray absorption fine structure (EXAFS). The conductivities of REALD YSZ films were found to be both a function of the thickness of YSZ film and the yttrium content in the film. The presence of conductivity enhancement effect on YSZ-SrTiO₃ nanoparticles are investigated as well.

5:00pm EN+TF-WeA10 ALD-enabled Tunneling and Transparent Conductive Oxide Layers for Novel Silicon Nanowire Solar Cells, M. Toivola, Picosun, Finland, C.L. Dezelah, Picosun USA, LLC

In order to enable more efficient harvesting of solar energy in the future, the recently ended (Dec 2011) EU 7th FP project ROD-SOL has successfully developed a novel, high efficiency solar cell based on Si nanostructures. The photoactive layer of this solar cell is a dense “forest” of adjacent Si nanowires (SiNW) deposited on metal or glass substrates. The 3D nanostructure of the NW forests offers various benefits over planar cell geometry, namely, more efficient light absorption due to light scattering in the NW forest, i.e. the NWs work as a light-trapping, antireflective layer.

The best solar cells in the project have already reached a promising value of near 10% efficiency and good long term stability. They were prepared with semiconductor-insulator-semiconductor concept, in which a 1–2 nm layer of ALD-deposited Al₂O₃ functions as a tunneling layer for the minority charge carriers between the SiNWs and the current collecting transparent conductive oxide (TCO) layer on the front side of the cell. Due to the high aspect ratio of the SiNWs ALD is the only method with which ultra-thin but highly uniform, conformal and pinhole-free tunneling layers can be coated on them. Also ALD-deposited, few hundreds of nm thick Al-doped ZnO (AZO) layer works as the TCO in SiNW solar cells, and we have investigated and optimized the electrical and optical properties of these layers.

AZO layers were prepared from trimethyl aluminum (TMA), diethyl zinc (DEZ) and deionized water (DIW). The varied parameters in AZO layers were deposition temperature (100 - 250 °C) and the percentage of Al in the ZnO matrix (0 - 11 %). The effects of post-ALD annealing and different TMA/DEZ/DIW pulsing orders were also tested.

The best conductivity (1–2 * 10⁻³ Ωm specific resistance) was achieved at 200 °C with a pulsing ratio of 5 % TMA and 95 % DEZ, equaling ~2 % elemental Al in ZnO. Reverse pulse order, i.e. starting the process with oxidant pulse instead of metal precursor, didn't result in significant performance improvement, neither did the annealing.

Optically, the ALD AZO films had high transparency over the visible wavelengths (no significant dependence on deposition temperature and/or Al doping-%) and refractive index 1.8 – 2, so the films work efficiently as conformal antireflective coatings on Si.

In short, ALD-deposited TCO layers offer a potential alternative to indium-doped tin oxide (ITO) and other scarce element containing TCO materials in solar cells. In the novel nanostructured photovoltaic devices ALD is typically the only method with which thin enough coatings of high quality material (i.e. dense, uniform, conformal, crack- and pinhole-free) can be deposited.

5:20pm EN+TF-WeA11 Effect of Top Electrodes on the Photovoltaic Properties of Ferroelectric PLZT Thin Film Capacitors, V. Nampoori, S. Kotru, The University of Alabama

Ferroelectrics are emerging as potential candidate materials for energy harvesting and storage. A recent report suggesting the possibility of above band gap voltages from ferroelectric materials has attracted the interest of research community to study these materials for the applications towards non-conventional solar cells devices. Although these ferroelectric solar cells materials do not exhibit very high conversion efficiency compared to the conventional solar devices, but the control of the PV characteristics with controlled polarization in these materials, gives it an edge over the semi-conducting counterparts. It is now, widely agreed that the PV effect in a ferroelectric material is induced by internal polarization of the material

which in turn separates the photo generated electron-hole pairs. However apart from controlling the polarization of the material, there are various other factors which could contribute to the PV output, choice of electrodes, is one among them.

In this work, PV response of ferroelectric PLZT thin film capacitors was investigated. The films were prepared using chemical solution deposition process. Capacitor type solar cells were fabricated from these films using various top electrodes. The IV curves were measured for each device. The ferroelectric/metal barrier as well as the bulk depolarizing field was shown to influence IV characteristics. Use of a metal top electrode with lower work function was found to increase the open circuit voltage (V_{oc}) from 0.17 V to 0.37 V. It was seen that use of a transparent conducting electrode could increase the V_{oc} further to $\sim 1.3V$. This in turn resulted in enhancement of PV efficiency of the devices. Such increase is attributed from the contribution of ferroelectric/metal barrier rather than from the bulk ferroelectric. These results indicate that choosing an appropriate top electrode can result in significant increase in the efficiency of the ferroelectric photovoltaic devices.

5:40pm **EN+TF-WeA12 Synthesis of Nano-structured Zn_3P_2 as a Solar Cell Absorber**, *P.S. Vasekar, S.P. Adusumilli, D. Vanhart, T. Dhakal*, Binghamton University

With rise in the prices and non-abundance of the materials like indium and gallium current research trends in thin film solar cells have been moving toward development of earth-abundant solar cell materials which can be synthesized using low-cost processes. Also zinc based hetero-junction partners are getting preference over toxic cadmium based compounds such as cadmium sulfide. Zn_3P_2 is also an important semiconductor from the II-V group and is used for optoelectronic applications. Zinc phosphide exhibits favorable optoelectronic properties such as direct bandgap of 1.5 eV which corresponds to the optimum solar energy conversion range. Also zinc phosphide has a large optical absorption coefficient of $>10^4 \text{ cm}^{-1}$, hence it can be positively used as a p-type absorber. Also due to its long minority diffusion length of $\sim 10 \mu\text{m}$, high current collection efficiency can be yielded. Zinc and phosphorous are quite abundant in earth's crust. It makes their cost-effective development quite feasible when it comes to large scale production. We have developed a very simple process using chemical reflux technique with Tri-octyl-phosphine (TOP) as a source of phosphorous. Zn_3P_2 has been synthesized in both nanowire and bulk form on zinc foil as well as glass substrates and initial results are quite encouraging. It has been observed that depending on the exposure method with TOP, either nanowire or bulk phase forms. Zinc metal when in contact with liquid TOP, develops nanowires in the range of 50-100 nm and the formation of nanowires exhibits a solution-liquid-solid (SLS) mechanism at the reaction temperature around 350 °C. To the best of our knowledge, zinc phosphide nanowire formation at this low temperature has been observed for the first time. Analysis has been carried out using SEM, XRD, TEM, XPS and PL.

Thursday Morning, November 1, 2012

Energy Frontiers Focus Topic

Room: 15 - Session EN+NS-ThM

Batteries and Fuel Cells

Moderator: Y. Wu, Purdue University

8:00am EN+NS-ThM1 Advanced Polymer Electrolyte Materials for Fuel Cell Applications, A.M. Herring, Colorado School of Mines INVITED

Proton exchange membrane (PEM) fuel cells are still the most desirable component of future zero emission, high efficiency automobiles fueled with hydrogen. However, their unit cost, ease of operation, and reliability must be reduced which includes eliminating the humidifier from the fuel cell system. Currently the commercial PEM is fabricated from a perfluorosulfonic acid (PFSA) polymer such as Nafion[®]. Unfortunately PFSA ionomers must be fully hydrated to achieve practical levels of proton conductivity which can only be achieved in vehicles operating at an inlet RH of 85% which still necessitates the use of a humidifier and undesirable complex water management and recovery. To achieve the goal of a PEM that can operate at temperatures from freezing to 120°C using dry inlet gases it will be necessary to develop new PEMs that are based on new chemistries or dramatically improved morphologies of existing chemistries. The versatility of the polymer electrolyte fuel cell could be expanded to more complex fuels with the use of an anion exchange membrane (AEM). An AEM fuel cell could potentially utilize less expensive metal catalysts and have the ability to oxidatively cleave carbon-carbon bonds.

Ionomers are generally perceived as being phase separated materials. However, the optimal morphology that an ionomer should adopt and that would be practical is still being debated. This situation is not helped by the uncertainty of the morphology adopted under operating fuel cell conditions of the incumbent material. Here I will describe a study that contrasts fully amorphous materials with materials designed to have phase separated morphologies of known symmetries and dimensions. While the designed materials allow us to probe certain concepts of ion conduction with pore shape and size, they do not necessarily out perform the amorphous materials. Curiously we show that the role of water has more to do with morphological changes in flexible materials than enhancing ion conduction in non-sulfonic acid based materials. This has implications for the fabrication of thin robust films that will be needed for an operating fuel cell. In the case of AEMs while a cation has yet to be found that is stable under hot and dry operation, water may be a necessary evil rather than an enhancer of anion conduction.

8:40am EN+NS-ThM3 Rational Design of Competitive Electrocatalysts for Hydrogen Fuel Cells, S. Stolbov, M. Alcántara Ortigoza, University of Central Florida

The large-scale commercial application of hydrogen fuel cells requires efficient and cost-effective electrocatalysts for the oxygen reduction reaction (ORR), which occurs on the cathode. We demonstrate that rational design can render electrocatalysts possessing both virtues. In this work, by unifying the knowledge on surface morphology, composition, electronic structure and reactivity, we find that tri-metallic sandwich-like structures are an excellent choice for optimization. Their constituting species are designed to couple synergistically rendering reaction-environment stability, cost-effectiveness and high catalytic activity. This cooperative-action concept enabled us to predict two Pt-free ORR electrocatalysts: Pd/Fe/W(110) and Au/Ru/W(110) [1]. Density functional theory calculations of the reaction free-energy diagrams indicate that these materials are more active toward ORR than the so far best Pt-based catalysts.

1. S. Stolbov and M. Alcántara Ortigoza; *J. Phys. Chem. Letts.* **3**, 463 (2012)

9:00am EN+NS-ThM4 Nanocomposite Materials for Lithium Ion Batteries, G. Yushin, Georgia Institute of Technology INVITED

High power energy storage devices, such as supercapacitors and Li-ion batteries, are critical for the development of zero-emission electrical vehicles, large scale smart grid, and energy efficient cargo ships and locomotives. The energy storage characteristics of supercapacitors and Li-ion batteries are mostly determined by the specific capacities of their electrodes, while their power characteristics are influenced by the maximum rate of the ion transport. The talk will focus on the development of nanocomposite electrodes capable to improve both the energy and power storage characteristics of the state of the art devices. Carbon-polymer and carbon-metal oxide nanocomposites have been demonstrated to greatly

exceed the specific capacitance of traditional electrodes for supercapacitors. Selected materials showed the unprecedented ultra-fast charging and discharging characteristics. Intelligently designed silicon-carbon-polymer composites showed up to 8 times higher specific capacity than graphite, the conventional anode material in Li-ion batteries, and stable performance for over 1000 cycles. In order to overcome the limitations of traditional composites precise control over the materials' structure and porosity at the nanoscale was required.

9:40am EN+NS-ThM6 Engineering Li_xAl_ySi_zO Ionic Conductive Thin Films by Atomic Layer Deposition for Lithium-ion Battery Applications, Y.-C. Perng, J. Cho, D. Membreno, N. Cirigliano, B. Dunn, J.P. Chang, University of California, Los Angeles

Lithium (Li)-ion batteries have drawn much attention for their outstanding performance in portable electronics applications with the potentials to function as a power source for further miniaturized devices, including micro-systems through the utilization of 3-dimensional electrodes based on high aspect ratio pillars. To realize this potential, an ultra-thin and highly conformal electrolyte layer is needed to coat the 3D electrode array. The ionic conductor lithium aluminosilicate (LiAlSiO₄) synthesized by atomic layer deposition (ALD) is a promising electrolyte material for 3D battery applications not only due to its high ionic conductivity along its c-axis resulting from channels formed by the alternating tetrahedra of aluminum-oxygen (Al-O) and silicon-oxygen (Si-O), but also expected to provide similar improved cell cyclability, as reported in the preliminary studies of ultra-thin metal-oxide ALD coatings on electrodes.

The self-limiting characteristic of ALD allows for precise control of thickness and composition of complex oxides and results in a highly conformal and pinhole-free coating suitable in 3D micro-battery applications or electrolyte surface coatings. The metal precursors used in this work are tetraethyl orthosilicate (TEOS), trimethylaluminum (TMA) and lithium t-butoxide (LTB). These precursors, along with water vapor as the oxidant, were used to deposit SiO₂, Al₂O₃ and Li₂O, with the deposition rates in the range of 0.8–2Å/cycle, respectively. The deposition rate of stoichiometric LiAlSiO₄ was ~20Å/cycle at a temperature of 290°C. The concentration of each metal element in Li_xAl_ySi_zO (LASO) thin films was found to correlate closely to ALD cycles and the associated incubation times. The crystallinity of the films after post-deposition rapid thermal annealing (RTA) was a function of cation atomic percentage. Li-ionic conductivities and the activation energy of as-deposited LASO films with respect to lithium contents as well as their relation to the film thickness were studied. The LASO ALD coating on 3D features, such as NWs and nanoparticles (NPs), were confirmed to be conformal and uniform by transmission electron microscopy (TEM) imaging. The cell performance as well as cyclability enhancement from Li_xAl_ySi_zO was investigated for a silicon-nanowire 3D microbattery, where SiNW was used as an anode, to explore the potentials of a solid-state SiNW battery with a solid-oxide electrolyte.

10:40am EN+NS-ThM9 Titanium Oxide and Lithium Titanium Oxide Coated 3D Nanoelectrodes for Li-ion Microbatteries, G. Pattanaik, J. Haag, M.F. Durstock, Air Force Research Laboratory

Titanium oxide based materials, including both Li-titanates and various TiO₂ polymorphs are promising alternatives to carbonaceous anode materials for Li-ion rechargeable batteries because of their higher voltage operation (enhanced safety), relatively small volume expansion upon lithiation, minimal electrode/electrolyte interface reactivity (nonexistent SEI layer), inexpensive and biocompatible non-toxic nature. Nanoscale three-dimensional (3D) architectures of current collectors for microbatteries would significantly increase the areal capacity over their planar counterparts, if the active Li-insertion electrode material could be coated conformally. The nanoscale thickness of the active electrode layer in combination with an electronically conducting 3D nanoarchitecture of the current collector should enable high areal capacity and fast charge-discharge rates.

Atomic layer deposition (ALD) is capable of growing conformal ultra thin films on complex 3D surface morphologies. We have used ALD to grow conformal layers of titanium oxide and lithium titanium oxide on various 3D nanoarchitectures including high aspect ratio nanoporous Al₂O₃ templates, template-electrodeposited 3D metal nanowire arrays and carbon nanotube buckypapers. The precursors for ALD used in this study include lithium t-butoxide, tetrakis(dimethylamido)titanium (TDMAT) and water. We have been able to grow conformal layers with controllable thickness at nanometer scale uniformly coated around the high aspect ratio features.

A significant increase in areal capacity (up to two orders of magnitude) was obtained in anatase TiO₂ coated Ni nanowire arrays over 2D thin film

electrodes of a similar footprint. ALD TiO₂ coated buckypapers showed specific capacities in excess of 200 mAh/g at C/10, with 70% of the capacity retained at 5C. At 1C, 95% of the initial capacity is retained after 500 charge/discharge cycles. ALD deposition of LiOx and TiOx and subsequent thermal annealing leads to a combination of TiO₂ and spinel lithium titanium oxide (Li₄Ti₅O₁₂) phases. The presence of these phases is reflected in XRD as well as electrochemical charge-discharge curves. This presentation will discuss a systematic study of the ALD growth of 3D titanium oxide and lithium titanium oxide nanostructures and their electrochemical characterization.

11:20am EN+NS-ThM11 **The Contribution of Auger Electron Spectroscopy to a Better Understanding of the Lithiation Process Occurring in Si-based Anodes Designed for Li-ion Batteries.** E. Radvanyi, E. De Vito, W. Porcher, S. Jouanneau, CEA Grenoble, France

With a specific capacity of almost 3580 mAh.g⁻¹ at room temperature (corresponding to the Li₁₅Si₄ alloy), silicon is a promising element for designing new efficient anodes in Li-ion battery technology. However, because of huge material volumic expansion (around 300%) during the lithiation process¹, leading to a quick pulverization of the electrode², silicon has been used only as an additive to graphite in commercial cells so far³. In order to improve Si-based electrodes cyclability, a better understanding of the lithium insertion mechanisms is among the key issues⁴. The study of the lithiation process in silicon particles is particularly challenging. Indeed, a complete amorphization of the material during cycling⁴ makes difficult the use of surface characterization techniques based on beam diffraction (e.g. X-rays or electrons). In this study, we have used Auger Electron Spectroscopy (AES) to study these mechanisms. Poor attention has been focused on AES in the battery research field so far^{5,6}. In this work we emphasize its interest, notably for the study of the lithiation mechanisms in silicon particles. The first part of this work is dedicated to the study of Li-Si alloys by using AES. Several crystalline Li_xSi alloys (Li₇Si₃, Li₁₃Si₄ and Li₂₂Si₅) have been synthesized and characterized by X-Ray diffraction and AES. It appears that the atomic relative concentrations obtained by AES for the elements Li and Si are accurate with a tolerance of approximately 10%. The effect of Ar⁺ sputtering has also been investigated. After this initial work, six electrodes based on silicon particles have been analyzed by using AES for different "State Of Charge" (SOC) within the first electrochemical cycle.

For each SOC, several silicon particles have been investigated individually. Li and Si depth concentration profiles have been achieved by following Li (KLL) and Si (LVV) Auger transitions. Thanks to the good spatial resolution (17 nm at 10kV/InA), it is possible to detect inhomogeneities of Li concentration at the particle surface. Based on the results obtained on different silicon particles at several SOC, a lithiation model is proposed and discussed.

- (1) Beaulieu, L. Y.; Hatchard, T. D. ; Bonakdarpour, A. ; Fleischauer, M. D.; Dahn, J. R. *J. Electrochem. Soc.* **2003**, *150*(11), A1457-A1464
- (2) Kasavajjula, U.; Wang, C.; Appleby, A. J. *J. Power Sources* **2007**, *163* (2), 1003-1039
- (3) www.hitachi.com
- (4) Zhang, W. J. *J. Power Sources* **2011**, *196* (1), 13-24
- (5) Morigaki, K. I.; Ohta, A. *J. Power Sources* **1998**, *76* (2), 159-166
- (6) Kim, Y. J., Lee, H.; Sohn, H. J. *Electrochem. Comm.* **2009**, *11* (11), 2125-2128

11:40am EN+NS-ThM12 **Organic/Inorganic Composite Materials as Anodes for Lithium Ion Batteries**, M. Thakur, R.B. Pernites, Rice University, M. Isaacson, Lockheed Martin Space Systems, M.S. Wong, Rice University, S.L. Sinsabaugh, Lockheed Martin MS2, S.L. Biswal, Rice University

Silicon continues to draw great interest as an anode material for lithium ion batteries due to its large specific capacity for lithium. Electrochemical etching silicon is one of several anode materials of interest, but its energy density is oftentimes limited due to its attachment to an unreactive silicon substrate. Here, we present a novel "liftoff" method by which a freestanding macroporous silicon film (MPSF) is electrochemically detached from the underlying bulk silicon and combined with pyrolyzed polyacrylonitrile (PAN), a conductive polymer. We report the performance of these silicon thin films with and without pyrolyzed PAN.

Surface Science

Room: 21 - Session SS+EN+OX-ThM

Catalysis and Photocatalysis on Oxides

Moderator: Z. Dohnalek, Pacific Northwest National Laboratory

8:00am SS+EN+OX-ThM1 **Photoelectrochemical Water Splitting under Sunlight Irradiation using Oxynitride Electrodes Fabricated by Particle Transfer Method**, K. Domen, J. Kubota, The University of Tokyo, Japan **INVITED**

Hydrogen production through the photoelectrochemical (PEC) water splitting is one of the attractive ways to convert solar energy to storable chemical energy. The availability of powder semiconductor materials through coating methods for preparing photoelectrodes is a one of strong point of PEC cells. Even if the surface is a rough particle layer, the electrolyte solution automatically forms the desirable solid-liquid interface for whole semiconductor surfaces, where photoexcited carriers are separated by electric field.

Oxynitride and oxysulfide materials are promising candidates for photoelectrodes for water splitting. Among them, LaTiO₂N has a proper band structure from the view point of driving solar water splitting. The material shows photocatalytic hydrogen and oxygen evolutions in half reactions using sacrificial reagents, indicating that the material have a proper band structure to drive PEC water splitting. LaTiO₂N absorbs visible light up to 600 nm ($E_g = 2.1$ eV), so that they can capture more solar energy than oxide photocatalysts, which typically have absorption in the UV region. Photoelectrodes based on the material have been studied extensively, however, the photocurrent was low due to the lack of good preparation method of the electrode.

In the present study, we report a novel fabrication method of photoelectrodes for PEC water splitting using semiconductor powders. This method, which we have termed the particle transfer (PT) method, is shown to be applicable to a variety of semiconductor powders. LaTiO₂N was demonstrated to exceed those prepared by the conventional method of photoelectrode fabrication from powder materials.

8:40am SS+EN+OX-ThM3 **Multi-step Photooxidation of CO on TiO₂(110)**, G.A. Kimmel, N.G. Petrik, Pacific Northwest National Laboratory

TiO₂ is an important photocatalyst with many practical applications. However, a detailed understanding of the relevant physical and chemical processes for the photocatalysis remains elusive. We have studied the photooxidation of CO adsorbed on rutile TiO₂(110) during UV irradiation with ~1 ms time resolution. Previous investigations with ~0.1 s resolution found that the maximum CO₂ photon-stimulated desorption (PSD) signal occurred for the first data point and then decreased monotonically with increasing irradiation time. However our experiments with improved time resolution show that the initial rate of CO₂ production is zero, and then increases smoothly to a maximum before decreasing at longer irradiation times. Experiments varying the UV photon flux show that the CO₂ PSD kinetics are proportional to the photon fluence but are independent of the photon flux (for the range investigated). The photon fluence required to reach the maximum CO₂ PSD signal increases as the initial coverage of chemisorbed O₂ increases – an effect that we attribute to changes in the initial charge state of the chemisorbed O₂. These results demonstrate that the production of CO₂ proceeds through the formation of stable precursor. The angular distribution of the photodesorbing CO₂, which is peaked at ~40° with respect to the surface normal perpendicular to the BBO rows, is also consistent with the production of CO₂ from a precursor state. Previously, the photooxidation of CO on TiO₂(110) was believed to occur in a single non-thermal reaction step: CO + O₂ + hv -> CO₂ + O_{ad}. However, our results show that the photooxidation of CO requires at least two non-thermal reaction steps – one to form the precursor and a second to produce the CO₂. We will compare the experimental results to DFT calculations and discuss the role of photo-generated electrons and holes in the photooxidation of CO. These results show that the photooxidation of CO on TiO₂ is more complicated than previously appreciated.

9:00am SS+EN+OX-ThM4 **Design of Band Engineered Photocatalysts using Titanium Dioxide**, S.W. Ong, D.E. Barlaz, E.G. Seebauer, University of Illinois at Urbana Champaign

Difficulties in achieving control over carrier concentration have impeded progress toward tailoring the electric fields in semiconducting oxide photocatalysts based upon principles of electronic band engineering drawn from classical optoelectronics. The present work demonstrates such principles using the model case of methylene blue photo-oxidation over

thin-film anatase TiO₂ grown by atomic layer deposition. The carrier concentration in the polycrystalline semiconductor is controlled over a range of 2.5 orders of magnitude via an unconventional means - film thickness, which indirectly influences the concentration of electrically active donor defects at grain boundaries. Over this range, the reaction rate constant varies by more than a factor of 10, and is well described by a quantitative one-dimensional model for photocurrent. The model suggests that the changes in rate result fundamentally from variations in the width of the space charge layer near the surface. Electrical characterization of the films by capacitance-voltage measurements and ultraviolet photoelectron spectroscopy, together with detailed physical characterization by a variety of techniques, confirm this picture. Prospects for better control of grain boundary donor defects through film synthesis procedures are discussed.

9:20am **SS+EN+OX-ThM5 Adsorption of CO₂ on Oxygen Precovered TiO₂(110) Surfaces.** X. Lin, Y. Yoon, N.G. Petrik, G.A. Kimmel, Z. Li, Z.-T. Wang, B.D. Kay, I. Lyubinetsky, R. Rousseau, Z. Dohnalek, Pacific Northwest National Laboratory

Rutile TiO₂(110) was employed as a model oxide surface to investigate the adsorption behavior of CO₂ by means of scanning tunneling microscopy (STM) and density functional theory (DFT). STM images of partially reduced TiO₂(110) surfaces obtained before and after *in-situ* dosing of CO₂ molecules at 50 K show that CO₂ adsorbs preferentially on oxygen vacancy (V_O) sites. Since the reaction of CO₂ with oxygen adatoms (surface hydroxyl groups) may lead to the formation of carbonate (bicarbonate), O₂ (H₂O) was pre-dosed to form oxygen adatom (hydroxyl) covered TiO₂ surfaces. On the oxygen precovered surfaces, CO₂ molecules were found to preferentially bind on the Ti sites next to oxygen adatoms (O_a's) and form CO₂/O_a complexes, while on hydroxylated surfaces no interactions were observed between CO₂ and hydroxyl groups. CO₂ binding to O_a's is weak as revealed by the dissociation of the CO₂/O_a complexes at 50 K where CO₂ diffuses away along the Ti row. The weak binding indicates that CO₂ is bound to O_a only via dispersion forces. Temperature dependent studies (100 - 150 K) show that the CO₂ binding energy next to O_a's is smaller by ~20 mV than that on V_O's. At 50 K, however, the adsorption of CO₂ on V_O is partially hindered by the higher adsorption barrier. CO₂ molecules diffusing between two CO₂/O_a complexes are found to move fast compared to the STM sampling rate and are imaged as a time average of all CO₂ binding configurations on Ti sites. DFT studies reveal the rotation-tumbling mechanism for CO₂ diffusion with a very low diffusion barrier (~ 50 meV) in agreement with the experiment.

X.L. is grateful for the support of the Linus Pauling Distinguished Postdoctoral Fellowship Program at PNNL. This work was supported by the US Department of Energy, Office of Basic Energy Sciences, Division of Chemical Sciences, Geosciences & Biosciences. A portion of the research was performed using EMSL, a national scientific user facility sponsored by the Department of Energy's Office of Biological and Environmental Research and located at Pacific Northwest National Laboratory (PN NL). PNNL is a multiprogram national laboratory operated for DOE by Battelle.

9:40am **SS+EN+OX-ThM6 Probe of NH₃ and CO Adsorption on the Very Outermost Surface of a Porous TiO₂ Adsorbent Using Photoluminescence Spectroscopy.** A. Stevanovic, J.T. Yates, Jr., University of Virginia

The photoluminescence (PL) of powdered TiO₂ at 529.5 nm (2.34 eV) has been found to be a sensitive indicator of UV-induced band structure modification. As UV irradiation occurs, the positive surface potential changes and shifts the depth of the depletion layer. It was found that UV light (3.88 eV) induces a positive surface potential which diminishes band bending in n-type TiO₂ and enhances PL1. Also, adsorbates modify the PL intensity by exchanging charge with TiO₂, producing a change in the surface band bending structure.

In addition, we employ photoluminescence (PL) spectroscopy to probe the development of adsorbed layers on the very outermost surface sites of a porous solid adsorbent (TiO₂) in a depth of 20 nm where the meso-pores, separating 30-80 nm TiO₂ particles, join the gas phase. In parallel, we also employ transmission infrared (IR) spectroscopy to gain insight into the extent of adsorption averaged over the entire depth of the diffusion process. The combination of the two surface spectroscopies (PL and IR) allows one to observe the kinetics of transport of adsorbate molecules between the very outermost surface region (where adsorption first occurs) and the interior of the powdered substrate. The transport is governed by the surface mobility of the adsorbate molecules, and hysteresis effects in adsorption/desorption are observed.

References:

1. Stevanovic, A.; Buttner, M.; Zhang, Z.; Yates, J. T., Jr., Photoluminescence of TiO₂: effect of UV light and adsorbed molecules on

surface band structure. *Journal of the American Chemical Society* **2012**, *134*, (1), 324-32.

2. Stevanovic, A.; Yates, J. T., Jr., Probe of NH₃ and CO Adsorption on the Very Outermost Surface of a Porous TiO₂ Adsorbent Using Photoluminescence Spectroscopy. *Langmuir : the ACS journal of surfaces and colloids* **2012**, *28*, (13), 5652-9.

Work supported by the Army Research Office.

10:40am **SS+EN+OX-ThM9 Site-Specific Photocatalytical Reactions of O₂ on TiO₂(110).** Z.-T. Wang, Pacific Northwest National Laboratory, N.A. Deskins, Worcester Polytechnic Institute, I. Lyubinetsky, Pacific Northwest National Laboratory

Photo-stimulated reactions on TiO₂ have attracted much attention due to the variety of potential applications ranging from a hydrogen production by water splitting to environmental remediation through organic pollutant oxidation. In majority of these processes, the oxygen plays a crucial role. A better understanding of the fundamental aspects of oxygen on TiO₂ can potentially lead to improvements or developments of the TiO₂ applications. We present the direct observation at an atomic level with high-resolution scanning tunneling microscopy of photostimulated reactions of single O₂ molecules on reduced TiO₂(110) surfaces at 50 K. The critical relation between photoreactivity and adsorption sites on TiO₂ is demonstrated. Two distinct reactions of O₂ desorption and dissociation occur at different active sites of terminal Ti atoms and bridging O vacancies, respectively. These two reaction channels follow very different kinetics. While hole-mediated O₂ desorption is promptly and fully completed, electron-mediated O₂ dissociation is much slower and is quenched above some critical O₂ coverage. Density functional theory calculations indicate that both coordination and charge state of an O₂ molecule chemisorbed at specific site largely determine a particular reaction pathway.

11:00am **SS+EN+OX-ThM10 Bond Selectivity in the Activation of n-alkanes on PdO(101).** J.F. Weaver, A. Antony, C. Hakanoglu, F. Zhang, University of Florida, A. Asthagiri, The Ohio State University

We have investigated initial C-H bond selectivity in the activation of propane and n-butane on PdO(101) both experimentally and computationally. Temperature-programmed experiments using different propane isotopologues reveal a strong preference toward primary C-H bond cleavage of propane on PdO(101); about 90% of the propane molecules which react do so by primary C-H bond activation. Direct measurements of the initial dissociation probability of various n-butane isotopologues also demonstrate a high selectivity for primary C-H bond activation of n-butane on PdO(101) at low coverages. Unlike propane, however, TPRS experiments show that the preference for primary C-H bond cleavage of n-butane diminishes with increasing molecular coverage. Calculations using dispersion-corrected DFT reproduce the selectivity toward primary C-H bond cleavage of propane and n-butane on PdO(101), and predict that alkane C-H bond scission occurs heterolytically on the oxide surface. The calculations suggest that greater substituent polarization in the 1-alkyl transition structures is responsible for the lower energy barriers for primary vs. secondary C-H bond activation of alkanes on PdO(101).

11:20am **SS+EN+OX-ThM11 Photoresponse, Electronic Transport and Magnetic Properties of Ti-doped (Cr_xFe_{1-x})₂O₃.** S.E. Chamberlin, T.C. Kaspar, M.E. Bowden, V. Shuthanandan, S.A. Chambers, M.A. Henderson, Pacific Northwest National Laboratory

There is widespread interest in discovering materials that can effectively harvest sunlight in the visible region of the electromagnetic spectrum in order to drive chemical processes on surfaces. Hematite (Fe₂O₃) has received renewed interest recently as the active photoanode in photoelectrochemical (PEC) water splitting to store solar energy as H₂. Hematite has three key advantages which make it appealing: it is very abundant, it has a bandgap of 2.2 eV, which is suitably narrow to harvest incident solar radiation, and it is sufficiently stable in the aqueous solutions required for PEC water splitting. However, hematite is a charge-transfer insulator with extremely poor electron and hole mobilities, which results in short hole diffusion lengths and ultrafast recombination of photogenerated electron/hole pairs before charge separation can occur. Substitutional Ti(IV) at an Fe(III) site should be a donor, and epitaxial Ti-doped α-Fe₂O₃ exhibits significantly enhanced conductivity relative to pure hematite when grown under certain conditions by oxygen-assisted molecular beam epitaxy (OAMBE) on α-Al₂O₃(0001) substrates.¹ In addition, Mashiko *et al.*² have shown that the bandgap of pure hematite can be reduced to 1.7 eV by alloying with Cr(III) in epitaxial films. Combining these approaches is expected to result in material with both a reduced bandgap and favorable electrical conductivity, which will facilitate visible-light photoactivity. Heteroepitaxial thin films of (Fe_{1-x}Cr_x)₂O₃ and (Fe_{1-x}Cr_xTi_y)₂O₃ were deposited on α-Al₂O₃(0001) substrates by OAMBE. Film quality was monitored *in situ* by reflection high energy electron diffraction (RHEED).

In situ x-ray photoemission spectroscopy (XPS) was utilized to characterize the charge states of the cations. Film crystallinity and lattice parameters were determined *ex situ* by high resolution x-ray diffraction (HRXRD). Rutherford backscattering spectrometry (RBS) in both random and channeling geometries confirmed the film stoichiometry, and elucidated the degree of substitution of the cations in the lattice. Preliminary optical absorption measurements and photochemistry experiments will be presented.

1. B. Zhao, T. C. Kaspar, T. C. Droubay, J. McCloy, M. E. Bowden, V. Shutthanandan, S. M. Heald, and S. A. Chambers, *Phys. Rev. B* 84, 245325 (2011).

2. H. Mashiko, T. Oshima, and A. Ohtomo, *Appl. Phys. Lett.* 99, 241904 (2011).

11:40am **SS+EN+OX-ThM12 A Nonadiabatic Mechanisms of Inequilibrium Charge Carriers Production in Pd/n-GaP Schottky Nanodiode Exposed to Atomic Hydrogen, S.V. Simchenko, V. Styrov, Azov State Technical University, Ukraine**

Since the recent discovery of production of electronic flows in Schottky diodes with nanosized "top" metal layer due to ballistic metal-to-semiconductor transport of hot electrons formed by the surface exoergic chemical reaction, e.g. [1], this effect attracts attention of scientists owing to its fundamental and practical potential. Here we investigate a new system of that kind, namely Pd-(n)GaP planar Schottky diode (15 nm Pd-layer) placed in the atmosphere of atomic hydrogen. We found the steady-state current flow through the system under consideration in perpendicular direction to the metal surface on which the hydrogen atoms stationary recombine into molecules.

We elaborated a new approach to detect production of the inequilibrium charge carriers via nonadiabatic channel by observing the current-voltage characteristic of the Schottky diode in the presence and absence of the atomic flux incident on the structure. The nonequilibrium nature of the additional carriers is confirmed by kinetics measurements: the current drops to its initial value in the absence of atoms practically momentarily once the atoms are "switched off" and jumps immediately to its excited value when atoms are "switched on" (at the given temperature of the structure and the fixed forward voltage bias on the structures). We were able to draw some quantitative information about the processes of generation of nonequilibrium electron-hole pairs in the reaction of recombination of hydrogen atoms on Pd-surface and their transport in the metal film. The short circuit current is expressed in terms of yield of the chemoexcited carriers and probability of their survival while traveling through the Pd-film.

For a 1V forward bias the current drastically grows from 3 nA to 950 uA; thus the bias allows gaining chemi-current value as large as five orders of magnitude. This result can be of significant importance for the practical applications of the nonequilibrium chemiconductance and chemi-currents in Schottky nanostructures including sensing and chemical-to-electricity energy conversion.

[1] B. Georgen, H. Nienhaus, W.H. Weinberg, E. McFarland. *Science*, 294, 2521 (2003)

Transparent Conductors and Printable Electronics

Focus Topic

Room: 7 - Session TC+EM+AS+TF+EN-ThM

Transparent Conductors and Devices

Moderator: L.M. Porter, Carnegie Mellon University

8:20am **TC+EM+AS+TF+EN-ThM2 High Conductivity in Thin ZnO:Al Deposited by Means of the Expanding Thermal Plasma Chemical Vapor Deposition, K. Sharma, H.C.M. Knoops, M.V. Ponomarev, Eindhoven University of Technology, The Netherlands, R. Joy, M. Velden, D. Borsa, R. Bosch, Roth and Rau BV, Germany, W.M.M. Kessels, M. Creatore, Eindhoven University of Technology, The Netherlands**

Session: Transparent Conductors and Devices

The ever-increasing demand for transparent conducting oxides (TCO) for application in flat panel displays, light emitting diodes (LEDs), and thin film photovoltaics drives the present research in the field of TCOs. Aluminum-doped zinc oxide (ZnO:Al) is often referred to as a potential alternative to e.g. indium tin oxide. The ZnO:Al is considered appealing due to the relatively low cost, high abundance, non-toxicity, resistance to H₂ etching and, under specific conditions, surface texturing for light management/trapping. Thin ZnO:Al films (~ 100 nm) with low resistivity

(2-5 * 10⁻⁴ ohm*cm) along with high transmission (> 85 %) are desirable in many devices. Furthermore, large area processing/ high throughput are essential pre-requisites for industrial applications.

ZnO:Al thin films (< 150 nm) have been deposited by using an in-line industrial expanding thermal plasma chemical vapor deposition (ETP-CVD) technique,^{1,2,3} by means of O₂/diethylzinc/trimethylaluminum mixtures. High diethyl zinc flow rate conditions² were applied, which enable the development of a conductive (5 · 10⁻⁴ Ω·cm), 300 nm-thick ZnO:Al layer by promoting the development of a densely packed structure at early stages of growth, as very recently reported.²

In the present contribution, the effect of the dopant, i.e. trimethylaluminum, is investigated to further improve the electrical quality of even thinner ZnO:Al layers. ZnO:Al films were analyzed with spectroscopic ellipsometry, four point probe, hall measurements, X-ray photon spectroscopy (XPS), Rutherford backscattering (RBS), elastic recoil backscattering (ERD), and X-ray diffraction (XRD).

A remarkable low resistivity of 5 · 10⁻⁴ Ω·cm was measured for a ZnO:Al film with thickness of only 120 nm, characterized by a carrier concentration of 1 · 10²¹ cm⁻³, with an electron mobility in the range of 10-25 cm²/V · s.^{2,3} The obtained mobility values are higher than previously reported value of 13 cm²/V · s for 300 nm thick ZnO:Al.² The improvement in terms of conductivity is attributed to the large hydrogen content (2-4 · 10²¹ at/cm³) promoting the chemical passivation of the grain boundaries.

A broad characterization of highly conductive thin ZnO:Al films along with insights on charge transport process will be presented.

Reference List

1. B. Hoex *et al.*, *Progress in Photovoltaics* **13**, 705 (2005).

2. M. V. Ponomarev *et al.* *Journal of Applied Physics* **112**, 043708 (2012).

3. M. V. Ponomarev, *et al.*, *Journal of Applied Physics* **111**, 063715 (2012).

8:40am **TC+EM+AS+TF+EN-ThM3 Recent Progress in Oxide Semiconductors and Oxide TFTs, H. Hosono, Tokyo Institute of Technology, Japan**

INVITED

Transparent conductive oxides (TCOs) and transparent oxide semiconductors (TOSs) have a long history since 1950s. The material design concept for TCOs looks almost established, i.e., ionic oxides p-block metals with an electronic configuration of (n-1)d¹⁰ns⁰ and a spatial spread of ns orbitals which is enough to have large overlap with neighboring metal ns orbitals irrespective of intervening oxygen ion¹. Concretely, most of the TCOs have been realized in the material systems of In₂O₃-SnO₂-CdO-Ga₂O₃-ZnO. Materials based on light metal oxides such as Al₂O₃ and SiO₂ have not been regarded as the candidates of TCOs. In 2002, we² reported high electronic conductivity in 12CaO·7Al₂O₃(C12A7) which had been a typical insulator and this discovery was followed by transparent conductivity in cubic SrGeO₃ in 2011.³ These two materials are TCOs realized by a new material design concept.

As for TOS, the striking advances are seen in transparent amorphous oxide semiconductors (TAOS) in science and technology due to strong demand for active layer materials in thin film transistors (TFTs). Amorphous In-Ga-Zn-O (IGZO) TFTs, which was first reported in late 2004,⁴ has adopted to drive high resolution displays of new iPad.⁵ This is a first mass production of TOS family. The major reasons for this adoption are high electron mobility (an order of larger than that of a-Si:H) and easy fabrication process. A major advance in TOS-TFTs is realization of p-channel TFTs and subsequent fabrication of C-MOS using ambipolar SnO.⁶

In this talk, I review these progresses viewed from electronic state of these materials.

1) H. Kawazoe, H. Yanagi, K. Ueda, and H. Hosono. *MRS Bull.* 25, 28 (2000)

2) K. Hayashi, S. Mitsuishi, T. Kamiya, M. Hirano, H. Hosono. *Nature* 419, 462 (2002).

3) H. Mizoguchi, T. Kamiya, S. Mitsuishi, H. Hosono. *Nat. Commun.*, 2, 470 (2011).

4) K. Nomura, H. Ohta, A. Takagi, T. Kamiya, M. Hirano, H. Hosono. *Nature* 432, 488 (2004).

5) Sharp Press Release April 6, 2012

6) K. Nomura, T. Kamiya, and H. Hosono. *Adv. Mater.*, **23**, 3431 (2011)

9:20am **TC+EM+AS+TF+EN-ThM5 Surface Functionalization of Amorphous Zinc Tin Oxide Thin Film Transistors, G.S. Herman, M.S. Rajachidambaram, Oregon State University, A. Pandey, S. Vilayurganapathy, P. Nachimuthu, S. Thevuthasan, Pacific Northwest National Laboratory**

Amorphous zinc tin oxide semiconductor materials have been studied primarily as the active semiconducting material for thin film transistors

(TFT) for applications including transparent and flexible electronics. Due to the amorphous nature of these materials excellent uniformity can be obtained over large areas while still having reasonably high electron mobilities ($>10 \text{ cm}^2/\text{Vs}$). Considerable control over the electrical properties of ZTO can be maintained, where insulating, semiconducting, and conductive films can be obtained by varying the processing and post-annealing conditions. We have recently characterized sputter-deposited zinc tin oxide (ZTO) as the active material for TFTs and found that the switching properties of ZTO are closely related to deposition, post-annealing, and electrical test conditions. In this presentation we will discuss bias stress induced instabilities for ZTO TFTs. We have found that devices with a backchannel exposed to the atmosphere have a positive subthreshold shift under positive bias, which can be well explained by a stretched exponential model. Using this model the shifts may be related to either electron trapping at the dielectric semiconductor interface or due to metastabilities of the active material. We have found that the adsorption of a self-assembled monolayer (SAM) on the backchannel of the TFT effectively passivates the device and significantly reduces the bias stress induced instabilities. In this study we will present contact angle measurements and x-ray photoelectron spectroscopy to better understand the interaction of the SAM with the ZTO surface, and the improved the stability of the ZTO TFTs will be discussed in regards to the interfacial chemistry of the backchannel.

9:40am **TC+EM+AS+TF+EN-ThM6 Work Function and Valence Band Structure of Oxide Semiconductors and Transparent Conducting Oxides Grown by Atomic Layer Deposition**, *A. Yanguas-Gil*, Argonne National Laboratory, *R.T. Haasch*, University of Illinois at Urbana Champaign, *J.A. Libera, J.W. Elam*, Argonne National Laboratory

Atomic Layer Deposition offers a low-temperature, scalable route to the synthesis of a wide range of oxide semiconductors and transparent conducting oxides both in flat and high aspect ratio surfaces. We have carried out studies on the influence of concentration and spatial distribution on the electrical properties within the $\text{ZnO-SnO}_2\text{-In}_2\text{O}_3$ compositional map, including standard TCO materials such as Al:ZnO and ITO. We will present results on the work function and valence band structure of transparent conducting oxides grown by ALD using ex-situ UPS measurements, including the influence of the surface termination on the interfacial properties of the materials. Finally, the ability of ALD to tailor the surface and interfacial properties of TCOs based on its layer-by-layer nature will be discussed.

10:40am **TC+EM+AS+TF+EN-ThM9 Low Temperature, High Performance Solution-Processed Metal Oxide Thin Film Transistors formed by a 'Sol-Gel on Chip' Process**, *H. Sirringhaus*, University of Cambridge, UK **INVITED**

N-type amorphous mixed metal oxide semiconductors, such as ternary oxides, where M^1 and M^2 are metals such as In, Ga, Sn, Zn, have recently gained momentum because of high carrier mobility and stability and good optical transparency, but they are mostly deposited by sputtering. To date only limited routes are available for forming high-performance mixed oxide materials from solution at low process temperature $< 250^\circ \text{C}$. Ionic mixed metal oxides should in principle be ideal candidates for solution processible materials because the conduction band states derived from metal s-orbitals are relatively insensitive to the presence of structural disorder and high charge carrier mobilities are achievable in amorphous structures. Here we report the formation of amorphous metal oxide semiconducting thin films via a 'sol-gel on chip' hydrolysis approach from soluble metal alkoxide precursors, which affords unprecedented high field-effect mobilities of $10 \text{ cm}^2/\text{Vs}$, reproducible and stable turn-on voltages $V_{\text{on}} \gg 0\text{V}$ and high operational stability at maximum process temperature as low as 230°C . We discuss the effect of film composition on device performance and stability.

11:20am **TC+EM+AS+TF+EN-ThM11 In Situ Measurements of Interface States and Junction Electrical Properties of Electrically Biased Metal / $\beta\text{-Ga}_2\text{O}_3$ Structures**, *H. Pham, X. Zheng, B. Krueger, M.A. Olmstead, F.S. Ohuchi*, University of Washington

A significant issue in application of wide-band-gap transparent conducting oxides is formation of reliable ohmic and rectifying metal contacts. The metal-oxide interface properties are dominated by chemical reactions during growth and the resultant interface state distribution once the interface is formed. We have investigated interface formation between the wide band gap TCO $\beta\text{-Ga}_2\text{O}_3$ ($E_g = 4.8 \text{ eV}$) and the metals Pd, Ni, Ti and Al with in-situ x-ray photoemission spectroscopy (XPS) both during growth and during sputter profiling. The two techniques give very similar results, demonstrating that in this case sputter profiling does not significantly alter the interface chemistry. Consistent with the relative compound heats of formation, Ni and Pd show very little interface reaction with either Ga or O, while Ti interacts strongly with both Ga and O and Al interacts primarily with oxygen. Electrically, Ni and Pd have similar Schottky barriers on the intrinsically n-type oxide (about 0.9 eV), Ti forms a symmetric, nearly

ohmic contact, while Al exhibits a smaller barrier (about 0.6 eV). To probe the nanoscopic origins of the Schottky contact behavior through the interface state energy distribution, we combined *in-situ* deposition of thin metal layers and application of forward/reverse biases to the metal-oxide junction with XPS measurements of the relative positions of the Ga_2O_3 bands (via the Ga 3d or O 1s core level) and the metal Fermi level. The density of interface states determines the rate at which the Fermi level can be moved through the oxide band gap, so variation of the oxide core-level shift with respect to the bias voltage yields the interface state density. We find the metal and oxide bands maintain their relative alignment under forward bias (back-plane negative with respect to metal), while they separate at a rate about half that of the applied bias under reverse bias (positive bias with respect to metal).

11:40am **TC+EM+AS+TF+EN-ThM12 Atmospheric Pressure Dielectric Barrier Discharge (DBD) Post Annealing of Aluminium Doped Zinc Oxide (AZO) Films**, *Y.L. Wu, E. Ritz, J. Hong, T.S. Cho, D.N. Ruzic*, University of Illinois at Urbana Champaign

Aluminum-doped Zinc Oxide (AZO) is a material that has high electrical conductivity while being highly transparent at the same time. It could find many useful applications in our daily lives such as displays, mobile devices, solar cells, etc. Currently AZO films are considered as attractive alternatives to materials such as Indium Tin Oxide (ITO) due to its much cheaper cost and comparable high electrical conductivity. A process of depositing AZO film by dual DC magnetron system has been developed. Film thicknesses were measured to be about 300nm by stylus contact profilometer and transparency of greater than 90% in the visible range were measured with spectrophotometry methods. Film conductivities were in the order of 10^{-3} Ohm-cm with the four-point probe method. By using a Dielectric Barrier Discharge operating at atmospheric pressure, conductivity of film can be further lowered. A $500\text{mm} \times 30\text{mm}$ line source operating at a Nitrogen flow of 250L/min was used and $\sim 0.4\text{L/min}$ Hydrogen gas was also introduced into the discharge system to create Hydrogen radicals. A 10%-15% decrease in electrical resistance was observed with no changes in the optical properties of the AZO films. The elemental composition of the film was measured by X-ray photoelectron spectroscopy (XPS) and the change of crystal structure after DBD post annealing was measured by X-ray diffraction (XRD).

Thursday Afternoon, November 1, 2012

Energy Frontiers Focus Topic
Room: 15 - Session EN+AS-ThA

Characterization of Energy Materials and Systems

Moderator: L. Lohstreter, Medtronic, Inc.

2:00pm **EN+AS-ThA1 Growth Temperature and Stoichiometry Effects on the Inherent Stability of CdS/CdTe Solar Cells**, *D.S. Albin, T.A. Gessert, R. Dhere, S.-H. Wei, J. Ma, D. Kuciauskas, A. Kanevce, R. Noufi*, National Renewable Energy Laboratory **INVITED**

Capacitance-voltage (CV) measurements are commonly used to characterize semiconductor junctions. A common observation when performing such measurements on polycrystalline CdTe solar cells is that the measured capacitance is a strong function of the voltage scan direction. These results in a noticeable hysteresis in the C-V profile when capacitance data is collected using both forward (fwd) and reverse (rev) voltage scan directions. Similarly, hysteresis curves for the usual derived quantities such as net carrier density, N_a , and depletion width, W , naturally follows. We have recently observed that in particular, the hysteresis in calculated carrier acceptor density, $N_{a, \text{hys}}$, arbitrarily defined as $N_{a, \text{fwd}} - N_{a, \text{rev}}$ decreases as the CdTe growth temperature is reduced. At higher CdTe growth temperatures, this value is positive and shifts to negative values at lower growth temperatures. This behavior is believed to reflect a transition of the CdTe stoichiometry in CdS/CdTe solar cells from Cd-poor at higher temperatures to Cd-rich at lower temperatures based upon recently published CdTe binary phase diagrams.

The impact of Cd/Te stoichiometry on cell performance is suspected. Cd-poor stoichiometry favors the formation of Cd-vacancies (V_{Cd}), a beneficial acceptor, but it also simultaneously increases the formation of the Te antisite (Te_{Cd}), an important recombination center in CdTe. Recent theoretical calculations using the hybrid Heyd-Scuseria-Ernzerhof (HSE) functional also suggests that Te interstitials (Te_i) may be an important recombination center under Cd-poor conditions. Increased Cd chemical potential will reduce the formation of these recombination centers, but also reduce hole carrier density. Thus, an optimal growth condition, which could include extrinsic p-type doping, may be needed for leading to higher performance CdTe solar cells.

Not discussed to date however is whether stoichiometry has an inherent impact on the stability of CdTe solar cells. In this talk, we contrast accelerated lifetime study results for CdTe cells grown at different growth temperatures. Open-circuit voltage (V_{oc}) stability in cells grown at lower temperatures was noticeably improved. $N_{a, \text{hys}}$ in the latter cells was considerably smaller. Both V_{oc} and FF were well correlated with this capacitance-derived parameter. $N_{a, \text{hys}}$ was observed to be relatively unchanged in devices where V_{oc} did not degrade. Finally, time-resolved photoluminescence lifetimes of nearly 10 ns were measured in these cells made at lower temperatures relative to values of around 2 ns measured in higher temperature devices.

3:00pm **EN+AS-ThA4 XPS Characterization of Organic Gradients in Organic Photovoltaic and Organic Light Emitting Devices Using Ar GCIB Depth Profiling**, *S.N. Raman, J.S. Hammond, J.F. Moulder*, Physical Electronics

The use of organic materials for electronic applications such as Organic Photovoltaics (OPV's) and Organic Light Emitting Diodes (OLED's) is rapidly growing. The efficiencies of these devices are widely recognized to depend on the molecular gradients fabricated into the devices. Conversely, the degradation of these devices is suspected to depend on several factors including chemical degradation and chemical migration as a function of use. It is therefore very desirable to develop analytical techniques which can quantify chemical gradients as well as identify degradation products in these films.

Gas Cluster Ion Beam (GCIB) sources with low energy per atom $\text{Ar}_{2,000}^+$ ions have recently been demonstrated to provide a depth profiling technique for molecular species (1,2). GCIB depth profiling in an interleaved mode with the surface analysis spectroscopy of X-ray Photoelectron Spectroscopy (XPS) has been applied to model OPV and OLED devices. The 2 to 5 nm information depth of XPS, combined with the demonstrated "non-destructive" chemical information revealed after each GCIB sputter interval, facilitates the chemical gradient analysis of a series of model samples up to several 100 nm in depth with molecular depth resolution < 10 nm.

Selected model OPV and OLED samples were exposed to annealing and environmental degradation testing. The XPS depth profiles measured the

migration of organic components and dopants as a function of fabrication processes. This presentation will provide an overview of GCIB depth profiling with XPS as well as discuss the insights into efficiencies and degradation processes elucidated by this chemical gradient analysis technique.

1. T. Miyayama, et al. *Surf. Interface. Anal.* 42 (2010) 1453-1457.

2. T. Miyayama, et al. *J. Vac. Sci. Technology A*, 28 (2) (2010) L1-L4.

3:40pm **EN+AS-ThA6 Characterization of Degradation Mechanisms of Membrane Electrode Assemblies by XPS and SEM Imaging**, *A. Patel, K. Artyushkova, P. Atanassov*, University of New Mexico, *S. Wessel, V. Colbow, M. Dutta*, Ballard Power Systems, Canada

Durability of catalyst layer (CL) is of key importance in the deployment of PEMFCs. Catalyst layer (CL) degradation is linked to several failure mechanisms including Pt dissolution and agglomeration and support corrosion. X-ray photoelectron spectroscopy (XPS), a powerful technique to study chemical changes, has been applied to quantitatively analyze catalyst layer degradation in PEM fuel cells. More specifically, ionomer degradation was characterized by a decrease of CF_3 and CF_2 species and an increase in oxidized forms of carbon (e.g. C-O and C=O). Chemical speciation as determined by XPS for catalyst powders was correlated with electrochemical performance losses. MEAs using catalyst coated membranes that are composed of Pt catalyst supported on differing carbon supports were subjected to aging protocols to accelerate the degradation mechanisms of the cathode CL. In-situ and ex-situ diagnostics were used to quantify performance losses and structural changes of the CL.

Large area XPS was used for analysis of fresh, conditioned and aged cathode catalyst layers. Spectroscopic analysis, which provides an integral spectrum from approximately 1mm² area, may have a contribution from the GDL sublayer that was not fully removed from the catalyst layer side during separation of the MEA components. The GDL sublayer exhibits a peak in the same BE range as fully fluorinated carbons that are detected in the catalyst layer. Changes that have been detected in CL may not be due to the changes within the ionomer, but rather due to physical intermixing of layers caused by the testing protocols. XPS imaging enabled separation of the differing component contributions. Using Pt 4f imaging, regions are clearly identified where no Pt is present, indicating that GDL pieces adhere to the CL. Fluorine images at two different binding energies (one for the ionomer, and another for the GDL) confirm this. High resolution C 1s spectrum extracted from the area where catalyst is present does not show a high BE component in the C 1s spectrum of the area where GDL is present, confirming that the high BE component detected by large area spectroscopy are contributions from the GDL. High-resolution spectra acquired from the area where only catalysts layer is present shows higher amounts of oxidized forms of carbons. In addition, morphological changes of aged cathode catalyst layers have been evaluated by Digital Image Processing of SEM images for roughness, porosity and texture parameters.

4:00pm **EN+AS-ThA7 Selective Adsorption Behavior of CO₂ and C₂ Hydrocarbon Isomers over N₂ and Methane in a Flexible Metal Organic Frameworks**, *N. Nijem, P. Thissen*, University of Texas at Dallas, *P. Canepa*, Wake Forest University, *H. Wu, J. Li*, Rutgers University, *T. Thonhauser*, Wake Forest University, *Y.J. Chabal*, University of Texas at Dallas

Post combustion carbon capture is a complementary approach to research in renewable energy to combat the exponential increase of CO₂ emission and global warming. An important outcome of enhancing gas separation in materials, for example, is the decrease in energy needed for separation of hydrocarbons. Metal-organic Frameworks (MOFs) have shown promise in this area because their high surface area, porosity and chemical/structural tailorability contribute to the preferential selective adsorption of gases. This work explores the incorporation of CO₂ and hydrocarbons into a flexible framework, $\text{Zn}_2(\text{bpd})_2(\text{bpee})$, ($\text{bpd} = 4,4'$ -biphenyl dicarboxylate, $\text{bpee} = 1,2$ -bis(4-pyridyl)ethylene) using infrared (IR), Raman spectroscopy and van der Waals density Functional (vdW-DF) calculations. We present evidence for "gate opening" phenomenon, where the structure of the framework changes only upon adsorption of CO₂ and C₂ hydrocarbon isomers but not for N₂ or methane. Understanding the specifics of CO₂ interaction with the framework was explored to identify parameters affecting its selectivity. We find that the high quadrupole moment of CO₂ and its interaction through its carbon with the bpd linker induces the transformations. The flexibility of the framework was found to be primarily due to the specific connectivity of the Zn metal center to the ligands, at one end in a monodentate mode and at the other in a bidentate mode. The unexpected gate opening behavior in this same framework upon the adsorption of C₂ hydrocarbon isomers was also studied. We find that the

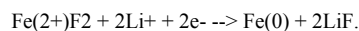
specific hydrogen bonding between the CH of the hydrocarbon and the C=O bond of the bpdc linker is responsible for this interesting behavior. Furthermore, the strength of the hydrogen bond was found to affect the gate opening pressure point. This effect points towards the potential of this framework for uses such as pressure swing adsorption based separation. In conclusion, we have identified specific interactions of CO₂ and hydrocarbons in a flexible framework that lead to their selective adsorption properties. This knowledge allows the design of frameworks with optimized properties.

4:20pm EN+AS-ThA8 Fabrication and Characterization of a PCBM-Terminated Organic Monolayer on a Si(111) Surface, *T.J. Miller, A.V. Teflyakov*, University of Delaware

The energy sector is a large, growing field in research and technology. A growing subset of the solar field is organic photovoltaics (OPV). Two areas that have long challenged researchers are efficiency and stability of the OPV devices. An area that is in need of fundamental understanding that may increase efficiency of these devices is the charge transfer. However, a precise nature of the bulk-heterojunction OPV donor/acceptor interface is difficult to pinpoint. Thus, model systems can be used initially to mimic these interactions. In the system presented here, the donor/acceptor interface is well-defined. Phenyl-C61-butyric acid methyl ester (PCBM) was reacted with an amino-terminated organic monolayer on a single crystalline Si(111) surface. Poly 3-hexylthiophene (P3HT) was then deposited onto this complex substrate, and the produced interface can be observed and investigated. Fourier transform infrared spectroscopy was used to identify the functional groups on the surface. The chemical and electronic states of the coating and the substrate were investigated by X-ray photoelectron spectroscopy, and the morphology was determined through atomic force microscopy. Preliminary charge carrier lifetime measurements will also be reported.

4:40pm EN+AS-ThA9 Conversion Reaction of Thin Film Metal Fluorides and Metal Oxides Exposed to Atomic Lithium, *R. Thorpe, S. Rangan, R.A. Bartyński*, Rutgers University

Modern Li-ion intercalation batteries use electrode materials that accommodate Li intercalation, enabling the exchange of Li ions during battery cycling without extensive alteration of the electrode's crystalline structure. Despite the stability of these materials to the intercalation process, the ability of such batteries to store energy is limited by the number of host sites in the electrodes to approximately one electron per formula unit. Conversion reaction materials could potentially store several times more energy than current generation batteries by utilizing the full range of charge states available to their constituent metal ions. For example, the following reaction occurs in a FeF₂ cathode:



Although conversion reaction materials have shown the promise of high energy storage density in electrochemical cells, their cycling stability is poor, and relatively little is known about the phase evolution and structural changes that occur during charge and discharge.

In order to study the fundamental properties of these materials, we have grown high purity thin films of conversion materials FeF₂, FeF₃, FeOF, FeOx, and CoO. By exposing these films to atomic Li in vacuum, can follow the evolution of these materials as they approach the reaction products reached in the discharge of a conversion battery. We have used UV and inverse photoemission to measure the electronic structure of the valence and conduction bands respectively. Using these techniques in tandem, we are able to measure the band gap of these materials, which can then be related to their electronic conductivity. Using x-ray photoemission, we have measured the stoichiometry and valence states of the compounds involved in these reactions. In addition, we have examined the structure of these nano-scale materials using TEM and LEED.

For FeF₂, our XPS results show immediate reaction upon exposure to Li, fully reducing the Fe to the metallic state and forming LiF, with no evidence of intermediary phases in the film due to the high mobility of lithium. TEM of the initial and final films indicates a drastic morphology alteration, leading to a local precipitation of Fe₀ and LiF formation, with an overall particle size reduction from 10nm to 2nm, consistent with what is found in electrochemical studies.

However, the Li-CoO and Li-FeOx reactions appear to diverge from the results of Li⁺ electrochemical reactions, leading to the simultaneous formation of both Li₂O and Li₂O₂, the latter of which hinders further reduction of the Fe and Co. These observations will be contrasted with results obtained from the related conversion reaction compounds FeOx_{Fy} and FeF₃.

Energy Frontiers Focus Topic Room: 7 - Session EN+NS-ThA

Thermophotovoltaics, Thermoelectrics and Plasmonics

Moderator: R.A. Quinlan, Naval Surface Warfare Center, Cardercock Division

2:00pm EN+NS-ThA1 Structuring of the Radiative Thermal Emission in Tungsten Inverse Opals for Thermophotovoltaic Applications, *M.D. Losego*, North Carolina State University, *K.A. Arpin*, University of Illinois at Urbana Champaign, *B. Kalanyan*, North Carolina State University, *P.V. Braun*, University of Illinois at Urbana Champaign, *G.N. Parsons*, North Carolina State University

Materials with photonic bandgaps are generated by periodic mesostructuring at length-scales comparable to visible wavelengths. While photonic bandgaps are often used to control the interaction of incident light with a material (e.g. reflect incident light over a narrow bandwidth), these structures can also be used to tune the thermal emission of light. Consequently, a heated metallic photonic crystal could be used in a thermophotovoltaic (TPV) device scheme. Such a TPV would (1) absorb broadband incident solar radiation, (2) heat up, and (3) re-emits the radiation over a narrow band of energies. This narrow-band radiation could then be converted to electricity with high efficiencies using a simple single-junction solar cell. However, demonstrating narrow-band thermal emission from a multidimensional architecture remains elusive. The central challenge is finding a materials set that demonstrates the required combination of thermal stability and dielectric function in a nanostructured architecture capable of high-temperature radiant emission.

This talk will examine our development of refractory tungsten inverse-opal structures designed for thermal emission in the visible spectrum. The first generation of these structures were constructed from silica opals infiltrated with electrodeposited tungsten. While ultrathin (<20 nm) oxide ALD layers were found to improve high temperature stability (>1000°C, 12 hours) by restricting surface diffusion and limiting sintering, difficulties with massive structural cracking during the molten-salt electrodeposition process could not be overcome. Second generation devices are now being developed using a lower temperature tungsten atomic layer deposition (ALD) process. Besides the avoidance of massive structural cracking, these ALD materials appear to be denser than electrodeposited materials, further reducing the unwanted sintering effects at high temperatures. Room temperature spectra collected from these structures indicate photonic effects not seen in planar tungsten films and suggest enhanced thermal emission at visible wavelengths.

2:40pm EN+NS-ThA3 Nanowires and Nanowire Heterostructures for Thermoelectric Energy Harvesting, *Y. Wu*, Purdue University INVITED

Substantial efforts have been devoted to use nanostructured materials for thermoelectric energy harvesting and solid-state cooling in the past decade. However, the majority of the research is still limited in lab scale due to the incapability to mass-produce well-defined nanostructured materials with low yet industrial-compatible process. In addition, a lot of widely used thermoelectric materials contain toxic and expensive elements that prevent the large-scale deployment of the thermoelectric devices. In this presentation, we will discuss our research on the development of mass production of molecular scale nanostructures of chalcogenides and metal oxides, as well as their heterostructures, for the manufacture of thermoelectric generators operating at different temperature ranges. Particularly, we will talk about our approach to discover and investigate the non-toxic and abundant nanostructured materials to achieve an environmentally friendly process. Our preliminary research indicated that thermoelectric figure of merit (ZT) close to 2 can be achieved in the molecular scale nanowires of certain chalcogenide due to significantly enhanced power factor and reduced thermal conductivity as a result of quantum confinement.

3:40pm EN+NS-ThA6 Plasmonic Polymer Solar Cells with Spectrally Tuned Au/SiO₂ Core/Shell Nanorods incorporated in Active Layers, *V. Jankovic, J.P. Chang*, UCLA

Octadecyl tri-methoxysilane (OTMS) functionalized Au/SiO₂core/shell nanorods were incorporated into the active layers of two different polymer bulk heterojunction (BHJ) systems: a broad band gap polymer (poly(3-hexylthiophene)(P3HT):[6,6]-phenyl-C61-butyric acid methyl ester (PCB60M)) and a low band gap polymer poly{2,6-4,8-di(5-ethylhexylthienyl)benzo[1,2-b;3,4-b']dithiophene-alt-5-dibutylthio-3,6-bis(5-bromothiophen-2-yl) pyrrolo[3,4-c]pyrrole-1,4-dione} (PBDDT-DPP):PC60BM. The extinction peaks of the Au nanorod scattering centers was tuned to match the band edge of the two polymers by controlling their

aspect ratio. For the P3HT:PC60BM system with a band edge around 700 nm, the addition of the core/shell nanorods of an aspect ratio 1:2.5 (resonant frequency peak is at around $\lambda=650\text{nm}$), resulted in 8% improvement in short circuit current (J_{sc}); for the low band gap polymer system PBDTT-DPP:PC60BM with band edge around 850 nm, we tuned the resonant frequency to near-infrared region by increasing the aspect ratio to 1:4 (resonant frequency peak is at around $\lambda=800\text{nm}$), the addition of the core/shell nanorods resulted in 18% improvement in short circuit current (J_{sc}). The J_{sc} enhancement was consistent with external quantum efficiency (EQE) measurements and the EQE improvement factor matched the absorption resonance spectrum of Au/SiO₂ nanorods in both systems. This work will instruct us on how to utilize and manipulate plasmon resonance of metallic nanoparticles to improve device efficiency in different polymer solar cell systems.

4:00pm **EN+NS-ThA7 Optics and Photonics Research Priorities and Grand Challenges as Relating to Today's Energy Frontiers, E.B. Svedberg**, The National Academies

A new report from the National Research Council of the National Academies identifies research priorities and grand challenges to fill gaps in optics and photonics, a field that has the potential to advance not only the energy field but also the economy of the United States and the world, the report provides visionary directions for future technology applications, and ensure progress in energy related research. As one of its recommendations the report recommends that the federal government develop a "National Photonics Initiative" to bring together academia, industry, and government to steer federal research and development funding and activities.

Eight particular areas of technological application are discussed in separate chapters: communications, information processing, and data storage; defense and national security; energy; health and medicine; advanced manufacturing; advanced photonic measurements and applications; strategic materials for optics; and displays. Each chapter reviews updates that have occurred since the 1998 National Research Council report *Harnessing Light: Optical Science and Engineering for the 21st Century*, as well as the technological opportunities that have risen from recent advances in optical science and engineering. This presentation will focus on the energy section of the report that deals not only with energy generation but also how to reduce excessive usage of energy. The report additionally recommends actions for the development and maintenance of the photonics-driven sector of the energy industry, including both near-term and long-range goals, likely participants, and responsible agents of change.

The recommended National Photonics Initiative will help manage the breadth of rapidly expanding applications of photonics technologies, allowing both governments and industry to develop coherent strategies for technology development and deployment in the energy sector. The initiative should also spearhead a collaborative effort to improve the collection and reporting of research, development, and economic data on this sector.

Thursday Afternoon Poster Sessions

Energy Frontiers Focus Topic

Room: Central Hall - Session EN-ThP

Energy Frontiers Poster Session

EN-ThP1 Tungsten Carbide: Synthesis and Reactivity with Oxygen on the Nanoscale, *J.B. McClimon, P. Reinke*, University of Virginia

Transition metal carbides have shown considerable promise as catalysts, which is often attributed the similarities in electronic structure between noble metals and transition metal carbides. The addition of tungsten carbide to microbial fuel cells, and their use as an anode material has proven to be quite advantageous. However, the bottleneck in the use of tungsten carbide lies in the loss of function due to partial or complete oxidation of the surface. We study the reactivity of tungsten, and carbon-rich tungsten carbide clusters with oxygen to investigate the progression of oxidation. We suggest that carbon-rich carbide surfaces are less susceptible to oxidation and can be regenerated by annealing.

The tungsten and tungsten carbide clusters are made by the co-deposition of W and C₆₀ which enables us to fine-tune composition in a wide range. The morphology and electronic structure of the surface is probed with STM in-situ, which is supplemented by chemical analysis with XPS, and structural analysis with TEM. The progression of oxidation is observed with bandgap maps with spatial resolution in the nm-range. The experiments were performed on graphite substrates, where the metal clusters remain highly mobile and do not react in the temperature regime of our work (< 650 K).

We begin with a discussion of the synthesis of clusters with compositions ranging from pure W-clusters, to carbon-rich surfaces. The cluster sizes are between 5-30 nm, and the carbon is introduced either by co-deposition of W and C₆₀ or by the deposition of fullerenes on pure W-clusters (and vice-versa). The C₆₀ aggregates to large islands and a reaction with the W-clusters is only initiated by annealing, and leads to carbon-terminated metallic clusters. The motion of fullerene molecules is reflected in the sawtooth signature of tip induced displacement, which is also a probe for the surface chemistry. The co-deposition of W and C₆₀ (and W deposition on C₆₀) leads to the formation of spherical structures whose granularity reflects the dimensions of the C₆₀ cage. We assume that the C₆₀ cage reacts with surface W but the low temperature prevents collapse. The oxidation of tungsten clusters has been observed as a function of oxygen partial pressure, and shows the progression of the reaction as a function of cluster size and surface morphology. We will present a complete set of bandgap maps, which are recorded during the oxidation at room temperature and elevated temperature for the different carbide structures. A model describing the oxidation as a function of carbide structure and composition will be presented.

EN-ThP2 F-doped ZnO Thin Films Deposited by Pulse DC Magnetron Sputtering of Zinc Target, *B.-H. Liao*, Instrument Technology Research Center, Taiwan, Republic of China

In this study, Fluorine doped ZnO (FZO) films were deposited on glass substrate by pulse DC magnetron sputtering of zinc targets with Ar, H₂, O₂ and CF₄ containing gas mixtures at room temperature. Increasing CF₄ gas in ZnO films can increase the carrier concentrations but slightly decrease the mobility. After introducing 1 sccm CF₄ gas in ZnO films we can get the lowest resistivity 7.6×10^{-4} ($\Omega\text{-cm}$) with mobility $12.4 \text{ cm}^2/\text{V-s}$ and carrier concentrations $6.6 \times 10^{20} \text{ cm}^{-3}$. Besides, its average transmittance in the visible region was over 82.95%. All of the results indicate that we have found a cost effective and mass production process suitable for the application of manufacture in the real-world industry.

EN-ThP3 Photoresponse of PbS Nanoparticle - Quaterthiophene Films Prepared by Gaseous Deposition as Probed by XPS, *M. Majeski, D. Pleticha, I. Bolotin, L. Hanley*, University of Illinois at Chicago, *E. Yilmaz, S. Suzer*, Bilkent University, Turkey

Semiconducting lead sulfide (PbS) nanoparticles were cluster beam deposited into evaporated quaterthiophene (4T) organic films, which in some cases were additionally modified by simultaneous 50 eV acetylene ion bombardment. Surface chemistry of these nanocomposite films was first examined using standard X-ray photoelectron spectroscopy (XPS) and laser desorption/ionization mass spectrometry. XPS was also used to probe photoinduced shifts in peak binding energies upon illumination with a CW green laser and the magnitudes of these peak shifts were interpreted as changes in relative photoconductivity. The four types of films examined all displayed photoconductivity: 4T only, 4T with acetylene ions, 4T with PbS nanoparticles, and 4T with both PbS nanoparticles and acetylene ions. Furthermore, the ion-modified films displayed higher photoconductivity,

which was consistent with enhanced bonding within the 4T organic matrix and between 4T and PbS nanoparticles. PbS nanoparticles displayed higher photoconductivity than the 4T component, regardless of ion-modification. Finally, development of a new instrument is discussed that will allow analysis of films without prior exposure to air.

EN-ThP4 The Investigation of the Shunt Resistance using Conductive AFM and EL Measurements in Si Based Thin Film Solar Cells, *M.H. Joo, J.M. Lee, K.H. Park*, LG Electronics Advanced Research Institute, Republic of Korea

Silicon (Si)-based solar cells are of great interest for photovoltaic applications, such as bulk type, thin film type, and heterojunction type. Recently amorphous silicon based thin film solar cells have attracted much attention from researchers and engineers because of low consumption of raw materials and low temperature deposition. However, the conversion efficiency of these solar cells is still very poor compared to other types of solar cells. An improved understanding on defects in Si based thin film solar cells is required to further enhance cell performance. Due to the short exposure time and high spatial resolution, camera-based techniques, such as photoluminescence (PL), electroluminescence (EL) and dark lock-in thermography (DLIT), have recently emerged as powerful characterization tools for the investigation of different loss mechanisms in solar cells and modules. And the combination of these techniques with high resolution electrical and structural analysis such as conductive atomic force microscopy (c-AFM) and transmission microscopy (TEM) allow for advanced studies on shunt and for determination of recombination current.

In this report, we studied the evolution of the shunt resistance in Si based thin film solar cells. The solar cell ($1 \times 1 \text{ cm}^2$) structures have a configuration of glass/Al-doped ZnO (AZO)/a-Si/a-SiGe/Al. AZO and Al are top and bottom electrodes respectively, deposited with DC magnetron sputter. A-Si and a-SiGe are used for absorption layers prepared by plasma enhanced chemical vapor deposition (PE-CVD). AZO was textured for the light management before the deposition of absorption layers. For defect investigation of solar cells, we measured the samples with both EL and c-AFM. Electroluminescence is driven by injecting a constant current from a power source into the cell. After EL measurements, current distributions in the local area of the cells were evaluated with c-AFM. EL results show the recombination loss of defect area, which is correlated with high leakage current area of c-AFM results. In the result of TEM analysis, low shunt area in the cells evolved from the crack defects in absorption layers. The surface structures of AZO such as high angle textures and pinhole defects make an important role of crack evolution in the absorption layers. When the sample was controlled with low angle AZO texture and no pinhole defects, there was no recombination loss and leakage current in the cells.

EN-ThP5 Growth Methods and Applications of SiC Nanopowder and Nanowhiskers, *R. Dhiman*, University of Southern Denmark, *E. Johnson*, University of Copenhagen, Denmark, *P.K. Kristensen*, Aalborg University, Denmark, *P. Morgen*, University of Southern Denmark

Nanomaterials have in a number of cases shown physical and chemical properties differing from their macroscopic counterparts. These differences can be tailored through form and size of the nanostructured materials, related to the restriction of the electronic degrees of freedom in one-, two-, or three dimensions. In this study, nanoporous SiC has been produced through reactions at high temperatures between carbon nanoparticles and SiO gas, while SiC nanowhiskers are made from saw dust impregnated with TEOS, reacting at high temperatures in a complex set of reactions to produce SiC clusters with a high concentration of SiC nanowhiskers sticking out perpendicularly from planar areas on the clusters. After suitable separation and extraction procedures individual crystals or whiskers may be handled and studied, with SEM and TEM methods. The SiC nanopowder is successfully applied as support material for Pt nanoparticles in the fuel cell technology, while the individual whiskers show very interesting mechanical properties and one-dimensional semiconductor properties. They are also currently used, in agglomerate form, as a very stable and inert type of binder material for new water-electrolysis active membrane systems.

EN-ThP6 Epitaxial Growth of ZnInON Films for Piezo-Electric-Field Effect MQW Solar Cells, *K. Matsushima*, Kyushu University, Japan

Multi-quantum well (MQW) solar cells belong to the most promising "third generation photovoltaics" with ultra-high conversion efficiencies at low cost. In order to approach their theoretical maximum efficiency (>50%), a significant improvement in the extraction efficiency of photo-generated carriers is important. We have recently proposed piezo-electric-field effect (PEF) MQW solar cells that utilize novel oxynitride semiconductor ZnInON (ZION) films [1,2]. Our simulation predicts that the electron-hole recombination rate in ZION-QWs is noticeably low compared to those in

conventional QWs with III-V materials such as GaAs and InGaN. Here we fabricate epitaxial ZION films on GaN and ZnO templates aiming at realization of PEF-MQW solar cells. Furthermore, we also demonstrate coherent growth of ZION films in order to study the piezo-electric field in ZION-QWs which can prevent the recombination and thus enhance the extraction efficiency of photo-generated carriers.

Epitaxial ZION films were fabricated by RF magnetron sputtering, which is suitable for large-area and low-cost fabrication. Commercial GaN templates that were fabricated by metal-organic chemical vapor deposition (MOCVD) and sputtered ZnO templates were used as epitaxial substrates. The ZnO templates were fabricated by RF magnetron sputtering at 700°C in Ar-O₂ atmosphere on ZnO buffer layers that were fabricated via nitrogen mediated crystallization (NMC) in N₂-Ar atmosphere at 700°C [3,4]. On GaN and ZnO templates, ZION films were deposited in N₂-Ar atmosphere at the total pressure of 0.2-0.5 Pa. The applied RF power was 10-90 W and the deposition temperature was 400°C. The film thickness was 30-700 nm.

X-ray diffraction measurements show that the ZION films have wurtzite crystal structure and the full width at half maximum (FWHM) of rocking curve from (002) plane for the films is noticeably small of 0.115°, indicating small fluctuation of the crystalline orientation. Furthermore, measurements of reciprocal lattice map of (105) plane suggest that the ZION films are grown coherently on GaN templates, indicating that a piezo-electric field can be generated. From these results, we conclude that ZION films are full of promise for Piezo-Electric-Field effect MQW solar cells that can be fabricated at low cost.

[1] N. Itagaki, *et al.*, Jpn. Patent Application No. 2012-49805 (2012) (in Japanese).

[2] N. Itagaki, *et al.*, U.S. Patent Publication No. 2010/0109002 (2010).

[3] N. Itagaki, *et al.*, Appl. Phys. Express 4 (2011) 011101.

[4] K. Kuwahara, *et al.*, Thin Solid Films 520 (2012) 4674.

EN-ThP7 Texture-Etched Surface Structure Control of Transparent Conductive Impurity-Doped ZnO Films Deposited by r.f. Power Superimposed d.c. Magnetron Sputtering. T. Minami, T. Fujita, T. Miyata, J. Nomoto, Kanazawa Institute of Technology, Japan

This paper describes the influence of the supplied r.f. power on the light scattering characteristics and the surface texture formation obtainable by wet-chemical etching transparent conducting impurity-doped ZnO thin films prepared by an r.f. power superimposed d.c. magnetron sputtering deposition (rf+dc-MSD) using a high-density-sintered rectangular Al- or Ga--doped ZnO (AZO or GZO) target (127 mm×275 mm) : prepared with an Al₂O₃ content of 1 or 2 wt.% or Ga₂O₃ content of 5.7 wt.%, respectively. Both AZO and GZO thin films were prepared with a film thickness of either 1000 or 2000 nm on OA-10 glass substrates at a temperature of 200°C by varying both the supplied d.c. and r.f. power used in the rf+dc-MSD: d.c. power in the range of 0-800 W and r.f. power in the range of 0-1000 W. The surface texture formation was carried out by wet-chemical etching (in a 0.1% HCl solution at 25°C) conducted after heat-treatment with rapid thermal annealing (RTA) at 500 or 550°C for 5 min in air. It was found that the light scattering characteristics and surface texture formation obtainable for texture-etched AZO (or GZO) thin films were considerably dependent on both the ratio of supplied r.f. to d.c. power as well as the Al (or Ga) content doped into the films. In particular, the haze value was significantly improved at wavelengths up to about 1200 nm in the near-infrared region in surface-textured AZO films prepared with an increased ratio of supplied r.f. power to d.c. power and etched after being heat treated with RTA, whereas the film deposition rate was found to decrease with the increased power ratio. The obtained haze value improvement is attributable to an increase of etch pit size as well as a decrease of carrier concentration. In addition, the obtainable improvement in texture-etched AZO thin films was also found to be considerably dependent on the Al content doped into the films. In particular, texture-etched AZO thin films that are appropriate for transparent electrode applications in thin-film solar cells were obtained with the following preparation conditions: rf+dc-MSD using an AZO target with an Al₂O₃ content of 2 rather than 1 wt.%, r.f. power superimposed at an appropriate value and wet-chemical etching after heat-treatment with RTA. A high haze value above 80% at wavelengths up to 1100 nm in the near-infrared region was attained in texture-etched AZO thin films prepared by rf+dc-MSD (700 W r.f. component added to a constant d.c. power of 570 W) using an AZO target with an Al₂O₃ content of 2 wt.%.

EN-ThP8 Thermoelectric Properties of Sb₃ Doped Bi₂Te₃+Bi₂Se₃ Alloys by Mechanical Alloying and Spark Plasma Sintering. M. Babu, S.J. Hong, Kongju National University, Republic of Korea

Thermoelectric (TE) materials and its devices provide attractive increasing attention because of their potential applications in the field of energy conversion, cooling for electronic devices and thermal sensors. For enhancing the thermoelectric performance, we fabricated the micro-sized n-

type Bi₂Te₃+Bi₂Se₃ (Bismuth-Tellurium-Selenium) with different compositions doped with 0.05 wt%SbI₃ alloys via high energy mechanical alloying which is associated with vacuum atmosphere. The milled powder was consolidated by Spark Plasma Sintering (SPS) technique at the temperature range of 400°C with a holding time of 10 minutes at 50 MPa pressure. The effects of milling time and temperatures were investigated. In order to investigate microstructural analysis of the samples, both Optical microscope (OM) and Scanning Electron Microscope (SEM) were used. The phase of different compounds was characterized by X-ray Diffraction (XRD). Mechanical properties were calculated by measuring the density and micro Vickers hardness of the samples. The temperature dependence of the Seebeck coefficient, electrical resistivity and hall coefficient were determined for the alloys samples with different compositions. From the experimental results, the thermoelectric properties are mainly influenced by the milling time, vacuum condition and temperature. The maximum values of Figure-of-merit (ZT) for the different compounds of samples were calculated using the thermoelectric properties.

EN-ThP9 Structure-to-Function Relationship in Porous Pt/TiO₂/Ti Planar Nanostructures with a Potential Barrier for Chemicurrent Related Applications. S. Dasari, M. Ariyan, M. Hashemian, E. Karpov, University of Illinois at Chicago

Recent observations of enhanced chemicurrent effects of heterogeneous reactions on porous MIM structures with an intrinsic potential barrier make them promising for novel sensing and energy conversion applications. This presentation describes relationships between morphological features of Pt/TiO₂/Ti nanostructures, derived from XRD and SEM studied, and chemicurrent production capabilities of this material system. In particular, samples containing anatase phase in the oxide film layer show significantly greater chemicurrent effect of catalytic hydrogen oxidation on the nanostructure surface and chemical to electrical energy conversion efficiency than those with a dominant rutile phase. Strategies of thin oxide film growth by plasma electrolytic oxidation method leading to porous anatase TiO₂ thin films are also presented.

EN-ThP10 Investigation of the Molecular Interaction between CdSe Quantum Dots and P3HT for Hybrid Solar Cell Applications. A.S. Karakoti, P. Nachimuthu, S. Thevuthasan, Pacific Northwest National Laboratory

We took a systematic approach to study the interaction between CdSe quantum dots (QDs) and regioregular P3HT polymer using spectroscopic and imaging tools. Photoluminescence (PL) measurements following the titration of CdSe quantum dots with P3HT showed evidence of charge transfer between the CdSe QDs and the P3HT matrix. The titration led to an immediate quenching of main PL emission from both CdSe and P3HT and a new emission in low energy region of the electromagnetic spectrum starts appearing from the recombination of electrons in CdSe with holes in P3HT. The effect of the size of QDs on charge transfer as a function of reaction time following the addition of CdSe quantum dots in to a fixed concentration of P3HT was monitored. The time course PL measurements show the quenching of main PL emission from P3HT follow the order 6.6 nm<3.3 nm<2.1 nm while no significant changes was observed in the absorbance spectrum. These results suggest that the size-dependent interaction between QDs and P3HT. However, dynamic light scattering measurements (DLS) from the ligand capped CdSe QDs indicate a strong tendency for agglomeration of smaller QDs in the presence of P3HT. Addition of P3HT to a known concentration of CdSe QDs increases their average diameter for 2.1nm and 3.3nm QDs in toluene while the average diameter of QDs with 6.6nm in toluene remains unchanged at the same concentrations. This suggests that the interaction between CdSe QDs and P3HT is controlled by the agglomeration of QDs and not by the size of the dots. Findings from these results and the effect of changing the capping ligands of CdSe QDs on the charge transfer will be discussed.

EN-ThP11 Low-Damage Deposition of Thin Silicon Films for Solar Panel Production using Surface-Wave Plasma Source. J. Peck, University of Illinois at Urbana Champaign, P. Zonooz, Starfire Industries LLC and University of Illinois at Urbana Champaign, D. Curreli, University of Illinois at Urbana Champaign, M. Reilly, R. Stubbers, B. Jurczyk, Starfire Industries, LLC, D.N. Ruzic, University of Illinois at Urbana Champaign

An innovative kind of plasma source for the deposition of thin silicon films used in semiconductor manufacturing is currently under development at Starfire Industries LLC and CPMI Center for Plasma Material Interaction, University of Illinois Urbana Champaign. The source, operating in the microwave range, is able to efficiently generate high-density and low-electron-temperature SiH₄-H₂ plasmas, and can easily be scaled upward to the deposition of thin films on large-area surfaces. The silicon films deposited at low RF power on glass substrates have been characterized using multiple techniques, comprising SEM, Ellipsometry and Raman

Spectroscopy. Spectroscopic data in the UV-VIS-NIR range have been acquired during the discharge operations for plasma characterization. By using Raman spectroscopy, the crystalline volume fraction of the deposited films has been obtained for several input mass-flows of silane, as a function of the substrate temperature and for several pressures of the Hydrogen gas. The averaged film growth rate has been obtained from both ellipsometry measurements and SEM imaging. From the results of the preliminary characterization, the possibility to obtain low-damage growth of a-Si:H and nc-Si:H thin films has been assessed. The trend of the crystallinity as a function of the electron temperature has also been presented, and its relationship with the low potential-drop allowed by this source at plasma-substrate interface has been discussed.

EN-ThP12 Relationship Between Interface Microstructures and Obtainable Photovoltaic Properties in ZnO/Cu₂O Heterojunction Solar Cells, Y. Nishi, S. Abe, T. Miyata, T. Minami, N. Ikenaga, O. Ueda, Kanazawa Institute of Technology, Japan

In this paper, we present our investigation into the relationship between the observable microstructure at heterojunction interfaces and the obtainable photovoltaic properties in ZnO/Cu₂O heterojunction solar cells fabricated with various structures on thermally oxidized Cu₂O sheets. Recently, we reported that high efficiencies of 2.19 and 4.12% as well as open circuit voltages of 0.5 and 0.72 V were obtained in heterojunction solar cells fabricated with an Al-doped ZnO (AZO)/Cu₂O or AZO/non-doped ZnO/Cu₂O structure, respectively: solar cells fabricated by depositing thin films on thermally oxidized Cu₂O sheets at room temperature using a pulsed laser deposition (PLD) method [1,2]. The improvement in obtained photovoltaic properties suggests that it is necessary to stabilize the surface of Cu₂O sheets as well as develop low-damage and low-temperature deposition techniques for forming and applying heterojunctions. In addition to improvements in the surface condition of Cu₂O sheets, the significant improvement of obtained photovoltaic properties exhibited in AZO/non-doped ZnO/Cu₂O heterojunction solar cells is attributable to enhanced potential barrier height and carrier lifetimes near the interface, resulting from the inserted buffer layer functioning as an n-type ZnO layer as well as an active layer in the n-p heterojunction. Cross-sectional views of ZnO/Cu₂O heterojunctions obtained by transmission electron microscopy revealed interface microstructures that differed significantly between high-efficiency and low-efficiency solar cells, fabricated with different deposition conditions, irrespective of the device structure used. For example, in AZO/non-doped ZnO/Cu₂O heterojunction solar cells fabricated with both the AZO and non-doped ZnO thin films prepared by PLD at the same deposition temperatures, either RT or 200°C, the solar cells formed at RT exhibited higher efficiency than those formed at 200°C. A smooth heterojunction was observed near both the interfaces within AZO/non-doped ZnO/Cu₂O heterojunction solar cells fabricated at RT; this contrasts with many dislocations observable near both of these interfaces of solar cells fabricated at 200°C, *i.e.*, between the non-doped ZnO layer and the Cu₂O and between the AZO and non-doped ZnO layers. Thus, the TEM observations of the heterojunction solar cells fabricated by forming both thin films at RT indicate that the higher efficiency results from an increase of carrier lifetimes, a consequence of suppressing carrier recombination and trapping near the interfaces of the heterojunctions.

[1] Y. Nishi et al., *Thin Solid Films*, 520 (2012) 3819.

[2] Y. Nishi et al., *J. Vac. Sci. Technol. A* 30 (2012) 04D103.

Friday Morning, November 2, 2012

Energy Frontiers Focus Topic

Room: 15 - Session EN+SS-FrM

Photocatalysis and Solar Fuels

Moderator: N.G. Petrik, Pacific Northwest National Laboratory

8:20am EN+SS-FrM1 **Atomic Layer Deposition for Electronic Band Engineering of Silicon Photoelectrochemical Cells.** *B. Kalanyan, M.D. Losogo, D.H. Kim, G.N. Parsons*, North Carolina State University

Nanostructured semiconductor materials are generating considerable interest for application in photoelectrochemical cells (PEC) for solar water splitting. A key challenge is improving the long-term chemical and operational stability of semiconductor electrodes. Our research in PEC devices focuses on utilizing atomic layer deposition (ALD) as a means to engineer the semiconductor-liquid interface of photoelectrodes. ALD modification can both impart chemical stability and tune the electronic band structure at the semiconductor's surface. P-type silicon photocathodes are a model PEC system capable of high photocurrents (>10 mA/cm²) in aqueous electrolytes under AM 1.5 illumination. Here we will detail our efforts to improve the reproducibility of silicon photocathode fabrication and to use TiO₂ ALD coatings for band engineering that permits planar catalyst integration.

This talk will discuss silicon photocathodes fabricated from p-type Si (100) wafers with ~ 1 cm² functional area. Electrodes were tested in a three-electrode electrochemical cell containing sulfuric acid electrolyte (0.5M, pH ~ 0), a Pt mesh (>5 cm²) counter electrode, and a Ag/AgCl reference electrode. To ensure similar dopant profiles, experiments were run using a range of silicon samples from the same wafer. We will first discuss the effects of varying the processing schemes for forming an ohmic back contact. We find a large and distinct effect on both the photocurrent saturation value and the photocurrent onset potential with the size and composition of this back contact. Through contact optimization, series resistance of the back contact can be reduced by 5x, as measured by impedance spectroscopy.

The second portion of our talk will describe our results using ALD TiO₂ thin films to engineer the electronic band structure at the photocathode/electrolyte interface. Deposition of a coalesced Pt thin film catalyst layer directly on p-type silicon is well known to form an Ohmic contact that pins the silicon's Fermi level in a nearly flat band state. Without the internal bias caused by surface carrier depletion, photoelectrode activity is eliminated. However, by inserting an interfacial TiO₂ layer with sub-nanometer thickness control, a p-n junction can be formed which generates the necessary electric field for photoelectrode operation. Here, we will demonstrate how uniform ALD layers are capable of providing the necessary electronic band engineering to form completely planar p-Si/TiO₂/Pt structures with photocurrents exceeding 10 mA/cm² with no applied bias.

8:40am EN+SS-FrM2 **Photochemical Hole Scavenging Reactions of Methanol on TiO₂: Identification of Active Species and Water Coadsorption Study.** *M. Shen, M.A. Henderson*, Pacific Northwest National Laboratory

Molecular and dissociative forms of adsorbed methanol were prepared on the rutile TiO₂(110) surface to study their relative photocatalytic activity for hole-mediated oxidation. Molecular methanol is the dominant surface species on the vacuum-annealed TiO₂(110) surface in ultrahigh vacuum (UHV). Coadsorption of methanol with oxygen results in $\sim 20\%$ of the adsorbed methanol decomposing to methoxy and OH. Subsequent heating of the surface to 350 K leaves a surface with only adsorbed methoxy groups. Using temperature-programmed desorption, we show that adsorbed methoxy is at least an order of magnitude more reactive than molecularly adsorbed methanol for hole-mediated photooxidation. Methoxy photodecomposes through cleavage of a C-H bond forming adsorbed formaldehyde and a surface OH group. These results suggest that methoxy, and not molecular methanol, is the effective hole scavenger in photochemical reactions of methanol on TiO₂. Same reactions were also studied with water coadsorption.

9:00am EN+SS-FrM3 **Nanostructured Antimony Doped Tin Oxide Enhances Photoelectrochemical Water Splitting by Supported TiO₂.** *Q. Peng*, Duke University, *B. Kalanyan*, North Carolina State University, *M. Andrew, P. Hoertz*, Research Triangle Institute, *L. Alibabaei*, University of North Carolina at Chapel Hill, *J. Liu*, Duke University, *T.J. Meyer*, University of North Carolina at Chapel Hill, *G.N. Parsons*, North Carolina State University, *J.T. Glass*, Duke University

Photoelectrochemical (PEC) water splitting devices hold great promise for harvesting solar energy, however, existing electrodes suffer from either stability or efficiency limitations. Owing to its low production cost, environmental compatibility, and remarkable stability, TiO₂ has been widely investigated as a PEC electrode since 1972. However, the solar-to-fuel conversion efficiency of TiO₂ PEC electrodes is still much lower than the theoretical value. This is partially due to the dilemma of short minority carrier diffusion length and long optical absorption length, as well as the low electron mobility. Nanostructured conductive scaffolds show promise to solve this challenge by decoupling light absorption and charge carrier diffusion while enhancing conductivity. In this research, we synthesized TiO₂ PEC electrodes on a conductive scaffold comprised of antimony doped tin oxide particles (ATO-particle film). These structures, which are a cost effective alternative to semiconductor supported TiO₂ electrodes, yielded a photocurrent density of 0.58 mA/cm². This is approximately 3 \times the corresponding current density for planar TiO₂ PEC electrodes on FTO glass. Our results have shown that the porosity of ATO-particle film has limited the further efficiency improvement, which can be addressed by optimizing particle size, thickness, and assembly strategy for ATO-particle films. Owing to its transparency in a wide range of wavelengths, the ATO-particle scaffold also has great potential to boost the efficiency of devices using other narrow bandgap PEC materials, e. g. Fe₂O₃.

9:20am EN+SS-FrM4 **Plasmon-Mediated Charge Transfer in Au-TiO₂ Heterostructures for Visible Light Water-Splitting.** *J. DuChene, B. Sweeny*, University of Florida, *A. Johnston-Peck, D. Su*, Brookhaven National Laboratory, *W.D. Wei*, University of Florida

Solar water splitting to produce hydrogen represents a potential approach to satisfy the global energy demand in a sustainable manner. Recently it has been reported that the incorporation of plasmonic nanoparticles into semiconductor architectures offers a potential route to increase the efficiency of photoelectrochemical water splitting due to the unique optical properties of plasmonic nanomaterials. We investigated the energetics and dynamics of electron flow in Au-TiO₂ heterostructures following excitation of the Au nanoparticles surface plasmon resonance with visible light. Our results show that the incorporation of Au nanoparticles into wide band gap semiconductors has promise for use as visible light sensitizers. Moreover, we have studied the role of the hole scavenger methanol in the plasmon-mediated charge transfer process in order to ascertain the nature of possible thermodynamic or kinetic limitations involved in this process. These results demonstrate that the excited-state lifetime of these hot electrons in the TiO₂ conduction band is dramatically extended relative to direct band gap excitation within the semiconductor itself, suggesting a possible strategy for improving the efficiency of photocatalytic reactions.

9:40am EN+SS-FrM5 **Narrowing of Band Gap in 1D Arrays of TiO₂ Nanoparticles for Photocatalysis: Studies using X-ray Spectroscopies with In Situ Water Exposure and Heating.** *Y. Liu, J. Taing*, University of California Irvine, *C.C. Chen*, SLAC National Accelerator Lab, *A. Sorini*, Lawrence Livermore National Lab, *M.H. Cheng*, University of California Irvine, *H. Bluhm, Z. Liu*, Lawrence Berkeley National Lab, *T. Devereaux*, SLAC National Accelerator Lab, *J.C. Hemminger*, University of California Irvine

Titanium(IV) oxide (TiO₂) has a wide range of applications in energy science and acts as a stable support for photocatalysts and sensitizers. Utilizing ambient pressure synchrotron x-ray photoelectron and absorption spectroscopies, we explore the properties of TiO₂ thin films and ordered linear arrays of TiO₂ nanoparticles under *in situ* water vapor exposure and heating. Our nondestructive depth profiles (obtained by varying the photoelectron kinetic energy) of electronic and surface structures, combined with density-functional theory calculations, indicate an enhancement of the density of states (DOS) near the Fermi level due to surface Ti³⁺ and oxygen vacancies. Introducing water on the interface suppresses this DOS enhancement. The Ti L-edge and O K-edge absorption spectra, in combination with atomic multiplet calculations, provide information on crystal field effects and multiplet interactions, helping to determine the phases of the TiO₂ particles. Our *in situ* studies suggest that isolated TiO₂ nanoparticles may enhance solar absorption efficiency, and the TiO₂ band gap can be tuned reversibly under water exposure and heating.

10:00am **EN+SS-FrM6 A Theoretical Study of Carbon Dioxide Reduction on Catalysts**, *T. Liang, Y.-T. Cheng, S.R. Phillpot, S.B. Sinnott*, University of Florida

Catalytic reduction of carbon dioxide into fuels would provide an ideal storage medium for intermittent renewable energy sources. Copper and copper oxides electro-catalysts have been found to be capable of producing significant quantities of hydrocarbons or alcohols from CO₂ in aqueous solutions. Selectivity to methanol is speculated to be due to Cu(I) species in electrochemical systems; however, these pathways have not been experimentally verified. Here, the third-generation charge optimized many body (COMB3) potentials, which are proven to be successful to characterize different types of bonding in the heterogeneous systems, are employed to investigate the atomic scale mechanisms associated with catalytic reactions on Cu surfaces and clusters supported on metal oxide surfaces. In particular, the reaction free energies of selected CHO molecules on the Cu (211) surface are investigated and validated with density functional theory calculations. The electrochemical systems are simulated with room temperature, low-energy (5 or 10 eV) deposition of CO₂ or CO₂+H₂O on the Cu (211) surface and Cu cluster interface with the ZnO (101-1) surface. The results suggest that the higher incident energy and the presence of water molecules facilitate CO₂ dissociation. The charge state of the Cu cluster and the charge transfer process are predicted to play significant roles in the selectivity of the catalysts. In particular, the Cu(I) species at the Cu/ZnO interface are predicted to be preferable sites for CO₂ reduction and dissociation, which is consistent with experimental observations. This work was supported as part of the Center for Atomic Level Catalyst Design, an Energy Frontier Research Center funded by the U.S. Department of Energy, Office of Science, Office of Basic Energy Sciences under award number DE-SC0001058.

10:20am **EN+SS-FrM7 Doping Effects on the Electronic Structure of Graphitic C₃N₄ Photocatalysts: Insights from First Principles**, *S. Zuluaga, S. Stolbov*, University of Central Florida

Band gap engineering and facilitating charge separation in the graphitic C₃N₄ semiconductors are promising means for improving the photocatalytic activity of these materials. A number of experiments suggest that doping of C₃N₄ is an efficient way to increase the rate of hydrogen production from water using this photocatalyst. In this work we apply a first principles computational approach to reveal the main factors controlling the S and P doping effects on the properties of C₃N₄. Our density-functional-theory-based calculations show that these dopants are bound to the edges of the triazine elements rather than substituting N or C. Valence charge density analysis provides detailed description of the charge transfer upon doping. We show, for example, that S does not work as an anion in these materials: it does not accept, but donates electronic charge to the C – N system. Using the GW method we calculate with high accuracy the electronic structure, including the band gap, of the pristine and doped C₃N₄. We show that sufficiently large S doping make the system a conductor. The obtained results shed light on how doping affect the catalytic properties of C₃N₄.

Authors Index

Bold page numbers indicate the presenter

— A —

Abdulagatov, A.: TF+EN-MoA3, 5
Abe, S.: EN-ThP12, 32
Adam, T.N.: EL+TF+AS+EM+SS+PS+EN+NM-MoM9, 2
Adusumilli, S.P.: EN+TF-WeA12, 21
Agarwal, S.: EN+PS-WeM4, 17
Ahn, J.R.: NS+EN-TuM1, 11
Aihara, T.: EN+TF-TuA11, **14**; EN+TF-TuA12, 14
Albin, D.S.: EN+AS-ThA1, **27**
Alcantara Ortigoza, M.: EN+NS-ThM3, 22
Alibabaei, L.: EN+SS-FrM3, 33
Andersen, J.N.: IS+AS+SS+EN-TuM12, 10
Anderson, T.J.: EN+TF-TuM10, 8
Andrew, M.: EN+SS-FrM3, 33
Antony, A.: SS+EN+OX-ThM10, 24
Anuniwat, N.: MI+EN+BI-TuA7, **15**
Ariyan, M.: EN-ThP9, **31**
Arman, M.A.: IS+AS+SS+EN-TuM12, 10
Arnold, M.S.: EN+TF-TuA3, **13**
Arpin, K.A.: EN+NS-ThA1, 28
Arregi, J.A.: MI+EN+BI-TuA12, **15**
Artyushkova, K.: EN+AS-ThA6, 27; IS+AS+SS+EN-TuM6, **10**
Aryal, P.: EL+TF+AS+EM+SS+PS+EN+NM-MoM1, 1
Asthagiri, A.: SS+EN+OX-ThM10, 24
Atanassov, P.: EN+AS-ThA6, 27; IS+AS+SS+EN-TuM6, 10
Attygalle, D.: EL+TF+AS+EM+SS+PS+EN+NM-MoM1, 1
Atwater, H.A.: EN+TF-TuA1, **13**
Axnanda, S.: IS+AS+SS+EN-TuM4, **9**
Aydil, E.S.: EN+TF-MoA8, 4; EN+TF-MoA9, 4; EN+TF-TuM9, 8

— B —

Babu, M.: EN-ThP8, 31
Bader, S.D.: MI+EN+BI-TuA1, **14**
Baek, H.-J.: EN+NS-MoM1, 2
Bao, Y.: MI+EN+BI-TuA9, **15**
Barlaz, D.E.: SS+EN+OX-ThM4, **23**
Barton, D.: EL+TF+AS+EM+SS+PS+EN+NM-MoM10, 2
Bartynski, R.A.: EN+AS-ThA9, 28
Baruth, A.: EN+TF-MoA9, 4
Beard, M.C.: EN+NS-MoM3, 3
Berger, A.: MI+EN+BI-TuA12, 15
Besnier, J.-F.: EL+TF+AS+EM+SS+PS+EN+NM-MoM3, 1
Biegalski, M.D.: IS+AS+SS+EN-TuM5, 9
Bindl, D.J.: EN+TF-TuA3, 13
Biswal, S.L.: EN+NS-ThM12, **23**
Bluhm, H.: EN+SS-FrM5, 33; IS+AS+SS+EN-TuM1, **9**; IS+AS+SS+EN-TuM5, 9
Bol, A.: TF+EN-MoA4, 5
Bolotin, I.: EN-ThP3, 30
Booth, J.-P.: EN+PS-WeM5, 17
Bora, D.: IS+AS+SS+EN-TuM3, 9
Borkowski, M.: AC+EN-TuM9, 7
Borsa, D.: TC+EM+AS+TF+EN-ThM2, 25
Bosch, R.: TC+EM+AS+TF+EN-ThM2, 25
Bowden, M.E.: SS+EN+OX-ThM11, 24
Braun, A.: IS+AS+SS+EN-TuM3, 9
Braun, P.V.: EN+NS-ThA1, 28
Brehmer, F.: EN+PS-WeM3, 17
Butler, W.H.: MI+EN+BI-TuA3, 15

— C —

Campbell, C.: EN+TF-TuM10, 8
Campbell, S.A.: EN+TF-TuM9, 8
Canepa, P.: EN+AS-ThA7, 27
Cavanagh, A.: TF+EN-MoA3, 5
Ceccone, G.: NS+EN+GR-TuA2, 15
Chabal, Y.J.: EN+AS-ThA7, 27; EN+TF-WeA7, 20

Chamberlin, S.E.: SS+EN+OX-ThM11, **24**
Chambers, S.A.: SS+EN+OX-ThM11, 24
Chang, J.P.: EN+NS-ThA6, 28; EN+NS-ThM6, 22; EN+TF-WeA9, 20
Chen, C.C.: EN+SS-FrM5, 33
Chen, J.: EL+TF+AS+EM+SS+PS+EN+NM-MoM4, 1
Chen, X.: TF+EN-MoA6, **5**
Cheng, M.H.: EN+SS-FrM5, 33
Cheng, Y.-T.: EN+SS-FrM6, 34
Chhowalla, M.: NS+EN+GR-TuA8, **16**
Chichester, H.J.M.: AC+EN-TuM1, 7
Cho, H.K.: NS+EN+GR-TuA11, 16
Cho, J.: EN+NS-ThM6, 22; EN+TF-WeA9, **20**
Cho, T.S.: TC+EM+AS+TF+EN-ThM12, 26
Choi, J.W.: EN+NS-MoM5, **3**
Christen, H.M.: IS+AS+SS+EN-TuM5, 9
Chupas, P.: IS+AS+SS+EN-TuM9, 10
Cirigliano, N.: EN+NS-ThM6, 22
Clark, M.D.: EN+TF-TuA7, 13
Cleveland, E.: NS+EN-TuM2, 11
Colbow, V.: EN+AS-ThA6, 27
Collins, R.W.: EL+TF+AS+EM+SS+PS+EN+NM-MoM1, **1**; EL+TF+AS+EM+SS+PS+EN+NM-MoM4, 1
Colpo, P.: NS+EN+GR-TuA2, 15
Constable, E.C.: IS+AS+SS+EN-TuM3, 9
Creatore, M.: EL+TF+AS+EM+SS+PS+EN+NM-MoM6, 2; TC+EM+AS+TF+EN-ThM2, 25
Crumlin, E.: IS+AS+SS+EN-TuM5, **9**
Cunningham, G.B.: EN+NS-MoM11, 3
Curreli, D.: EN-ThP11, 31
Curtiss, L.: TF+EN-MoA1, 5
Czarnetzki, U.: EN+PS-WeM12, 18; EN+PS-WeM9, 18

— D —

Dasari, S.: EN-ThP9, 31
Dawahre, N.: NS+EN-TuM3, 11
De Vito, E.: EN+NS-ThM11, **23**
Delattre, P.A.: EN+PS-WeM5, 17
Deskins, N.A.: SS+EN+OX-ThM9, 24
Devereaux, T.: EN+SS-FrM5, 33
Dezelah, C.L.: EN+TF-WeA10, **20**
Dhakal, T.: EN+TF-WeA12, 21
Dhere, N.: EN+TF-TuM11, 8
Dhere, R.: EN+AS-ThA1, 27
Dhiman, R.: EN-ThP5, **30**
Diebold, A.C.: EL+TF+AS+EM+SS+PS+EN+NM-MoM9, **2**
Ding, M.: MI+EN+BI-TuA7, 15
Dogan, I.: EN+PS-WeM4, **17**
Dohnalek, Z.: SS+EN+OX-ThM5, 24
Dohnalova, K.: EN+PS-WeM4, 17
Domen, K.: SS+EN+OX-ThM1, 23
Doris, B.: EL+TF+AS+EM+SS+PS+EN+NM-MoM9, 2
Dornstetter, J.-C.: EL+TF+AS+EM+SS+PS+EN+NM-MoM3, **1**
DuChene, J.: EN+SS-FrM4, **33**
Dudney, N.: EN+TF-WeA1, **20**
Dunn, B.: EN+NS-ThM6, 22; EN+TF-WeA9, 20
Durstock, M.F.: EN+NS-ThM9, 22
Dutta, M.: EN+AS-ThA6, 27
Dutta, P.: EN+TF-TuA8, 13

— E —

Elam, J.W.: IS+AS+SS+EN-TuM9, 10; TC+EM+AS+TF+EN-ThM6, 26; TF+EN-MoA1, **5**
Engeln, R.: EN+PS-WeM3, **17**

— F —

Fauzi, M.E.: EN+PS-WeM11, **18**
Feliciano, D.M.: EN+NS-MoM6, 3
Ferekides, C.S.: EN+TF-TuM1, 7
Filler, M.: NS+EN-TuM4, 11

Fujita, T.: EN-ThP7, 31
Fukuyama, A.: EN+TF-TuA12, 14

— G —

Galtsyan, E.: EN+TF-TuA8, 13
Gao, Y.: EN+TF-TuA8, 13
Gartstein, Yu.N.: EN+TF-WeA7, 20
Gembocki, O.J.: NS+EN-TuM2, 11
George, S.M.: TF+EN-MoA3, 5
Gessert, T.A.: EN+AS-ThA1, 27; EN+TF-MoA1, 4
Glass, J.T.: EN+SS-FrM3, 33
González-Díaz, J.B.: MI+EN+BI-TuA12, 15
Grånäs, E.: IS+AS+SS+EN-TuM12, 10
Grätzel, M.: IS+AS+SS+EN-TuM3, 9
Greeley, J.: IS+AS+SS+EN-TuM9, 10; TF+EN-MoA1, 5
Gregorkiewicz, T.: EN+PS-WeM4, 17
Gregory, C.W.: EN+NS-MoM11, 3
Guo, J.H.: IS+AS+SS+EN-TuM3, **9**
Guo, X.: NS+EN-TuM11, 12

— H —

Haag, J.: EN+NS-ThM9, 22
Haasch, R.T.: TC+EM+AS+TF+EN-ThM6, 26
Hakanoglu, C.: SS+EN+OX-ThM10, 24
Halevi, B.: IS+AS+SS+EN-TuM6, 10
Hall, S.: EN+NS-MoM11, 3
Hammond, J.S.: EN+AS-ThA4, 27
Han, L.: EN+PS-WeM10, **18**
Hanley, L.: EN-ThP3, 30
Hanrath, T.: EN+NS-MoM5, 3
Hanus, J.: NS+EN+GR-TuA2, 15
Hashemian, M.: EN-ThP9, 31
Hawley, C.J.: NS+EN-TuM6, **12**
Hayes, S.L.: AC+EN-TuM1, 7
Hemminger, J.C.: EN+SS-FrM5, 33
Henderson, M.A.: EN+SS-FrM2, 33; SS+EN+OX-ThM11, 24
Herman, G.S.: TC+EM+AS+TF+EN-ThM5, **25**
Herring, A.M.: EN+NS-ThM1, **22**
Hettiarachchi, C.: EN+NS-MoM6, **3**
Hillhouse, H.W.: EN+TF-MoA3, **4**
Hoertz, P.: EN+SS-FrM3, 33
Hoffman, R.S.: EN+NS-MoM5, 3
Hofman, G.L.: AC+EN-TuM1, 7
Holliday, K.S.: AC+EN-TuM10, 7
Hone, J.C.: NS+EN-TuM11, 12
Hong, J.: TC+EM+AS+TF+EN-ThM12, 26
Hong, S.J.: EN-ThP8, **31**
Hong, W.T.: IS+AS+SS+EN-TuM5, 9
Hosono, H.: TC+EM+AS+TF+EN-ThM3, **25**
Hu, L.: TF+EN-MoA6, 5
Hu, W.: EN+PS-WeM11, 18
Hu, X.: TF+EN-MoA7, 6
Hwang, H.H.: EN+NS-MoM1, 2

— I —

Idigoras, O.: MI+EN+BI-TuA12, 15
Igarashi, M.: EN+PS-WeM11, 18
Ikari, T.: EN+TF-TuA12, **14**
Ikenaga, N.: EN-ThP12, 32
Isaacson, M.: EN+NS-ThM12, 23
Ishigami, M.: NS+EN-TuM11, 12
Ishikawa, T.: NS+EN-TuM5, 12
Itagaki, N.: EN+NS-MoM2, 3

— J —

Jang, J.S.: EN+NS-MoM1, 2
Jankovic, V.: EN+NS-ThA6, **28**
Jespersen, M.L.: EN+TF-TuA7, 13
Johnson, E.: EN-ThP5, 30
Johnson, E.V.: EN+PS-WeM5, **17**
Johnson, M.: EN+TF-MoA8, 4; EN+TF-MoA9, 4
Johnston-Peck, A.: EN+SS-FrM4, 33
Joo, M.H.: EN-ThP4, **30**
Jouanneau, S.: EN+NS-ThM11, 23

- Joy, R.: TC+EM+AS+TF+EN-ThM2, 25
Jurczyk, B.: EN-ThP11, 31
- **K** —
- Kabir, A.K.: MI+EN+BI-TuA8, 15
Kalanyan, B.: EN+NS-ThA1, 28; EN+SS-FrM1, 33; EN+SS-FrM3, 33; TF+EN-MoA8, 6
Kamataki, K.: EN+NS-MoM2, 3
Kanevce, A.: EN+AS-ThA1, 27
Karakoti, A.S.: EN-ThP10, 31
Karim, A.M.: IS+AS+SS+EN-TuM10, 10
Karpov, E.: EN-ThP9, 31
Kasouit, S.: EL+TF+AS+EM+SS+PS+EN+NM-MoM3, 1
Kaspar, T.C.: SS+EN+OX-ThM11, 24
Kaul, A.: EN+TF-TuM11, 8
Kay, B.D.: SS+EN+OX-ThM5, 24
Kennedy, J.R.: AC+EN-TuM1, 7
Kessels, W.M.M.:
EL+TF+AS+EM+SS+PS+EN+NM-MoM6, 2;
TC+EM+AS+TF+EN-ThM2, 25; TF+EN-MoA4, 5
Kiefer, B.: IS+AS+SS+EN-TuM6, 10
Kim, D.H.: EN+SS-FrM1, 33; NS+EN+GR-TuA10, 16; TF+EN-MoA8, 6
Kim, J.H.: NS+EN+GR-TuA11, 16
Kim, K.J.: EN+NS-MoM1, 2
Kim, S.H.: EN+TF-TuM12, 8
Kim, S.M.: NS+EN-TuM3, 11
Kim, W.K.: EN+TF-TuM10, 8
Kim, Y.S.: AC+EN-TuM1, 7
Kimmel, G.A.: SS+EN+OX-ThM3, 23;
SS+EN+OX-ThM5, 24
Klem, E.J.D.: EN+NS-MoM11, 3
Knoops, H.C.M.:
EL+TF+AS+EM+SS+PS+EN+NM-MoM6, 2;
TC+EM+AS+TF+EN-ThM2, 25
Knudsen, J.: IS+AS+SS+EN-TuM12, 10
Koga, K.: EN+NS-MoM2, 3
Koirala, P.: EL+TF+AS+EM+SS+PS+EN+NM-MoM4, 1
Kondoh, H.: IS+AS+SS+EN-TuM12, 10
Koshihara, S.: NS+EN-TuM5, 12
Kotru, S.: EN+TF-WeA11, 20
Krafcik, J.: NS+EN-TuM3, 11
Krishnan, R.: EN+TF-TuM10, 8
Kristensen, P.K.: EN-ThP5, 30
Krueger, B.: TC+EM+AS+TF+EN-ThM11, 26
Kubota, J.: SS+EN+OX-ThM1, 23
Kuciauskas, D.: EN+AS-ThA1, 27
Kung, M.: TF+EN-MoA1, 5
Kung, P.: NS+EN-TuM3, 11
- **L** —
- Law, M.: EN+TF-MoA6, 4
Le, D.: NS+EN+GR-TuA7, 16
Lee, J.H.: EN+TF-TuM12, 8
Lee, J.M.: EN-ThP4, 30
Lee, K.M.: NS+EN+GR-TuA10, 16; TF+EN-MoA8, 6
Lee, Y.H.: EN+TF-TuM12, 8
Leever, B.J.: EN+TF-TuA7, 13
Lei, Y.: IS+AS+SS+EN-TuM9, 10
Leick, N.: EL+TF+AS+EM+SS+PS+EN+NM-MoM6, 2
Leick-Marius, N.: TF+EN-MoA4, 5
Leighton, C.: EN+TF-MoA8, 4; EN+TF-MoA9, 4
Lewis, J.: EN+NS-MoM11, 3
Li, J.: EN+AS-ThA7, 27
Li, Z.: SS+EN+OX-ThM5, 24
Lian, T.: EN+NS-MoM8, 3
Liang, T.: EN+SS-FrM6, 34
Liao, B.-H.: EN-ThP2, 30
Libera, J.A.: TC+EM+AS+TF+EN-ThM6, 26
Lin, X.: SS+EN+OX-ThM5, 24
Liu, B.: IS+AS+SS+EN-TuM9, 10
Liu, J.: EN+SS-FrM3, 33
Liu, Y.: EN+SS-FrM5, 33
Liu, Z.: EN+SS-FrM5, 33; IS+AS+SS+EN-TuM4, 9; IS+AS+SS+EN-TuM5, 9
- Losego, M.D.: EN+NS-ThA1, 28; EN+SS-FrM1, 33
Lu, J.: IS+AS+SS+EN-TuM9, 10
Lu, J.W.: MI+EN+BI-TuA7, 15
Lucchini, J.-F.: AC+EN-TuM9, 7
Luther, J.M.: EN+NS-MoM3, 3
Lyubinetzky, I.: SS+EN+OX-ThM5, 24;
SS+EN+OX-ThM9, 24
- **M** —
- Ma, J.: EN+AS-ThA1, 27
Ma, M.: EN+PS-WeM3, 17
Mackus, A.J.M.: TF+EN-MoA4, 5
Majeski, M.: EN-ThP3, 30
Majkic, G.: EN+TF-TuA8, 13
Malko, A.V.: EN+TF-WeA7, 20
Mann, H.S.: TF+EN-MoA7, 6
Manno, M.: EN+TF-MoA8, 4; EN+TF-MoA9, 4
Mao, B.: IS+AS+SS+EN-TuM4, 9
Mariani, R.D.: AC+EN-TuM1, 7
Marshall, C.: TF+EN-MoA1, 5
Marsillac, S.: EL+TF+AS+EM+SS+PS+EN+NM-MoM1, 1; EL+TF+AS+EM+SS+PS+EN+NM-MoM4, 1
Masters, A.E.: TF+EN-MoA7, 6
Matsushima, K.: EN-ThP6, 30
McClimon, J.B.: EN-ThP1, 30
McGuckin, T.: NS+EN-TuM6, 12
Medikonda, M.:
EL+TF+AS+EM+SS+PS+EN+NM-MoM9, 2
Melese, Y.G.: EL+TF+AS+EM+SS+PS+EN+NM-MoM6, 2
Membreno, D.: EN+NS-ThM6, 22; EN+TF-WeA9, 20
Mewes, K.A.: MI+EN+BI-TuA3, 15
Mewes, T.: MI+EN+BI-TuA3, 15
Meyer, T.J.: EN+SS-FrM3, 33
Miller, J.: IS+AS+SS+EN-TuM9, 10
Miller, T.J.: EN+AS-ThA8, 28
Minami, T.: EN-ThP12, 32; EN-ThP7, 31
Miyata, T.: EN-ThP12, 32; EN-ThP7, 31
Mohr, S.: EN+PS-WeM12, 18; EN+PS-WeM9, 18
Monya, Y.: IS+AS+SS+EN-TuM12, 10
Morgen, P.: EN-ThP5, 30
Morrish, R.: EN+TF-MoA10, 5
Moulder, J.F.: EN+AS-ThA4, 27
Mukherjee, D.: EN+NS-MoM6, 3
Mukherjee, P.: EN+NS-MoM6, 3
Muthinti, G.R.:
EL+TF+AS+EM+SS+PS+EN+NM-MoM9, 2
Mutoro, E.: IS+AS+SS+EN-TuM5, 9
Muzzillo, C.: EN+TF-TuM10, 8
- **N** —
- Nachimuthu, P.: EN-ThP10, 31;
TC+EM+AS+TF+EN-ThM5, 25
Nakano, Y.: EN+TF-TuA12, 14
Nampoori, V.: EN+TF-WeA11, 20
Nelson, A.J.: AC+EN-TuM10, 7; AC+EN-TuM3, 7
Nguyen, H.M.: EN+TF-WeA7, 20
Nguyen, S.: TF+EN-MoA1, 5
Nijem, N.: EN+AS-ThA7, 27
Nishi, Y.: EN-ThP12, 32
Nomoto, J.: EN-ThP7, 31
Notestein, J.: TF+EN-MoA1, 5
Noufi, R.: EN+AS-ThA1, 27
Nozaki, T.: EN+PS-WeM1, 17
Nozik, A.J.: EN+NS-MoM3, 3
- **O** —
- Oda, S.: NS+EN-TuM5, 12
Oh, D.-H.: NS+EN-TuM1, 11
Ohuchi, F.S.: TC+EM+AS+TF+EN-ThM11, 26
Olmstead, M.A.: TC+EM+AS+TF+EN-ThM11, 26
Omberg, R.P.: AC+EN-TuM1, 7
Ong, S.W.: SS+EN+OX-ThM4, 23
- **P** —
- Pandey, A.: TC+EM+AS+TF+EN-ThM5, 25
Park, C.-Y.: NS+EN-TuM1, 11
Park, J.H.: EN+NS-MoM1, 2
Park, K.H.: EN-ThP4, 30
Parracino, M.A.: NS+EN+GR-TuA2, 15
Parsons, G.N.: EN+NS-ThA1, 28; EN+SS-FrM1, 33; EN+SS-FrM3, 33; NS+EN+GR-TuA10, 16; TF+EN-MoA8, 6
Patel, A.: EN+AS-ThA6, 27
Pattanaik, G.: EN+NS-ThM9, 22
Payzant, E.A.: EN+TF-TuM10, 8
Peck, J.: EN-ThP11, 31
Peng, Q.: EN+SS-FrM3, 33
Peng, W.: EN+TF-WeA7, 20
Perez Roldan, M.J.: NS+EN+GR-TuA2, 15
Perng, Y.-C.: EN+NS-ThM6, 22
Pernites, R.B.: EN+NS-ThM12, 23
Pethe, S.: EN+TF-TuM11, 8
Petrik, N.G.: SS+EN+OX-ThM3, 23; SS+EN+OX-ThM5, 24
Pettit, C.: EN+TF-TuM9, 8
Pham, H.: TC+EM+AS+TF+EN-ThM11, 26
Phillpot, S.R.: EN+SS-FrM6, 34
Plaue, J.: AC+EN-TuM10, 7
Pleticha, D.: EN-ThP3, 30
Podraza, N.J.: EL+TF+AS+EM+SS+PS+EN+NM-MoM1, 1; EL+TF+AS+EM+SS+PS+EN+NM-MoM4, 1
Poepfmeier, K.: TF+EN-MoA1, 5
Ponduri, S.: EN+PS-WeM3, 17
Ponomarev, M.V.:
EL+TF+AS+EM+SS+PS+EN+NM-MoM6, 2;
TC+EM+AS+TF+EN-ThM2, 25
Poon, J.: MI+EN+BI-TuA7, 15
Porcher, W.: EN+NS-ThM11, 23
Porter, D.L.: AC+EN-TuM1, 7
Pouliquen, S.: EN+PS-WeM5, 17
Pradhan, P.: EL+TF+AS+EM+SS+PS+EN+NM-MoM1, 1
Prokes, S.M.: NS+EN-TuM2, 11
- **R** —
- Radvanyi, E.: EN+NS-ThM11, 23
Rahman, T.S.: MI+EN+BI-TuA8, 15;
NS+EN+GR-TuA7, 16
Raj, R.: TF+EN-MoA3, 5
Rajachidambaram, M.S.: TC+EM+AS+TF+EN-ThM5, 25
Raman, S.N.: EN+AS-ThA4, 27
Rangan, S.: EN+AS-ThA9, 28
Ranjan, V.: EL+TF+AS+EM+SS+PS+EN+NM-MoM1, 1
Reed, D.T.: AC+EN-TuM9, 7
Reilly, M.: EN-ThP11, 31
Reinke, P.: EN-ThP1, 30
Reznicek, A.: EL+TF+AS+EM+SS+PS+EN+NM-MoM9, 2
Ribeiro, F.: TF+EN-MoA1, 5
Richmann, M.K.: AC+EN-TuM9, 7
Ritz, E.: TC+EM+AS+TF+EN-ThM12, 26
Roca i Cabarocas, P.:
EL+TF+AS+EM+SS+PS+EN+NM-MoM3, 1
Rossi, F.: NS+EN+GR-TuA2, 15
Rousseau, R.: SS+EN+OX-ThM5, 24
Roussel, P.: AC+EN-TuM3, 7
Rubloff, G.W.: TF+EN-MoA6, 5
Ruzic, D.N.: EN-ThP11, 31;
TC+EM+AS+TF+EN-ThM12, 26
- **S** —
- Sabnis, V.A.: EN+TF-TuA9, 14
Samukawa, S.: EN+PS-WeM11, 18
Scarel, G.: TF+EN-MoA7, 6
Schnadt, J.: IS+AS+SS+EN-TuM12, 10
Schneller, E.: EN+TF-TuM11, 8
Schuengel, E.: EN+PS-WeM12, 18; EN+PS-WeM9, 18
Schulze, J.: EN+PS-WeM12, 18; EN+PS-WeM9, 18
Schwab, Y.: TF+EN-MoA7, 6
Seebauer, E.G.: SS+EN+OX-ThM4, 23
Seitz, O.: EN+TF-WeA7, 20

Selvamanickam, V.: EN+TF-TuA8, **13**
 Semonin, O.E.: EN+NS-MoM3, **3**
 Senior, D.J.: AC+EN-TuM1, **7**
 Seo, H.: EN+NS-MoM2, **3**
 Seo, J.-W.T.: NS+EN-TuM12, **12**
 Serov, A.: IS+AS+SS+EN-TuM6, **10**
 Seyhan, A.: NS+EN-TuM5, **12**
 Shafarman, W.N.: EN+TF-TuM3, **8**
 Shao-Horn, Y.: IS+AS+SS+EN-TuM5, **9**
 Sharma, K.: TC+EM+AS+TF+EN-ThM2, **25**
 Shea, M.J.: EN+TF-TuA3, **13**
 Shen, G.: NS+EN-TuM3, **11**
 Shen, J.: EN+TF-TuM10, **8**
 Shen, M.: EN+SS-FrM2, **33**
 Shin, N.: NS+EN-TuM4, **11**
 Shiradkar, N.: EN+TF-TuM11, **8**
 Shiratani, M.: EN+NS-MoM2, **3**
 Shutthanandan, V.: SS+EN+OX-ThM11, **24**
 Siebentritt, S.: EN+TF-TuM5, **8**
 Siekhaus, W.J.: AC+EN-TuM10, **7**; AC+EN-TuM6, **7**
 Silverstein, R.: EN+TF-MoA10, **5**
 Simanullang, M.: NS+EN-TuM5, **12**
 Simchenko, S.V.: SS+EN+OX-ThM12, **25**
 Sinnott, S.B.: EN+SS-FrM6, **34**
 Sinsabaugh, S.L.: EN+NS-ThM12, **23**
 Siringhaus, H.: TC+EM+AS+TF+EN-ThM9, **26**
 Sivula, K.: IS+AS+SS+EN-TuM3, **9**
 Smets, A.H.M.: EN+PS-WeM10, **18**
 Sohn, Y.H.: EN+TF-TuM10, **8**
 Song, L.: NS+EN-TuM1, **11**
 Sorini, A.: EN+SS-FrM5, **33**
 Spampinato, V.: NS+EN+GR-TuA2, **15**
 Spanier, J.E.: NS+EN-TuM6, **12**
 Stach, E.: TF+EN-MoA1, **5**
 Stair, P.C.: TF+EN-MoA1, **5**
 Steiner, M.B.: NS+EN-TuM9, **12**
 Stevanovic, A.: SS+EN+OX-ThM6, **24**
 Stolbov, S.: EN+NS-ThM3, **22**; EN+SS-FrM7, **34**
 Stubbers, R.: EN-ThP11, **31**
 Styrov, V.: SS+EN+OX-ThM12, **25**
 Su, D.: EN+SS-FrM4, **33**
 Sugiyama, M.: EN+TF-TuA12, **14**
 Suzer, S.: EN-ThP3, **30**
 Svedberg, E.B.: EN+NS-ThA7, **29**
 Sweeny, B.: EN+SS-FrM4, **33**
 Synowicki, R.A.:
 EL+TF+AS+EM+SS+PS+EN+NM-MoM5, **1**

— **T** —

Taing, J.: EN+SS-FrM5, **33**
 Tan, X.: EL+TF+AS+EM+SS+PS+EN+NM-MoM4, **1**
 Temple, D.S.: EN+NS-MoM11, **3**
 Teplyakov, A.V.: EN+AS-ThA8, **28**
 Terauds, K.: TF+EN-MoA3, **5**
 Teslich, N.E.: AC+EN-TuM6, **7**
 Thakur, M.: EN+NS-ThM12, **23**
 Thevuthasan, S.: EN-ThP10, **31**;
 TC+EM+AS+TF+EN-ThM5, **25**
 Thissen, P.: EN+AS-ThA7, **27**
 Thonhauser, T.: EN+AS-ThA7, **27**
 Thorpe, R.: EN+AS-ThA9, **28**
 Toivola, M.: EN+TF-WeA10, **20**
 Tompkins, H.G.:
 EL+TF+AS+EM+SS+PS+EN+NM-MoM8, **2**
 Tosun, B.S.: EN+TF-TuM9, **8**
 Travis, J.: TF+EN-MoA3, **5**
 Tsuchikawa, R.: NS+EN-TuM11, **12**
 Turkowski, V.: MI+EN+BI-TuA8, **15**

— **U** —

Uchida, G.: EN+NS-MoM2, **3**
 Ueda, O.: EN-ThP12, **32**
 Urban, F.K.: EL+TF+AS+EM+SS+PS+EN+NM-MoM10, **2**
 Usami, K.: NS+EN-TuM5, **12**

— **V** —

van de Loo, B.W.H.:
 EL+TF+AS+EM+SS+PS+EN+NM-MoM6, **2**
 van de Sanden, M.C.M.: EN+PS-WeM3, **17**;
 EN+PS-WeM4, **17**
 Vanhart, D.: EN+TF-WeA12, **21**
 Vasekar, P.S.: EN+TF-WeA12, **21**
 Velden, M.: TC+EM+AS+TF+EN-ThM2, **25**
 Verheijen, M.A.: TF+EN-MoA4, **5**
 Vilayrganapathy, S.: TC+EM+AS+TF+EN-ThM5, **25**
 Vincent-Johnson, A.J.: TF+EN-MoA7, **6**

— **W** —

Wang, R.: EN+TF-TuA8, **13**
 Wang, Y.: EN+NS-MoM2, **3**; EN+TF-TuA12, **14**
 Wang, Z.-T.: SS+EN+OX-ThM5, **24**; SS+EN+OX-ThM9, **24**
 Waters, J.: NS+EN-TuM3, **11**
 Weaver, J.F.: SS+EN+OX-ThM10, **24**

Weber, J.W.: EL+TF+AS+EM+SS+PS+EN+NM-MoM6, **2**
 Weber, M.J.: TF+EN-MoA4, **5**
 Weber, P.K.: AC+EN-TuM6, **7**
 Weeks, S.L.: EN+PS-WeM4, **17**
 Wei, S.-H.: EN+AS-ThA1, **27**
 Wei, W.D.: EN+SS-FrM4, **33**
 Welzel, S.: EN+PS-WeM3, **17**
 Wenger, W.N.: EN+NS-MoM5, **3**
 Wessel, S.: EN+AS-ThA6, **27**
 Wiemer, M.: EN+TF-TuA9, **14**
 Winans, L.: TF+EN-MoA1, **5**
 Witanachchi, S.: EN+NS-MoM6, **3**
 Wolden, C.A.: EN+TF-MoA10, **5**
 Wolf, S.A.: MI+EN+BI-TuA7, **15**
 Won, S.-O.: EN+TF-TuM12, **8**
 Wong, M.S.: EN+NS-ThM12, **23**
 Woodroof, M.: TF+EN-MoA8, **6**
 Wright, A.E.: AC+EN-TuM1, **7**
 Wu, H.: EN+AS-ThA7, **27**
 Wu, M.-Y.: EN+TF-TuA3, **13**
 Wu, Y.: EN+NS-ThA3, **28**
 Wu, Y.L.: TC+EM+AS+TF+EN-ThM12, **26**

— **Y** —

Yacout, A.M.: AC+EN-TuM1, **7**
 Yang, M.: EN+TF-TuA8, **13**
 Yanguas-Gil, A.: TC+EM+AS+TF+EN-ThM6, **26**
 Yao, B.: EN+TF-TuM10, **8**
 Yates, Jr., J.T.: SS+EN+OX-ThM6, **24**
 Yilmaz, E.: EN-ThP3, **30**
 Yoon, J.-H.: EN+TF-TuM12, **8**
 Yoon, Y.: SS+EN+OX-ThM5, **24**
 Yuen, H.B.: EN+TF-TuA9, **14**
 Yushin, G.: EN+NS-ThM4, **22**

— **Z** —

Zeman, M.: EN+PS-WeM10, **18**
 Zhang, F.: SS+EN+OX-ThM10, **24**
 Zhang, L.: IS+AS+SS+EN-TuM3, **9**
 Zhang, X.: EN+TF-MoA8, **4**; EN+TF-MoA9, **4**
 Zhang, Z.: NS+EN-TuM11, **12**
 Zhao, H.: IS+AS+SS+EN-TuM9, **10**
 Zheng, X.: TC+EM+AS+TF+EN-ThM11, **26**
 Zhu, H.: TF+EN-MoA6, **5**
 Zhu, J.F.: IS+AS+SS+EN-TuM3, **9**
 Zonooz, P.: EN-ThP11, **31**
 Zuluaga, S.: EN+SS-FrM7, **34**